RESILIENCE-BASED BLAST DESIGN OF REINFORCED CONCRETE MASONRY SYSTEMS

RESILIENCE-BASED BLAST DESIGN OF REINFORCED CONCRETE MASONRY SYSTEMS

By

Shady Hesham Abdel-Mohaimen Bakr Salem

B.Sc., M.Sc.

A Thesis Submitted to the School of Graduate Studies in Partial Fulfillment of the Requirements for the Degree Doctor of Philosophy

McMaster University

July 2018

Doctor of Philosophy (2018) McMaster University

(Civil Engineering) Hamilton, Ontario

TITLE: RESILIENCE-BASED BLAST DESIGN FOR REINFORCED CONCRETE MASONRY SYSTEMS

AUTHOR: Shady Salem

B.Sc., M.Sc. (Ain Shams University)

SUPERVISORS: Dr. Wael El-Dakhakhni

Dr. Michael Tait

NUMBER OF PAGES: xvi,204

Abstract

The use of fully grouted reinforced masonry shear walls (RMSWs) has been growing in several areas around the world owing to their relative ease of construction and their in-plane ductile behavior. However, RMSWs possess low out-of-plane ductility which amplifies the vulnerability of such components under blast loading. Furthermore, the long time and high costs of recovery following devastating (deliberate or accidental) explosions have created a need for resilience-based design for risk mitigation, especially considering the different sources of associated uncertainty. As such, this study aims to lay out the foundations of a probabilistic resilience–based blast analysis and design framework. The framework should have the capability of quantifying the overall building post-blast functionality in order to estimate its recovery cost and time, and thus the building resilience following such a demand. The proposed framework will be specifically applied for RMSW buildings incurring blast loads through a profound investigation for the behavior of rectangular RMSWs as being a primary structural element in reinforced masonry buildings. The investigation will subsume an experimental and analytical evaluation for the performance of load-bearing RMSWs with different in-plane ductility levels subjected to out-of-plane quasi-static loading. This will be followed by a numerical investigation of RMSWs to conclude the blast probabilistic performance of RMSWs that can be applied within the proposed probabilistic resilience-based blast framework. The work in this dissertation presents a key step towards adopting resilience based analysis and design in future editions of blast-resistant construction standards and provides the decisionmakers with a complete insight into post-blast building functionality and its recovery.

Acknowledgment

First, I would like to acknowledge my supervisors Dr. Wael El-Dakhakhni and Dr. Michael Tait. I was lucky to be supervised by such respected experts, advocates, and supervisors. I will always consider them to be role models for advisors interested in life knowledge transfer, rather than typical academic supervisors. I am especially grateful for our discussions that significantly impacted the quality of my research. Special thanks are due to my supervisory committee members, Dr. Lydell Wiebe and Dr. Tracy Becker, for their valuable advice and suggestions. Their helpful comments and discussions during our meetings are greatly appreciated. Thanks are extended to Dr. Hani Salim from the University of Missouri for reviewing the thesis as the external examiner.

I would like to admit that without the patience and support of my brother Tarek El-Hashimy; the presented work here in this thesis would not have been completed. I would also like to acknowledge his great "N" family, Nehal, Noureen, and Nadin, for considering me their fifth family member. Special thanks to Noureen, the best niece I will ever have, for her endless hugs and smiles.

I would like to thank the Applied Dynamics Laboratory (ADL) team; Mr. Kent Wheeler, and Mr. Paul Heerema, for their unwavering help throughout the experimental phase of this study. I would also like to thank them as real friends who showed me their great culture as true Canadians. I owe a special thanks to my peers and colleagues who whom my study would not have been completed: Ahmed Ghith, Ahmed Ismail, Ahmed Yassin, Ahmed Yosri, Maysara Ghaith, Mohamed El-Sefy, Nathan Buccella, Yasser Al-Anany, Yasser Khalifa. Moreover, I would like to thank Dr. Manuel Campidelli as a great mentor and travelling companion. A great thank you note to my colleagues, mentors, and above all, friends, Dr. Ahmad Siam and Dr. Mohamed Ezzeldin, for their continuous academic and social support as they treated me like their younger brother.

I would not have sustained my fifty two month stay in the ADL offices (the Rock) without my cheerful roommates; especially: Adrian Crowder, Alexander Sciascetti, Changxuan Zhang, Clinton D'Souza, Feras Alsheet, Francesco Longo, Heba Bayoumy, Hossein Mohammadi, Joud Odeh, Kevin McNamara, Mahmoud Madany, Mehdi Shafikhani, Mohammadreza Najafi Jozani, Neda Salari, Scott Linde, Sylvia Mihaljevic, Taylor Steele, Vahid Mohsenzadeh.

I am thankful for the research funding support provided through the Natural Sciences and Engineering Research Council of Canada, and the Canada Masonry Design Centre. Many thanks to Mr. David Stubbs and Dr. Bennett Banting for providing valuable comments on the reinforced masonry practice in Canada, and the provisions by their expert masons. The supply of the scaled blocks by the Canadian Concrete Masonry Producers Association is gratefully acknowledged. Support was also provided by the McMaster University Centre for Effective Design of Structures, funded through the Ontario Research and Development Challenge Fund of the Ministry of Research and Innovation. Additional advancements have also been provided by the McMaster Institute for Multi-Hazard Systemic Risk Studies.

Finally, I can find no words to express my sincere gratitude to my family, to whom I would dedicate my work, for their selfless love, patience, and support. I would not have borne the burden of my studies pressure throughout my Ph.D. journey without the persisted encouragement of my father Hesham and my mother Heba. I am also indebted to my grandmothers for their endless prayers and motivations. I would like to thank my uncle Amr for his continuous faith in me. I would also have a sense of obligation towards my sister Shahinda for her initial motivating words that I kept in mind during my whole study period. I would like to thank her and my brother-in-law Mostafa for their continuous support. At last but not least, I would thank my newborn nephew, Yassin, for inspiring two chapters within this thesis with his chubby cheeks and smiles.

Co-Authorship

This dissertation had been prepared in accordance with the regulation for a sandwich thesis format, a compilation of research paper stipulated by the faculty of graduate studies at McMaster University. This research presents experimental and analytical work carried out solely by Shady Salem. Advice and guidance were provided for the whole thesis by the academic supervisors Dr. Wael El-Dakhakhni and Dr. Michael Tait. Dr. Mohamed Ezzeldin provided additional advice and guidance on the papers reported in Chapter 2 and 3. Dr. Manuel Campidelli provided editorial and several comments on the paper reported in Chapter 4. Dr. Ahmad Siam provided editorial and several comments on the paper reported in Chapter 5. Information presented from outside sources, which has been used towards analysis or discussion, has been cited where appropriate; all other materials are the sole work of the author. This thesis consists of the following manuscripts in the following chapters:

Chapter 2

Salem, S., Ezzeldin, M., El-Dakhakhni, W. W., & Tait, M. J. **Out-of-plane behaviour of load-bearing reinforced masonry shear walls**. *ASCE Journal of Structure Engineering,* submitted for publication in June 2018

Chapter 3

Salem, S., Ezzeldin, M., Tait, M. J. & El-Dakhakhni, W. W. **Blast fragility assessment for load-bearing reinforced masonry shear walls**. *ASCE Journal of Structure Engineering,* submitted for publication in July 2018

Chapter 4

Salem, S., Campidelli, M., El-Dakhakhni, W. W., & Tait, M. J. (2018). **Resilience-based design of urban centres: application to blast risk assessment**. Sustainable and Resilient Infrastructure, 3(2), 68-85.

Chapter 5

Salem, S., Siam, A., Tait, M. J. & El-Dakhakhni, W. W. **Probabilistic resilience-based blast design framework**. Engineering Structures, submitted for publication in September 2018.

TABLE OF CONTENTS

List of Figures

List of Tables

CHAPTER 1

INTRODUCTION

1.1 BACKGROUND AND MOTIVATION

The negative economic and/or societal impacts of different hazard risks have adverted the public attention to the design-for-multi-hazard paradigm (Cutter et al. 2014; Lindell and Prater 2003). These hazards, either natural or anthropogenic, can be classified as concurrent or nonconcurrent and dependent or independent (Li et al. 2012; Salman and Li 2017). For example, tsunamis, landslides, and fires can be considered as both concurrent and earthquake-dependent hazards, while hurricanes and earthquakes can be designated as nonconcurrent independent hazards (Salman and Li 2017). As such, numerous attempts have focused on enhancing the performance of different structural components subjected to multiple hazards. However, in some cases, performance enhancement under one type of hazard may cause an increased vulnerability under another hazard(s) (Bruneau et al. 2017). For example, increasing the mass of a component is considered an effective mitigation strategy to enhance the blast and wind uplift resistances, however, an increase in mass would typically increase the inertial forces during earthquakes (Bruneau et al. 2017), and thus the seismic demands.

The use of reinforced masonry shear wall (RMSW) systems within the context of modern construction has increased within the past few decades. This trend is attributed to the relative ease of construction and their in-plane ductile behavior when properly detailed (Priestley et al. 2007). Several experimental and analytical studies have demonstrated the ductile in-plane performance of RMSWs (El-Dakhakhni and Ashour 2017; Shedid et al. 2008; Siyam et al. 2016b; a). The demonstrated in-plane ductility is reflected in the current North American building codes (e.g. ASCE 41-17 2017; NRC 2015) and design standards (e.g. CSA 2014; TMS-402 2016) through the relaxation of the RMSWs systems design requirements. Conversely, RMSWs have been found

to have limited ductility in the out-of-plane loading, due to the typical single layer/ mid-cell reinforcement configuration (ElSayed et al. 2015). Out-of-plane loading may be induced by different types of hazards such as high wind, blast, impact, and others (Bui and Limam 2014). Conversely, the demand for blast-resistant civilian structures has increased, particularly after the 9/11 attacks (Marjanishvili 2004). This blast protection demand is sought in order to minimize the blast risk resulting from improvised explosive devices (IEDs) attacks, which constitute 60% of all terrorist attacks (Institute for Economics and Peace 2015). In this context, multiple studies have focused on hardening the structural components, especially RMSWs as the main structural components of reinforced masonry buildings, to decrease their blast vulnerability (Browning et al. 2014; Campidelli et al. 2016; Hoemann et al. 2015; Mayrhofer 2002; Oesterle et al. 2009; Smith et al. 2016). Past studies have focused on investigating and/or enhancing the blast performance of non-loadbearing walls (i.e. no axial loads) with well-defined boundary conditions, however, this does not represent the typical RMSWs used in the current construction systems. This limited research is attributed to the unaffordable nature of the blast field testing for RMSWs (considering the effect of axial load and realistic boundary conditions) (El-Dakhakhni et al. 2010). As such, non-linear dynamic analysis is typically used to assess the blast performance of different structural elements (El-Dakhakhni et al. 2009, 2010). Moreover, blast loading is characterized by high epistemic and aleatory uncertainties, even for a given design basis threat (Stewart 2008; Stewart et al. 2006). The blast epistemic uncertainties include parameter uncertainty (detonation charge, stand-off distance, etc.) and model uncertainty (accuracy of predictive models), while aleatory uncertainties include the inherent variability (weather, blast environment, etc.) (Stewart et al. 2006). These sources of uncertainty may propagate into significant variability of the structural response (Campidelli et al. 2015). As such, a reliable analytical model is required to assess the probabilistic blast performance of load-bearing RMSWs while considering realistic boundary conditions.

The current North American blast-resistant design standards, namely, the ASCE 59-11 (ASCE 2011) and CSA S-850 (CSA 2012), classify the entire structure's level of protection (LoP) based on the its components lowest performance. This assumption may lead to an overestimating analysis due to the large variation of blast overpressure on a target structure during most of the observed improvised explosive devices attacks (Salem et al. 2017). In addition, the LoPs prescribed in both design standards are neither related to the structure's post-hazard functionality nor to its downtime, which are key parameters for risk-informed decision–making. As such, a comprehensive probabilistic framework is required to account to account for the post-hazard structure functionality and the subsequent downtime.

The concept of resilience has been applied within multiple disciplines to assess systems post-disaster, resilience parameters, functionality and its recovery effectiveness (Rose and Krausmann 2013). In civil engineering, the concept of resilience has been applied within the context of assessing the post-hazards performance of multiple infrastructure components (acute care facilities, transportation, gas, and water networks) (Bruneau and Reinhorn 2007; Cimellaro et al. 2010, 2015, 2016; Mackie and Stojadinović 2006). More specifically, the concept of resilience has been considered for earthquake buildings assessment through introducing sensible post-hazard functionality targets, namely, re-occupancy, pre-disaster functionality, and full recovery (Almufti and Willford 2014). As such, the application of resilience-based blast design holds significant promise to overcome the current blast standards (ASCE 2011; CSA 2012) limitations.

In this respect, this study first reports the results of an experimental investigation of seven scaled RMSWs, with different in-plane ductility seismic classifications and axial (load) stress levels, subjected to out-of-plane loading. Following the experimental investigation, an assessment of the out-of-plane resistance function, developed by the *Unified Facilities Criteria 3-340* (USDOD 2014), is presented. In addition, a comprehensive analytical model is proposed to predict the out-

of-plane resistance function of RMSWs. Subsequently, a numerical model is developed to probabilistically assess the wavefront uncertainty/variability influence of RMSWs blast response. Next, a deterministic resilience-based blast design framework is presented to quantify the post-blast functionality and the subsequent recovery history. Finally, the probabilistic blast response of the RMSW is introduced into the proposed resilience framework to utilize the probabilistic estimation of the post-blast resilience parameters.

1.2 RESEARCH OBJECTIVES

The main objective of this dissertation is to introduce a novel approach for probabilistic resilience-based blast design for RMSW buildings. As such, the following objectives were identified:

1. Experimentally investigate the behaviour of load-bearing RMSWs, with different in-plane seismic classifications and axial stress levels, subjected to uniformly distributed quasi-static out-of-plane loading.
2. Assess the influence of the axial load and vertical reinforcement ratio on the out-of-plane behaviour of RMSWs.
3. Develop a reliable analytical resistance function to simulate the out-of-plane behavior of non-load bearing/load-bearing RMSWs.
4. Introduce a simplified numerical model to probabilistically assess the blast performance of RMSWs and to evaluate the influence of axial load and vertical reinforcement ratio on the dynamic behavior of RMSWs.
5. Propose a deterministic resilience-based blast design framework to evaluate building functionality and downtime.
6. Expand the above deterministic framework into a probabilistic framework by propagating blast demand and capacity uncertainties into the resilience aspects, functionality and repair time.

1.3 ORGANIZATION OF THE DISSERTATION

This section summarizes the content of each of the six chapters in the dissertation as follows:

- Chapter 1: introduces the background and motivation of the research as well as the dissertation objectives and an overview of its arrangement.
- Chapter 2: presents an experimental and analytical investigation for the out-of-plane behaviour of seven scaled RMSWs, with different in-plane seismic classifications and axial stress levels, subjected to uniformly distributed out-of-plane loads. This chapter first presents a comprehensive description of the experimental work, including the test matrix, material properties, test setup, loading protocol, and instrumentation. Test results reported include wall damage sequence, load-displacement hysteretic response, stiffness degradation and energy dissipation. The experimental results are used to quantify the influence of reinforcement ratios and axial load levels on the out-of-plane behavior of RMSWs. Finally, an analytical resistance function is developed and experimentally validated to simulate the out-of-plane load-displacement relationships of RMSWs. This chapter provides an out-of-plane resistance function that is used in predicting the blast performance of RMSWs.
- Chapter 3: contains a numerical investigation of RMSWs blast performance by adapting the Open System for Earthquake Engineering Simulation (OpenSees) software to blast analysis. The model utilizes the concentrated plasticity modeling approach to track material strain rate effects and implement their corresponding dynamic increase factors (DIF) within the wall response predictions. The model is statically validated against an experimental database, including the reported results of Chapter 2. In addition, the model is also validated against free-field explosion results and compared to a single degree of freedom analytical model, which is widely accepted in current blast standards. Furthermore, an iterative modeling framework, Blast OpenSees Simulation (BOSS) framework, is proposed to assess the variability/uncertainty

associated with the blast wavefront parameters on the response of fully grouted RMSWs, which is presented through a 3D fragility surface. Finally, the BOSS is applied to interrogate the probabilistic influence of the axial load at different vertical reinforcement ratios on the response of RMSWs.

- Chapter 4: presents the first attempt to apply the concept of resilience within blast design through quantification of the post-blast building functionality and the expected recovery time. Resilience-based blast design is achieved via a simplified framework, wherein two new metrics, namely the functionality loss index, and the resilience indicator are introduced. The framework adopts a deterministic approach, following that adopted within the current North American blast design standards, which would subsequently facilitate the direct adoption of the proposed resilience metrics within the standards. In addition, a case study example of an administrative RMSW building, subjected to hypothetical blast scenarios, is presented to demonstrate the utility of the proposed framework. The presented example shows the meaningful information provided by this framework, which can provide stakeholders with a wealth of information unparalleled by current practices. This information is useful in identifying the most cost-effective measure(s) for blast risk mitigation.
- Chapter 5: comprises the development of the deterministic framework discussed in Chapter 4 into a probabilistic resilience-based blast design framework considering different sources of blast uncertainties. This chapter's objective is to probabilistically integrate the building system loss and subsequent downtime into unified resilience indicators, to provide decision-makers with a comprehensive risk perspective. In this context, the proposed framework, based on a conditional probability, is applied using the probabilistic infrastructure resilience assessment toolbox (PIRAT) to facilitate the assessment repeatability. The probabilistic resilience aspects, functionality and repair time, are quantified and presented in graphical form, extending the 2D

resilience triangle into a 3D resilience surface. Where the PIRAT utilizes the conditional probability using previously developed fragility curves similar to that developed in Chapter 3 to derive the probabilistic resilience parameters. Finally, an illustrative example is applied to illustrate the applicability of the proposed probabilistic framework. The example demonstrates the influence of the blast probabilistic nature on the resilience parameters, which is considered a key point for stakeholders and risk analysts.

1.4 REFERENCES

Almufti, I., and Willford, M. (2014). "The REDi^{TM} rating system: A framework to implement resilience-based earthquake design for new buildings." *10th U.S. National Conference on Earthquake Engineering, Frontiers of Earthquake Engineering, July 21-25*.

ASCE. (2011). *Blast Protection of Buildings*. *ASCE 59-11*, (American Society of Civil Engineers, ed.), American Society of Civil Engineers, Reston, VA, VA.

ASCE 41-17. (2017). *Seismic Evaluation and Retrofit of Existing Buildings*. American Society of Civil Engineers, Reston, VA.

Browning, R. S., Dinan, R. J., and Davidson, J. S. (2014). "Blast Resistance of Fully Grouted Reinforced Concrete Masonry Veneer Walls." *Journal of Performance of Constructed Facilities*, 28(2), 228–241.

Bruneau, M., Barbato, M., Padgett, J. E., Zaghi, A. E., Mitrani-Reiser, J., and Li, Y. (2017). "State of the Art of Multihazard Design." *Journal of Structural Engineering*, 143(10), 03117002.

Bruneau, M., and Reinhorn, A. (2007). "Exploring the Concept of Seismic Resilience for Acute Care Facilities." *Earthquake Spectra*, 23(1), 41–62.

Bui, T. T., and Limam, A. (2014). "Out-of-plane behaviour of hollow concrete block masonry walls unstrengthened and strengthened with CFRP composite." *Composites Part B: Engineering*, 67, 527–542.

Campidelli, M., El-Dakhakhni, W., Tait, M., and Mekky, W. (2016). "Probabilistic risk assessment of masonry buildings exposed to improvised explosive devices." *Brick and Block Masonry*, CRC Press, 959–966.

Campidelli, M., El-Dakhakhni, W. W., Tait, M. J., and Mekky, W. (2015). "Blast Design-Basis Threat Uncertainty and Its Effects on Probabilistic Risk Assessment." *ASCE-ASME Journal of Risk and Uncertainty in Engineering Systems, Part A: Civil Engineering*, 1(4), 04015012.

Cimellaro, G. P., Reinhorn, A. M., and Bruneau, M. (2010). "Framework for analytical quantification of disaster resilience." *Engineering Structures*, 32(11), 3639–3649.

Cimellaro, G. P., Tinebra, A., Renschler, C., and Fragiadakis, M. (2016). "New Resilience Index for Urban Water Distribution Networks." *Journal of Structural Engineering*, American Society of Civil Engineers, 142(8), C4015014.

Cimellaro, G. P., Villa, O., and Bruneau, M. (2015). "Resilience-Based Design of Natural Gas Distribution Networks." *Journal of Infrastructure Systems*, 21(1), 05014005.

CSA. (2012). *CSA S850-12 Design and assessment of buildings subjected to blast loads*. Canadian Standards Association, Mississauga, ON, Canada.

CSA. (2014). *CSA S304-14 Design of Masonry Structures*. Canadian Standards Association, Mississauga, ON, Canada.

Cutter, S. L., Ash, K. D., and Emrich, C. T. (2014). "The geographies of community disaster resilience." *Global Environmental Change*, Elsevier Ltd, 29, 65–77.

El-Dakhakhni, W., and Ashour, A. (2017). "Seismic Response of Reinforced-Concrete Masonry Shear-Wall Components and Systems: State of the Art." *Journal of Structural Engineering*, 143(9), 03117001.

El-Dakhakhni, W. W., Changiz Rezaei, S. H., Mekky, W. F., and Razaqpur, A. G. (2009). "Response sensitivity of blast-loaded reinforced concrete structures to the number of degrees of freedomThis article is one of a selection of papers published in the Special Issue on Blast

Engineering." *Canadian Journal of Civil Engineering*, 36(8), 1305–1320.

El-Dakhakhni, W. W., Mekky, W. F., and Rezaei, S. H. C. (2010). "Validity of SDOF Models for Analyzing Two-Way Reinforced Concrete Panels under Blast Loading." *Journal of Performance of Constructed Facilities*, 24(4), 311–325.

ElSayed, M., El-Dakhakhni, W., and Tait, M. (2015). "Response Evaluation of Reinforced Concrete Block Structural Walls Subjected to Blast Loading." *Journal of Structural Engineering*, 141(11), 04015043.

Hoemann, J. M., Shull, J. S., Salim, H. H., Bewick, B. T., and Davidson, J. S. (2015). "Performance of Partially Grouted, Minimally Reinforced CMU Cavity Walls against Blast Demands. II: Performance under Impulse Loads." *Journal of Performance of Constructed Facilities*, 29(4), 04014114.

Institute for Economics and Peace. (2015). *Global Terrorism Index 2015: Measuring and Understanding the Impact of Terrorism*.

Li, Y., Ahuja, A., and Padgett, J. E. (2012). "Review of Methods to Assess, Design for, and Mitigate Multiple Hazards." *Journal of Performance of Constructed Facilities*, 26(1), 104–117.

Lindell, M. K., and Prater, C. S. (2003). "Assessing Community Impacts of Natural Disasters." *Natural Hazards Review*, 4(4), 176–185.

Mackie, K. R., and Stojadinović, B. (2006). "Post-earthquake functionality of highway overpass bridges." *Earthquake Engineering & Structural Dynamics*, 35(1), 77–93.

Marjanishvili, S. M. (2004). "Progressive Analysis Procedure for Progressive Collapse." *Journal of Performance of Constructed Facilities*, 18(2), 79–85.

Mayrhofer, C. (2002). “Reinforced masonry walls under blast loading.” *International Journal of Mechanical Sciences*, 44(6), 1067–1080.

NRC, (National Reasearch Council of Canada). (2015). *National Building Code of Canda (NBCC-15)*. Institute for Re- search in Construction, Ottawa.

Oesterle, M. G., Hegemier, G. A., and Morrill, K. B. (2009). “Response of Concrete Masonry Walls to Simulated Blast Loads.” *Structures Congress 2009*, American Society of Civil Engineers, Reston, VA, 1–10.

Priestley, M. J. N. M. N., Calvi, G. M., Kowalsky, M. J., and Park, T. (2007). *Displacement-based seismic design of structures*. IUSS Press, Pavia, Italy.

Rose, A., and Krausmann, E. (2013). “An economic framework for the development of a resilience index for business recovery.” *International Journal of Disaster Risk Reduction*, 5, 73–83.

Salem, S., Campidelli, M., El-Dakhakhni, W., and Tait, M. (2017). “Blast Resilient Design of Infrastructure Subjected to Ground Threats.” *Volume 4: Fluid-Structure Interaction*, ASME, Hawaii, USA, V004T04A018.

Salman, A. M., and Li, Y. (2017). “Multihazard Risk Assessment of Electric Power Systems.” *Journal of Structural Engineering*, 143(3), 04016198.

Shedid, M. T., Drysdale, R. G., and El-Dakhakhni, W. W. (2008). “Behavior of Fully Grouted Reinforced Concrete Masonry Shear Walls Failing in Flexure: Experimental Results.” *Journal of Structural Engineering*, American Society of Civil Engineers, 134(11), 1754–1767.

Siyam, M. A., El-Dakhakhni, W. W., Banting, B. R., and Drysdale, R. G. (2016a). “Seismic

Response Evaluation of Ductile Reinforced Concrete Block Structural Walls. II: Displacement and Performance–Based Design Parameters." *Journal of Performance of Constructed Facilities*, 30(4), 04015067.

Siyam, M. A., El-Dakhakhni, W. W., Shedid, M. T., and Drysdale, R. G. (2016b). "Seismic Response Evaluation of Ductile Reinforced Concrete Block Structural Walls. I: Experimental Results and Force-Based Design Parameters." *Journal of Performance of Constructed Facilities*, 30(4), 04015066.

Smith, N. L., Tait, M. J., El-Dakhakhni, W. W., and Mekky, W. F. (2016). "Response Analysis of Reinforced Concrete Block Infill Panels under Blast." *Journal of Performance of Constructed Facilities*, 30(6), 04016059.

Stewart, M. G. (2008). "Cost Effectiveness of Risk Mitigation Strategies for Protection of Buildings against Terrorist Attack." *Journal of Performance of Constructed Facilities*, 22(April), 115–120.

Stewart, M. G., Netherton, M. D., and Rosowsky, D. V. (2006). "Terrorism Risks and Blast Damage to Built Infrastructure." *Natural Hazards Review*, American Society of Civil Engineers, 7(3), 114–122.

The Masonry Society (TMS). (2016). *Building Code Requirements for Masonry Structures*. TMS 402-16/ACI 530-16/ASCE 5-16, Detroit, MI.

USDOD, (U.S. Department of Defense). (2014). *Structures to resist the effects of accidental explosions*. *Unified Facilities Criteria 4-340-02*, Washington D.C., USA.

Chapter 2

OUT-OF-PLANE BEHAVIOR OF LOAD-BEARING REINFORCED MASONRY SHEAR WALLS

2.1 ABSTRACT:

The increase in deliberate and accidental explosion events over the past two decades have necessitated evaluating the performance of blast-vulnerable structural components and develop subsequent risk mitigation strategies. In this context, several studies have focused on the out-of-plane behavior of either unreinforced masonry walls or non-load bearing reinforced masonry shear walls (RMSWs). However, to date, a limited number of studies are available on the interaction between the axial load and out-of-plane demands (e.g. when subjected to blast loads) on such walls. As such, the current study focuses on evaluating the out-of-plane behavior of seismically detailed RMSWs with different designs. Experimental results of seven scaled RMSW, with different in-plane ductility seismic classifications and axial stress levels, subjected to out-of-plane loading are presented. These results include the wall damage sequence, load-displacement response, stiffness degradation and energy dissipation. Subsequently, the resistance function prediction of the *Unified Facilities Criteria 3-340* is compared to the experimental results. Furthermore, an analytical resistance function is developed and experimentally validated to consider the post-peak behaviour of the RMSWs, including second-order effects. The study results demonstrate the influence of axial load and vertical reinforcement ratio on the wall displacement and force resistance capacities and the overall wall resistance function.

2.2 INTRODUCTION

The demand for blast-resistant structures has increased over the past few years due to increasing threats of terrorist attacks (Parisi and Augenti 2012), with a spike that followed the 9/11 attacks (Marjanishvili 2004). Subsequently, numerous blast risk mitigation strategies are proposed to protect structures through decreasing the structure's vulnerability (blast-resistant hardening schemes) and/or reducing the hazard intensity (augmenting the standoff distance or increasing the building envelope security) (FEMA-426 2011). However, the current strategies are often hampered by the lack of some structural component response understanding and may thus impose significant economic constraints, which can increase the facility construction cost by as much as 30% (Campidelli et al. 2015; Mueller et al. 2011). As such, experimental and analytical evaluations are still needed for several structural components that might be exposed to blast.

Reinforced masonry shear walls (RMSWs) are an attractive building system because of their relative ease of construction and their in-plane ductile behavior when the walls are properly detailed according to the relevant design standards (Priestley et al. 2007). This enhanced in-plane behavior of RMSWs has been recently reflected in the North American building codes (e.g. NBCC 2015, ASCE 2017) and design standards (CSA 2014a; The Masonry Society (TMS) 2016) through their corresponding design requirements. This is mainly based on several recent experimental and analytical studies that have demonstrated the ductile in-plane performance of properly detailed and constructed RMSWs compared to their unreinforced masonry or poorly constructed RMSWs (Shedid et al. 2008). Conversely, RMSWs showed limited ductility coupled with high vulnerability when loaded in the out-of-plane direction due to the mid-cell reinforcement configuration (ElSayed et al. 2015). This out-of-plane loading can occur during multiple extreme events such as hurricanes, blast, impact, etc. (Bui and Limam 2014). Therefore, this contrast between the wall's in-plane and

out-of-plane behavior may depict a trade-off in the application of RMSWs system within the context of multi-hazard mitigation.

Despite the high vulnerability (due to the reduced stiffness, strength, and ductility) of RMSWs under out-of-plane loading, limited research studies have been conducted to investigate and/or enhance the performance of these walls. To date, available research has been limited only to non-load bearing walls (i.e. no axial loads) with well-defined boundary conditions. For example, Bechara et al. (1996) tested six RMSWs under static out-of-plane four-point bending, however, ideal rollers were used and no axial loads were applied on these walls. The out-of-plane behavior of three flanged non-load-bearing RMSWs (i.e. supported on return walls at their ends) with openings were also investigated by Zhang et al. (2001); however, the configuration of such walls forced an atypical three-sided behavior. In addition, Browning et al. (2011) reported the results of three non-load-bearing RMSWs, two of which were attached to external veneer walls, tested under uniform pressure from a vacuum chamber; however, these walls were attached to steel frames, which may not be a reasonable representation of current construction practice. Recently, Elsayed et al. (2016) tested three one-third scale non-load-bearing RMSWs under quasi-static loading, however, these walls were welded to a steel frame, which did not fully represent actual boundary conditions, where the reinforcement would continue through the concrete floor slab, for example. The aforementioned limitations of boundary conditions have significant influences on altering the performance of RMSWs (Bui and Limam 2014; Shedid et al. 2008). Finally, although Porto et al. (2010) tested two systems of load-bearing perforated clay walls, these do not adequately represent the concrete masonry units used in North American construction practices.

Published literature shows that only a limited number of studies has been conducted to simulate the out-of-plane behavior of RMSWs. In addition, these studies have mainly focused on predicting the ultimate capacity of the wall without consideration of its post-peak behavior,

including the second order effects due to axial loads that may exist (e.g. Browning et al. 2011; Browning and Davidson 2011; USACE 2008; USDOD 2014). Browning et al. (2011) and Browning and Davidson (2011) integrated a simple piecewise linear moment-curvature function which efficiently predicted the wall's small deformations, but not its post-peak deformations since plasticity concentration was not considered. The USACE (2008) and USDOD (2014) also adopt a linear-elastic-perfectly-plastic resistance function that does not model failure. As such, a nonlinear resistance function is still needed to overcome the limitations of current models.

The current study experimentally and analytically investigates the out-of-plane behavior of seven scaled RMSWs, with different in-plane seismic classifications and axial stress levels, subjected to uniformly distributed out-of-plane loads. This investigation aims at providing out-of-plane resistance functions that can be used in further studies pertaining to the performance of load-bearing RMSWs subjected to blast loading scenarios. In this respect, the study first presents a comprehensive description of the experimental work including the test matrix, material properties, test setup, loading protocol, and instrumentation. Following the experimental work description, the test results are reported including the wall damage sequence, load-displacement hysteretic response, stiffness degradation and energy dissipation. The experimental results are used to quantify the influence of reinforcement ratios and axial load levels on the out-of-plane behavior of RMSWs. Finally, an analytical resistance function is developed and experimentally validated to simulate the out-of-plane load-displacement relationships (including the elastic, elastic-plastic, and plastic stages) of RMSWs. This function integrates the linear-elastic-perfectly-plastic with the concentrated plasticity concept to estimate the plastic deformations and to consider the subsequent moment redistribution.

2.3 EXPERIMENTAL PROGRAM

The experimental program in the current study includes seven half-scale fully-grouted (i.e. five load-bearing and two non-load bearing) RMSWs with different in-plane seismic design classifications. The five load-bearing walls were designed to maintain their axial load levels throughout the test while loaded in the out-of-plane direction using uniformly distributed loads across the wall's surface area. This section provides details on the wall selection, material properties, test setup, instrumentation and loading protocol.

2.3.1 Test Matrix

The experimental program focused on testing seven half-scale walls with 1,420 mm length, 90 mm thickness, 2,000 mm height and 1500 mm loading span. The difference (i.e. 500 mm) between the loading span and the total height, is to realistically simulate the reinforcement development length within the upper building floors. The walls were originally designed to represent the current in-plane seismic classifications (i.e. ordinary, intermediate and special) of RMSWs (TMS 2016). The main variables within the seven tested RMSWs, are the reinforcement ratio and the axial load level. The vertical reinforcement ratios (ρ_v) vary through 0.33%, 0.61% and 0.83% of the vertical gross area, while the horizontal reinforcement ratio(ρ_h) is 0.14% for all the walls except for the wall with the highest vertical reinforcement ratio (ρ_h = 0.28%). This increase in the horizontal reinforcement ratio is to resist the expected increase in the in-plane shear force. The axial stress levels vary from 0% to 15% of the axial compressive strength. The walls are identified in this study using a letter (i.e. L, M, H) to represent the vertical reinforcement ratio (i.e. low, moderate, and high) and a number so as to refer to the axial stress ratio (i.e. 0, 5,10,15%). For example, Wall M-05 is a moderately reinforced wall (ρ_v = 0.61%) with an axial stress ratio of 5%. Figure 2.1(a) shows the cross sections and reinforcement details of the tested walls, while Table 2.1 summarizes their

vertical and horizontal reinforcement ratios as well as their in-plane ductility classifications according to the TMS (2016).

2.3.2 Wall Details and Construction

The walls were constructed using half-scale concrete masonry units (CMU) units in a running bond pattern and face shell mortar bedding by certified masons, following the North American construction practices. The (90x90x185 mm) half-scale CMU units were resembling the standard two-cell 190mm full-scale CMU (Long et al. 2005). The scaled CMU were saw cut to 25 mm deep through their webs to allow the placement of the horizontal reinforcement. Each wall was constructed on a 1500 mm x700 mm isolated reinforced concrete foundation with a thickness of 400 mm. The vertical reinforcements were extended to the full height of their corresponding walls with no splices. The vertical reinforcements were also bent 90-degrees and tied to the lower mesh of the foundation with an extended leg of 150 mm, to ensure a full development length. The walls were constructed and grouted on two stages to facilitate the low-lift grouting technique (TMS 2016). The horizontal reinforcements were placed on top of the CMU notches with a 180-degree standard hook around the vertical edge rebars, as shown in Figure 2.1(a). In order to simulate a typical continuous wall loaded in the first story, the wall was horizontally supported at 1,500 mm from its base, resembling a scaled version of a first story wall with 3,000 mm height. With regard to the intermediate horizontal support, the walls were drilled and threaded bars were fitted/fixed using a non-shrinkable epoxy at the location of the support following the standard grouting and anchorage procedure of the American Concrete Institute (ACI committee 318, 2014). Figure 2.1(b) shows the typical three-dimensional view of the tested walls illustrating the tested area and the location of the top support.

2.3.3 Material Properties

The isolated foundation used for each wall had an average compressive strength of 71.0 MPa (coefficient of variation, c.o.v. = 6.3%) (ASTM 2018) within the walls testing period. Forty-three blocks for stretchers and seven blocks for half units were randomly selected and tested according to ASTM C140-16 (ASTM 2016a) and CSA A165 (CSA 2014b). The average compressive strengths (based on the net area) were 14.5 MPa (c.o.v. = 14.1%) and 16.4 MPa (c.o.v. = 6.7%) for the stretchers and half units, respectively. The construction of the walls was conducted with a running bond scheme using approximately 5-mm-thick mortar joint representing the scaled version of the common 10 mm joint in full-scale masonry construction. Pre-blended and pre-packaged Type S mortar was used in the wall construction with an average flow of 126%. The average compressive strength of the mortar, based on thirty standard mortar cubes taken from each batch during the construction, was 19.2 MPa (c.o.v. = 21.2 %), tested according to ASTM C780-16 and CSA A179-14 (ASTM 2016b; CSA 2015). The walls were grouted with fine grout, according to ASTM C476-16 (ASTM 2016c), having weight mixing portions of 1: 0.04: 3.9: 0.85 (Portland cement: lime: dry sand: water) and average slump of 230mm. Twenty-three grout cylinders were tested according to ASTM 1019-16 and CSA A179-14 (ASTM 2016d; CSA 2015) resulting in an average strength of 21.3 MPa (c.o.v. = 15.1%). Sixty-nine fully-grouted running bond masonry prisms were tested according to the ASTM C1314-16 (ASTM 2016e) −one block long by four block height− to evaluate the grouted masonry compressive strength normal to the bed joint. The average compressive strength was 11.8 MPa (c.o.v. = 13.4%); which resulted in 13.5 MPa standard average compressive strength −by multiplying the suggested correction factor of 1.15 – to account for the tested height-to-thickness ratio (ASTM 2016e).

Tensile tests were conducted for the used rebars – #3 and # 4 (used as the vertical reinforcement), D4 (used as horizontal reinforcement), and M10 (used in the foundation)−

according to CSA G30.18-09 (CSA 2014c) in order to determine their yield and ultimate strengths. The average yield strength of the M10 rebars (100 mm^2) was 436 MPa (c.o.v. = 1.32%), while the average yield strengths of the #3 (71 mm^2), #4 (129 mm^2), and the D4 (45 mm^2) rebars were 459, 436 and 517 MPa (c.o.v. = 4.60%, 0.92% and 6.90%), respectively. It should also be mentioned that the D4 reinforcement was heat treated to enhance its ductility based on the available literature (Heerema et al. 2015).

2.3.4 Test setup, Instrumentation and Loading Protocol

The test setup was designed to simulate the application of uniformly distributed out-of-plane loads on the load-bearing walls simultaneously with a uniform (and constant) axial load (P_A). The out-of-plane distributed loads were applied through a displacement-controlled (main) actuator with 500 kN capacity and 500 mm stroke. This actuator was exerted to the walls through nine-point/patch loads (300 mm x 300 mm) using nine (secondary) actuators, as shown in Figure 2.2(a). These actuators were connected in a closed loop hydraulic system to equate the applied forces and allow for different displacements without restrictions on the RMSWs deformations. The position of the swivel end of the main actuator was fixed in order to maintain the location of the resultant force at the center of mass of the wall loaded area, while the nine secondary actuators were pinned to a rigid steel frame supported on the main actuator. The nine actuators were capped with steel ball bearing ends to allow for the rotation of the loading pads on the tested walls. The loading pads consist of 200 mm x 200 mm rigid steel plates of 250 mm thickness and buttressed with 300 mm x 300 mm rubber pads of 40 mm thickness, in order not to restrain the wall deformations.

The load-bearing walls were vertically (i.e. axially) loaded by a separate loading mechanism, through fitted threaded bars, using two hydraulic actuators. These two actuators were attached to the top (horizontal) support; which only restrained the horizontal deformation and vertically slid on the testing frame. High-performance polymers were used to reduce the friction

between the testing frame and the top horizontal support. On the other side, the concrete foundations were attached to the testing frame using eight prestressed rods forming the bottom support. Figures 2.2 (a and b) depict the horizontal and vertical loading systems, and the walls' fixation mechanism.

The horizontal and vertical deformations of the tested walls were monitored using displacement potentiometers. More specifically, the horizontal deformations were monitored through seven potentiometers (A, B, C1, D, E, F and G) to capture the out-of-plane deflection profile, and one redundant potentiometer (C_2) at the control station so as to be used in case of the malfunction of the main potentiometer (C_1), as shown in Figure 2.3. One additional potentiometer (C') was also attached at the mid-height of the wall towards one of the edges, as shown in Figure 2.3, in order to evaluate the load-path distribution of the tested walls. In addition, fourteen displacement potentiometers (P_1 to P_{14}) were also attached vertically at every other course (h_{gauge}) on the front (North) and rear (South) surfaces of the tested walls a to monitor the wall's surface deformation along the wall height. Moreover, four potentiometers were used to record any displacements within the foundation (BR and BL) and the top support (TR and TL), as shown in Figure 2.3. Three strain gauges (S_1, S_2, and S_3) were also attached to the vertical reinforcement bars at the foundation, mid-height, and at the top support levels, respectively, as shown in Figure 2.3. Finally, while the uniformity of the acting out-of-plane forces, transferred from the main actuators to the nine actuators, was verified through three diagonally load cells so as to monitor any loading misalignment, the wall axial load was monitored using two load cells attached to the two vertical actuators, as shown in Figure 2.2(a).

The unidirectional cyclic loading protocol was designed to both capture the force-displacement capacity boundary and monitor the cracking propagation through different loading stages. As such, the walls were loaded to reach targeted chord rotations (θ) (displacements), then were unloaded until they reached zero loads. The chord rotations (i.e. defined as the ratio between

the mid-height displacement and half the wall height) have been utilized in the current study to align with the context of the current blast design standards (ASCE 2011; CSA 2012; USACE 2008; USDOD 2014) as shown in Figure 2.4. The absence of the strain hardening cycles (i.e. more than one cycle at the same chord rotation level) in the utilized loading protocol would yield the monotonic response of the tested walls (Applied Technology Council 2009). The loading cycles were based on fractions (i.e. one eighth) of the out-of-plane chord rotation, as shown in Figure 2.4, to assess the walls' performance at different chord rotation demands. The test was performed until a strength degradation of 70% of the ultimate strength was reached, to capture a wide range of the RMSW behavior.

2.4 EXPERIMENTAL RESULTS AND OBSERVATIONS

2.4.1 Load-displacement Behavior

Figure 2.5 shows the out-of-plane hysteretic load-displacement relationships for all the tested walls. In this figure, the total load, P, represents the resultant of the distributed loads acting on the wall loaded area (i.e. distributed through the nine secondary actuators), while the displacement, Δ, is measured at the mid-height of the wall (i.e. 750 mm from the foundation). Figure 2.5 is divided into three sub-sets/categories based on the wall's vertical reinforcement ratio, where each category illustrates the influence of the axial load on the out-of-plane behavior of the same wall. As can be seen in Figure 2.5, the wall ultimate load is highly dependent on the vertical reinforcement ratio as can be inferred by comparing the three sub-figure categories. For example, the ultimate load of Walls M-10 and H-10 is approximately 50% and 75%, respectively, higher than that of Wall L-10. The axial load has also an influence on the wall out-of-plane ultimate load, where the ultimate load of Wall M15, for example, is 19% higher than that of Wall M-00.

Figure 2.6 shows the resistance functions of the tested walls by illustrating their peak loads at each cycle with respect to the corresponding mid-height displacements and chord rotations. As can be observed from Figure 2.6, all the tested walls did not show similar initial stiffness values due to their different axial stress levels. For example, the initial stiffness values of the two non-load-bearing Walls L-00 and M-00 are on average 52% lower than those of the load-bearing Walls L-10 and M-10 with 10 % axial stress levels of their axial compressive strengths. This is mainly attributed to the direct relation between the wall effective moment of inertia and the applied axial stress level (Paulay and Priestley, 1992). Moreover, the effect of the axial stress level on the wall post-peak behavior is distinct, as shown in Figure 2.6, through the steep post-peak behavior of Wall M-15, for example, relative to Wall M-00, which is attributed to the second order effect, as will be discussed later.

The out-of-plane displacements of all the walls at different stations along their heights are linearly interpolated and shown in Figure 2.7 at different chord rotation levels. Figure 2.7 demonstrates that all the walls showed similar displacement profile regardless of their reinforcement ratios or axial load levels. For example, at $\theta = 1.0°$ and $3.0°$, the displacement values for all walls at 468mm above the foundation are 10 and 28.7 mm on average with standard deviation values of 3.3 and 2.4 mm., respectively. It worth mentioning that the linear interpolation between the measured displacement below and above the support yield to a negligible displacement at the support height as can be seen in Figure 2.7.

2.4.2 Damage Sequence and Failure Modes

This subsection presents the damage sequence and the failure modes of the tested walls. All the walls showed similar crack patterns especially at their early loading stages, characterized by horizontal cracks at the first bed joint above the foundation at the front wall face followed by similar cracks at the mid-height of the rear wall face. This crack pattern is mainly attributed to the fixed

support condition at the foundation level that localized more flexural stresses relative to those at the wall mid-height. This pattern is verified through the consistent strain propagation of the vertical bars, where the bar strain at the foundation level was not only always higher than that at the mid-height, but also exceeded the yield strain at an earlier stage of loading. At higher displacement levels, for all walls, the crushing started at the foundation level (rear face) before the wall reached its ultimate load. Subsequently, the wall experienced additional crushing at the mid-height of the front face, which was accompanied by a decrease in the wall load carrying capacity. This observation exemplifies the in-wall moment redistribution after the formation of a *perfect* plastic hinge (i.e. capable of transmitting limited or unlimited plastic deformation without transmitting an increase in the bending moment) at the foundation level according to Tichy and Rakosnik (1977). However, Wall H-10 did not reach its ultimate flexural capacity (typically identified through bottom rear or mid-height front face crushing) and had a distinctly different failure mode. This is concluded as the wall's vertical reinforcement of this wall did not reach the yielding strain throughout the test (brittle failure), and a shear failure was observed. More specifically, a front wall face crack (at the foundation level) propagated diagonally to the rear face (at the second-course level) leading to detaching/sliding of the wall. Figures 2.8 (a and b) show the rear face crack pattern of the walls at both the onset of vertical bar yielding and the ultimate load cycles, respectively. It is worth noting that the crack pattern of Wall H-10 is not shown in Figure 2.8(a) because the vertical bars of this wall did not reach the yield strain, as mentioned earlier.

2.5 ANALYSIS OF THE EXPERIMENTAL RESULTS

2.5.1 Displacement Ductility

Displacement ductility (μ_{Δ}) is generally defined as the ratio between the displacement at the ultimate load (Δ_u) to that associated with the displacement at the yield load (Δ_y). Displacement ductility has been indicated as an influential parameter in the blast performance (Krauthammer et al. 2008;

Thiagarajan et al. 2013). However, there is no consensus on the definition of the ductility parameters (Δ_y and Δ_u). Available literature focused on defining the ductility parameters based on either theoretical or experimental values; however, the integration of both values is not recommended as this may lead to inaccurate ductility prediction (Shedid et al. 2008). In this respect, the displacement ductility evaluation as used in the current study is based on the experimental results reported by Seif ElDin and Galal (2017).

In this study, two approaches were used to calculate the wall displacement ductility $\mu_{\Delta u}$. The first approach used the experimental displacement at the peak load (Δ_u), while ignoring any post-peak behavior ($\mu_{\Delta u} = \Delta_u / \Delta_y$). The second approach used the benefit of a reasonable amount of the strength degradation capacity, corresponding to displacements at degradation from 80% to 50% of the ultimate load (Ezzeldin et al. 2017; Haach et al. 2010; Siyam et al. 2016; Vasconcelos and Lourenço 2009). In this study, the second approach was based on the displacement corresponding to 70% degradation ($\Delta_{0.7u}$). This displacement was selected to fully account for the second-order effect due to the applied vertical load, without reaching the instability stage ($\mu_{\Delta 0.7u} = \Delta_{0.7u} / \Delta_y$). It should be noted that Δ_y was defined as the displacement at the onset of yielding for both approaches and subsequently, the displacement ductility of Wall H-10 was not considered. The results of the two approaches, summarized in Figures 2.9 (a and b), demonstrate the influence of the design parameters on the displacement ductility. As can be seen from both figures, the increase of the axial load reduces the out-of-plane displacement ductility regardless the approach that was used. For example, the displacement ductility values of Walls L-10 and M-15 were 28% and 65% lower than those of Walls L-00 and M-00, respectively, when the second approach was adopted as shown in Figure 2.9(b). Figures 2.9 (a and b) also illustrate the inverse relationship between the wall out-of-plane displacement ductility and its vertical reinforcement ratio. For example, the displacement ductility of Wall M-10 was 30% lower than that of Wall L-10, as shown in Figure 2.9(b). It should

be noted that Wall L-00 experienced early translation at the upper support during the test, which delayed the observed yielding relative to other walls and consequently reduced the displacement ductility, as shown in Figure 2.9.

2.5.2 Energy Dissipation

Energy dissipation (E_d) is considered to be an influential aspect of the dynamic response of structures when subjected to blast loading. E_d was determined in the current study as suggested by Hose and Seible (1999), by calculating the area enclosed by the resistance functions at different displacement levels, as shown in Figure 2.10. The figure shows that, as expected, for low displacement levels, E_d values were low with almost no sensitivity to the walls' vertical reinforcement ratio; while being highly influenced to the axial stress. However, at higher displacement levels, as can be seen in Figure 2.10, E_d is directly proportional to the wall vertical reinforcement ratio and the axial load. The figure shows that the E_d values at 5 and 35 mm mid-height displacements were 9% and 27% higher for Wall M-00, respectively, than those for Wall L-00. While E_d increased by 99% and 33% at 5 and 36 mm, respectively, when Wall M-10 is compared to Wall M-00. This is attributed to the direct dependency between these two parameters (i.e. axial load and vertical reinforcement ratio) and the wall's flexural capacity.

2.5.3 Secant Stiffness Degradation

Wall stiffness is another important parameter in the dynamic response since, in addition to influencing the wall's period and subsequently its blast response (i.e. being within the impulsive, dynamic, or quasi-static regime), is key to model the inelastic wall behavior. In this respect, Figure 2.11 presents the influence of the design parameters on the normalized secant stiffness (i.e. defined as the ratio between the wall secant stiffness (K_s) to its initial stiffness (K_i)) throughout the test. The figure shows a similar trend of stiffness degradation at low displacement levels, where the normalized secant stiffness values of all walls were reduced approximately by 30% at Δ=5mm. At

higher displacement levels, the wall's vertical reinforcement ratio and axial load influence its normalized secant stiffness values. For example, the normalized secant stiffness of wall M-00 is 16% and 20% higher than that of Walls L-00 and M-10, respectively, at Δ= 35mm, as shown in Figure 2.11.

2.5.4 Out-of-plane Curvature Profile

To assess the overall mechanism of the tested walls, the average out-of-plane curvatures (φ) were calculated at different wall's heights, at the average height of each two consecutive surface deformation potentiometers, using the front and rear displacement potentiometers (P_1 to P_{14}). The average curvature was calculated as the rotation across the wall thickness resulted from the front (Δ_f/h_{gauge}) and rear (Δ_r/h_{gauge}) strains, as presented in Eq. 1. Δ_f and Δ_r are the front and the rear wall vertical deformations, respectively, h_{gauge} is the difference between the surface potentiometers, P_1 to P_{14}, and t is the wall thickness.

$$\varphi = \frac{\frac{\Delta_f}{h_{gauge}} + \frac{\Delta_r}{h_{gauge}}}{t} \quad (1)$$

The average curvatures were calculated at the mid-point of each station, and subsequently linearly interpolated along the wall height, as shown in Figure 2.12. These curvatures are plotted at yield, ultimate, and the 70% strength degradation to illustrate the curvature profile propagation for all the walls (except Wall M-10 as errors were recorded at the front and rear wall face vertical deformations). Figure 2.12 demonstrates that all the walls showed a similar trend curvature profile, where two inflection points along the wall height were observed. It should be noted that the wall curvatures at the bottom and top supports were not linearly extrapolated, as it is expected to have curvature concentration within these supports at high displacement levels. This curvature concentration can be inferred in Figure 2.12 from the nonlinear behavior of the first and second

curvature stations (93 and 280 mm above the foundation level) at ultimate and post-peak stages. The trends of having higher curvatures, especially at early loading stages, at the lower level station above the bottom support compared to those at the wall mid-height are shown for the tested walls through Figure 2.12. For example, Figure 2.13 shows the absolute curvature propagation at these stations for wall M-05 against the normalized wall displacement (Δ/Δ_u). Higher curvatures at the lower level (φ_b), 93 mm above the foundation level, are observed than those at the mid-height (φ_m), 844 mm above the foundation level, especially prior to the wall reaching its ultimate strength. The small curvature recorded/calculated at the top level (φ_t), is attributed to the station location (i.e. 280mm below the top support) which fails to capture the curvature concentration at the support. However, the calculated curvature at the top level, (φ_t), aligns with its counterparts above (i.e. 280mm) the bottom support. It should be noted that the observed abrupt increase of the φ_m, at higher loading levels, compared to φ_b, and φ_t is attributed to the unrecorded curvature concentration within the lower/upper plastic hinges, as mentioned earlier.

2.6 BLAST RESISTANCE FUNCTION

The USACE (2008)/USDOD (2014) utilize a simplified linear-elastic-perfectly-plastic model, used as a blast resistance function, for predicting the flexural out-plane performance of RMSWs. However, this function does not consider the post-peak behavior of the wall, including the second order effect of the load-bearing walls. Therefore, the current study proposes an analytical resistance function to simulate the out-of-plane behavior of non-load bearing/load-bearing walls, considering the wall's post-peak behavior. Both the proposed- and the USACE (2008)/USDOD (2014) functions are discussed and subsequently validated against the experimental results of the tested walls in the current section.

It is important to note that most of the available analytical studies idealize the supports of their underlying structures as pinned or fixed to represent its boundary conditions (Zareian and

Kanvinde 2013), especially for the out-of-plane behavior of RMSWs (ElSayed et al. 2015, 2016; Smith et al. 2016). As such, the resistance functions discussed in the current section are based on a fixed-fixed boundary condition, which conforms with the observed curvature profiles shown earlier in Figure 2.12.

2.6.1 USACE (2008)/USDOD (2014)

The linear-elastic-perfectly-plastic resistance function proposed by the USACE (2008)/USDOD (2014) for the fixed-fixed walls is characterized by two distinctive points and a performance arbitrary point. This divides the out-of-plane response into three different stages, as shown in Figure 2.14. The three stages are the elastic, elastic-plastic, and the plastic stages. These stages are identified through elastic, Δ_e, elastic-plastic, Δ_{ep} and maximum, Δ_m, deflections as well as the elastic, P_e, and ultimate, P_u, loads. These distinctive loads, P_e and P_u, are derived through plastic analysis, while their corresponding deformations are evaluated using the relevant stiffness values, K_e and K_{ep}, as presented in Eqs. 2 to 5.

$$P_e = \frac{12 M_p \, L}{h^2} \tag{2}$$

$$K_e = \frac{384 E I_e}{L^4} \tag{3}$$

$$P_u = \frac{16 M_p \, L}{h^2} \tag{4}$$

$$K_{ep} = \frac{384 E I_e}{5 L^4} \tag{5}$$

Where P_e is the load at which the at least one of the critical sections reaches the plastic moment capacity (M_p). Subsequently, the moments at the top and bottom supports are expected to

reach M_p, simultaneously, due to the symmetric boundary conditions, as shown in Figure 2.14. However, P_u is the load at which all the critical sections reaches M_p, following the mechanism shown in Figure 2.14. L and h are the wall length and height, respectively, while E is the masonry modulus of elasticity and I_e is the effective moment of inertia, according to Eq. 6 (USDOD 2014). Where I_g and I_{cr} are the wall gross and cracked moment of inertia, respectively.

$$I_e = \frac{I_g + I_{cr}}{2} \tag{6}$$

The USACE (2008)/USDOD (2014) resistance function did not consider the ultimate deformation capacity of the wall which may result in an unexpected failure. This is demonstrated from the arbitrary performance limit, Δ_m, where no formula is assigned to evaluate such limit. The function also ignored the influence of the second-order effects of the axial load demands on the global response of the RMSWs, where an elastic-perfectly-plastic relationship was assumed. As such, an analytical resistance function is proposed in the following subsection to overcome the aforementioned drawbacks of the USACE (2008)/USDOD (2014).

2.6.2 Proposed Resistance Function

The proposed out-of-plane resistance function is based on four distinctive points and a performance arbitrary point. These points divide the out-of-plane wall performance into four stages, namely elastic, elastic-plastic, plastic, and degradation stages, as shown in Figure 2.15. These stages are defined through different displacement levels, the initiation of cracking (Δ_{cr}), elastic (Δ_e), elastic-plastic (Δ_{ep}), plastic (Δ_u), and maximum (Δ_m) displacements, and load demands, cracking (P_{cr}), elastic (P_e), ultimate (P_u), and post-peak (P_u') loads. The following subsections detail the four key points and the degradation stage of the proposed resistance function.

2.6.2.1 *Point 1: Cracking*

The cracking point is defined by the cracking load (P_{cr}) and the gross stiffness (K_g). P_{cr} is the load causing at least one the wall critical sections to reach the cracking moment (M_{cr}), as presented in Eq. (7). M_{cr} is evaluated based on both the gross section properties and the axial load of the wall, as shown in Eq. (8) (Drysdale and Hamid 2005). The gross stiffness, K_g, is based on a fixed-fixed boundary condition, as presented in Eq. 9. Where f_t is the masonry tensile strength, P_A is the axial compressive load, A_g is the gross cross-sectional area of the wall, S_g is the wall gross section modulus, and I_g is the wall gross moment of inertia.

$$P_{cr} = \frac{12 M_{cr}\ L}{h^2} \tag{7}$$

$$M_{cr} = \left(f_t + \frac{P_A}{A_g} \right) S_g \tag{8}$$

$$K_g = \frac{384 E I_g}{L^4} \tag{9}$$

2.6.2.2 *Point 2: Elastic*

The elastic point is defined by the elastic load (P_e) and the elastic displacement (Δ_e). P_e is calculated using the same equation proposed by the USACE (2008)/USDOD (2014) (i.e. Eq. 2), while Δ_e is derived through the integration of the curvature profile. The curvature profile is assumed to be in a parabolic distribution, similar to the expected bending moment diagram, as a linear behavior is assumed for the elastic point. Subsequently, a yielding curvature(φ_y) is assumed at both supports, while the middle section is assigned a $\varphi_y/2$, due to the assumed elastic-perfectly plastic moment-curvature (M-φ) relationship as shown in Figure 2.15. As such, the elastic displacement, Δ_e, is evaluated as shown in Eq. 10.

$$\Delta_e = \frac{\varphi_y L^2}{32} \tag{10}$$

2.6.2.3 Point 3: Elastic-plastic

The elastic-plastic point defines the onset of the plastic stage, where the wall capacity does not increase beyond this point. At this point, the moment is redistributed from the maximum moment location, at the supports, to other sections until reaching M_p to start a mechanism. As such, P_u is calculated using the upper bound plastic theorem using the same formulation of the USACE (2008)/USDOD (2014), as presented in Eq. 4. Although the three critical sections reached M_p as shown in Figure 2.15, only the two critical wall sections (i.e. at the top and bottom supports) are expected to exceed the yielding-curvature, φ_y, and the mid-height section was assumed to reach the onset of φ_y. However, for simplicity, Δ_{ep} is calculated based on the assumption that the three critical sections reached φ_y simultaneously as shown in Figure 2.15 and calculated using Eq. 11.

$$\Delta_{ep} = \frac{\varphi_y L^2}{12} \tag{11}$$

2.6.2.4 Point 4: Plastic

The plastic point defines the plastic stage and demonstrates the onset of the strength degradation. The plastic stage accounts for the plastic deformations that occur due to the moment-redistribution and the concentration of curvature until φ_u is reached at the critical sections. It also considers the strength degradation due to the second-order effects. The φ_u limit is derived from the uniqueness theorem which allows a statically admissible moment-redistribution (Tichy and Rakosnik 1977). The plastic point is defined using the plastic load (P_u') and the ultimate displacement (Δ_u'). P_u' is calculated using the upper bound plastic theorem as P_u, however, the moment capacity at the critical sections are reduced to M_p' as shown in Eq.12. M_p' is the reduced out-of-plane capacity of the wall due to the second order effects of the axial loads, as illustrated in Eq. 13.

$$P_u' = \frac{16 M_p' L}{h^2} \tag{12}$$

$$M_p' = M_p \left(1 - P_A / P_{cr}\right) \tag{13}$$

Where P_{cr} is the critical buckling load according to Eq. 14.

$$P_{cr} = \frac{\pi^2 E I_e}{h^2} \tag{14}$$

Δ_u'is the modified deformation resulted from curvatures at the ultimate stage, considering the second order effects according to Eq. 15.

$$\Delta_u' = \frac{\Delta_u}{1 - P_A / P_{cr}} \tag{15}$$

Where Δ_u is the ultimate deformation without any consideration of the second order effects. Δ_u is the deformation resulting from the summation of the Δ_{ep} and the plastic deformation, Δ_p, as shown in Eq. 16. Δ_p is the deformation resulted from the curvature concentration which can be idealized as a uniform concentration at the plastic hinge locations. The curvature idealization concept is used to model the curvature concentration at the critical locations along the plastic hinge zone after moment-redistribution, which is widely used within the context of seismic design (Siam et al. 2017).

$$\Delta_u = \Delta_{ep} + \Delta_p = \Delta_{ep} + 2\left(\varphi_u - \varphi_y\right) L_p \left(\frac{h - L_p}{2}\right) + \varphi_u L_{sp} \frac{h}{2} \tag{16}$$

Two plastic hinges at both supports are assumed, while the hinge at the mid-height location is not considered due to its small rotation arm compared to that at the supports sections.

The plastic hinge length (L_p) is derived based on the formula proposed by Bohl and Adebar (2011). This is facilitated by introducing the wall thickness (t) to replace the wall length in the formula due to the out-of-plane deformation orientation, as shown in Eq. (17), where z is the shear span ratio (distance from the maximum to zero bending moment).

$$L_p = \left(0.2t + 0.05z\right)\left(1 - 1.5\frac{P_A}{f_m' A_g}\right) \leq 0.8t \tag{17}$$

The strain penetration of the fully anchored vertical reinforcement causes bar slip along its anchorage length, which results in additional end rotations (Zhao and Sritharan 2007). A uniform curvature (φ_y) distribution is typically assumed within the strain penetration length (L_{sp}) (Shedid and El-Dakhakhni 2014). Several studies have been conducted to estimate the L_{sp} that mainly depends on the diameter (d_b) and the f_y of the vertical reinforcement (Berry et al. 2008; Goodnight et al. 2016; Paulay and Priestley 1992; Shedid and El-Dakhakhni 2014; Zhao and Sritharan 2007). In the current study, the model proposed by Zhao and Sritharan (2007) for evaluating the minimum development length is adopted, as illustrated in Eq. 18.

$$L_{sp} = \frac{1}{7}\frac{f_y}{\sqrt{f_c'}} d_p \tag{18}$$

2.6.2.5 *Strength degradation stage*

At the strength degradation stage, the curvature of all the critical sections surpasses φ_u, resulting in concentrated plastic hinges that entail the formation of a mechanism. The degradation stage limit, Δ_m, is left *arbitrary* according to the post-peak objective performance. At this stage, the capacity of all the critical sections start to decrease; which subsequently decreases the overall wall strength. As such, for simplicity of the proposed resistance function, the slope of the degradation stage is left equal to the slope connecting the ultimate stage to the plastic stage (i.e. from Point 3 to Point 4), as

shown in Figure 2.16. This simplification is due to the lack of information to define the backbone relationship beyond Point 4.

2.6.3 Resistance Function Assessment

This section validates the linear-elastic-perfectly-plastic resistance function proposed by the USACE (2008)/USDOD (2014) as well as the proposed function relative to the experimental results of the flexural walls tested in the current study. The M_p and the M-φ relationships used in the validation process are derived from an incremental fiber analysis (i.e. strain increments) accounting for the external axial stresses. The M-φ relationships are evaluated by calculating the RMSW average strain at different layers then estimates the subsequent stress values based on the corresponding material response that fulfills the equilibrium limits. For the RMSWs application, both the masonry and the reinforcement were modeled using the unconfined concrete model and the monotonic stress-strain relationships, respectively (Chang and Mander 1994). Figure 2.16 illustrates the response of the predictive resistance functions relative to the experimental results, while Table 2.2 summarizes the percentage of deviations at different displacement levels. The deviations for the USACE (2008) /USDOD (2014) were on average 48%, 10% and -11% at Δ_e, Δ_{ep}, and Δ_u, respectively, while the same deviations for the proposed resistance function were 12%, 5% and -6%. Furthermore, the ultimate load of both functions had an average deviation of 2% which confirms the M_p values assumed at the critical sections regardless the out-of-plane classification. This finding is attributed to the small plastic hinge length compared the wall height which allows for in-wall moment redistribution even if some hinges start to soften (Darvall 1984; Darvall and Mendis 1985).

2.7 CONCLUSION

The current study experimentally and analytically investigated the out-of-plane behavior of seven half-scale fully grouted (i.e. five load-bearing and two non-load bearing) RMSWs subjected to a

quasi-static unidirectional cyclic loading. In this respect, the wall damage sequence, load-displacement response, displacement ductility, stiffness degradation, energy dissipation and curvature profile were reported. The influences of reinforcement ratios and axial load levels on the out-of-plane behavior of RMSWs were quantified. All the walls exhibited a similar out-of-plane displacement profile regardless their design parameters. However, six of the tested walls had flexural dominated failures, while the failure of one wall (i.e. with the highest vertical reinforcement ratio) was shear dominated. In addition, increases in the wall vertical reinforcement ratio and axial load reduced significantly the out-of-plane displacement ductility. Moreover, the vertical reinforcement ratio was found to be directly proportional to the energy dissipated and the normalized secant stiffness. Finally, the axial load increased the wall energy dissipation, but reduced its corresponding normalized secant stiffness.

The USACE (2008)/USDOD (2014) resistance function was compared to the experimental results. This function showed inadequate experimental predictions, especially at the post-peak stage. As such, an analytical resistance function is developed and experimentally validated to simulate the nonlinear out-of-plane response of RMSW. The developed function accounted for the moment redistribution, curvature concentrations, and the second order effects. The resistance function accurately captured the load-displacement, with average deviations of 12%, 5% and 6% at the elastic, elastic-plastic and plastic stages, respectively. The developed function can be used, while incorporating the effects of the strain rate and the subsequent dynamic increase factors, within the context of the blast analysis (Biggs 1964).

Although the current study presented an experimental investigation that covered different seismically detailed RMSWs, additional experimental tests are still required. These additional tests should cover different horizontal reinforcement details, boundary conditions, and

axial load levels. In addition, the out-of-plane dynamic behavior of RMSWs should be also assessed to facilitate reliable applications within different multi-hazard events.

2.8 ACKNOWLEDGMENTS

Financial support has been provided through a Collaborative Research and Development Grant funded by the Natural Sciences and Engineering Research Council (NSERC) of Canada. Industrial support has been provided by the Canadian Concrete Masonry Producers Association (CCMPA) and the Canada Masonry Design Centre (CMDC). Additional support has been provided through the McMaster University Institute for Multi-Hazard Systemic Risk Studies.

2.9 NOTATION

The following symbols are used in this paper:

A_g = gross cross section area;

b= wall width;

d_b = vertical bar diameter;

f_c' = compressive strength of the adjacent concrete elements;

f_m' = masonry compressive strength;

f_t = masonry tensile strength;

f_y = vertical reinforcement yield strength;

h= wall height;

h_{gauge} = distance between the walls' surface potentiomentrs;

I_e = effective moment of inertia;

I_g = gross moment of inertia;

k = integration constant;

K_e = elastic flexural stiffness;

K_{ep} = elastic-plastic flexural stiffness;

K_g = gross flexural stiffness;

L= wall length;

L_p = plastic hinge length;

L_{sp} = strain penetration length;

M_{cr} = cracking moment;

M_p = ultimate moment;

P_A = axial load;

P_{cr} = cracking load;

P_e = elastic load;

P_u = ultimate load;

P_u'= reduced ultimate load due to the second order effects;

S_g = gross section modulus;

t = wall thickness;

z = shear span;

α = reduction factor;

$\Delta_{0.7u}$ = displacement at 70% degradation of the ultimate load;

Δ_{cr} = displacement at cracking load;

Δ_{e} = displacement at elastic load;

Δ_{ep} = displacement at elastic-plastic load;

Δ_{f} = wall front surface deformation;

Δ_{m}= maximum displacement;

Δ_{p} = plastic displacement;

Δ_{r} = wall rear surface deformation;

Δ_{u} = displacement at ultimate load;

Δ_{u}' = displacement at post-peak load;

Δ_{u}' = magnified ultimate displacement due to second order effects;

Δ_{y} = displacement at first rebar yielding;

δ_{φ} = curvature difference;

ρ_{h} = horizontal reinforcement ratio;

ρ_{v} = vertical reinforcement ratio;

φ_{b} = curvature at bottom support section;

φ_{cr} = curvature at cracking load;

φ_{m} = curvature at walls' approximate mid-height section;

φ_{t}= curvature at top support section;

φ_u = curvature at ultimate load;

φ_u' = curvature at post-peak load;

φ_u'= pseudo-ultimate curvature;

φ_y = curvature at first rebar yielding;

$\mu_{\Delta 0.7u}$= displacement ductility using displacement at 70% degradation of the ultimate load; and

$\mu_{\Delta u}$ = displacement ductility using ultimate displacement.

2.10 REFERENCES

ACI committee 318. (2014). *Building Code Requirements for Structural Concrete and Commentary (ACI 318M-14)*. *American Concrete Institute*, Farmington Hills, MI.

Applied Technology Council. (2009). *Improvement of Nonlinear Static Seismic Analysis Procedures*. *FEMA P440A*, Washington, D.C.

ASCE. (2011). *Blast Protection of Buildings*. *ASCE 59-11*, (American Society of Civil Engineers, ed.), American Society of Civil Engineers, Reston, VA, VA.

ASTM. (2016a). *Standard Test Methods for Sampling and Testing Concrete Masonry Units and Related Unit*. ASTM:C140/C140M-16, West Conshohocken, PA.

ASTM. (2016b). *Standard Test Method for Preconstruction and Construction Evaluation of Mortars for Plain and Reinforced Unit Masonry*. ASTM C780 - 16a, West Conshohocken, PA.

ASTM. (2016c). *Standard Specification for Grout for Masonry*. ASTM C476-16, West Conshohocken, PA.

ASTM. (2016d). *Standard Test Method for Sampling and Testing Grout*. ASTM C1019-16, West Conshohocken, PA.

ASTM. (2016e). *Standard Test Method for Compressive Strength of Masonry Prisms*. ASTM C1314-16, West Conshohocken, PA.

ASTM. (2018). *ASTM C39 / C39M-18, Standard Test Method for Compressive Strength of Cylindrical Concrete Specimens*.

Bechara, E. A., Ahmad, A. H., and Harrv, G. H. (1996). “Flexural Behavior of Reinforced

Concrete Masonry Walls under Out-of-Plane Monotonic Loads." *ACI Structural Journal*, 93(3).

Berry, M. P., Lehman, D. E., and Lowes, L. N. (2008). "Lumped-Plasticity Models for Performance Simulation of Bridge Columns." *ACI Structural Journal*, 105(3), 270–279.

Biggs, J. (1964). *Introduction to structural dynamics*. McGraw-Hill College, New York.

Bohl, A., and Adebar, P. (2011). "Plastic Hinge Length in High-Rise Concrete Shear Walls." *ACI Structural Journal*, 108(2), 148–156.

Browning, R. S., and Davidson, J. S. (2011). "Use of Empirical Constitutive Properties to Develop a Resistance Function for Reinforced Masonry." *Structures Congress 2011*, American Society of Civil Engineers, Reston, VA, 1310–1319.

Browning, R. S., Hoemann, J. M., and Davidson, J. S. (2011). "Large-Deflection Response of Fully Grouted Reinforced Masonry Walls to Static and Dynamic Out-of-Plane Pressure." *ACI special publication*, 281, 1–20.

Bui, T. T., and Limam, A. (2014). "Out-of-plane behaviour of hollow concrete block masonry walls unstrengthened and strengthened with CFRP composite." *Composites Part B: Engineering*, 67, 527–542.

Campidelli, M., Tait, M. J., El-Dakhakhni, W. W., and Mekky, W. (2015). "Inference of Blast Wavefront Parameter Uncertainty for Probabilistic Risk Assessment." *Journal of Structural Engineering*, 141(12), 4015062.

Chang, G., and Mander, J. (1994). "Seismic Energy Based Fatigue Damage Analysis of Bridge Columns: Part I - Evaluation of Seismic Capacity." *(NCEER) Technical Report 94-0006*.

CSA. (2012). *CSA S850-12 Design and assessment of buildings subjected to blast loads*. Canadian Standards Association, Mississauga, ON, Canada.

CSA. (2014a). *CSA S304-14 Design of Masonry Structures*. Canadian Standards Association, Mississauga, ON, Canada.

CSA. (2014b). *CSA A165-14, Standards on concrete masonry units*. Canadian Standards Association, Mississauga, ON, Canada.

CSA. (2014c). *CSA G30.18-09, Carbon steel bars for concrete reinforcement*. Canadian Standards Association, Mississauga, ON, Canada.

CSA. (2015). *CAN/CSA-A179-14, Mortar and Grout for Unit Masonry*. Canadian Standards Association, Mississauga, ON, Canada.

Darvall, P. L. (1984). "Load-Deflection Curves For Elastic-Softening Beams." *Journal of Structural Engineering*, 110(10), 2536–2541.

Darvall, P. L., and Mendis, P. A. (1985). "Elastic-Plastic-Softening Analysis of Plane Frames." *Journal of Structural Engineering*, 111(4), 871–888.

Drysdale, R. G., and Hamid, A. A. (2005). *Masonry structures behaviour and design*. (D. W. Stubbs, ed.), Canada Masonry Design Centre, Mississauga, ON, Canada.

ElSayed, M., El-Dakhakhni, W., and Tait, M. (2015). "Response Evaluation of Reinforced Concrete Block Structural Walls Subjected to Blast Loading." *Journal of Structural Engineering*, 141(11), 4015043.

ElSayed, M., El-Dakhakhni, W., and Tait, M. (2016). "Resilience Evaluation of Seismically Detailed Reinforced Concrete-Block Shear Walls for Blast-Risk Assessment." *Journal of*

Performance of Constructed Facilities, 30(4), 4015087.

Ezzeldin, M., El-Dakhakhni, W., and Wiebe, L. (2017). "Experimental Assessment of the System-Level Seismic Performance of an Asymmetrical Reinforced Concrete Block–Wall Building with Boundary Elements." *Journal of Structural Engineering*, 143(8), 4017063.

FEMA-426. (2011). *BIPS 06/FEMA 426: Reference Manual to Mitigate Potential Terrorist Attacks against Buildings*. U.S. Department of Homeland Security.

Goodnight, J. C., Kowalsky, M. J., and Nau, J. M. (2016). "Modified Plastic-Hinge Method for Circular RC Bridge Columns." *Journal of Structural Engineering*, 142(11), 4016103.

Haach, V. G., Vasconcelos, G., and Lourenço, P. B. (2010). "Experimental Analysis of Reinforced Concrete Block Masonry Walls Subjected to In-Plane Cyclic Loading." *Journal of Structural Engineering*, 136(April), 452–462.

Heerema, P., Shedid, M., Konstantinidis, D., and El-Dakhakhni, W. (2015). "System-Level Seismic Performance Assessment of an Asymmetrical Reinforced Concrete Block Shear Wall Building." *Journal of Structural Engineering*, 141(12), 4015047.

Hose, Y. D., and Seible, F. (1999). *Performance Evaluation Database for Concrete Bridge Components and Systems under Simulated Seismic Loads*. (Pacific Earthquake Engineering Research Center, ed.), PEER Rep. No. 1999/11.

Krauthammer, T., Astarlioglu, S., Blasko, J., Soh, T. B., and Ng, P. H. (2008). "Pressure–impulse diagrams for the behavior assessment of structural components." *International Journal of Impact Engineering*, Pergamon, 35(8), 771–783.

Long, L., Hamid, A., and Drysdale, R. (2005). "Small-scale modelling of concrete masonry using ½ scale units: a preliminary study." *10th Canadian*.

Marjanishvili, S. M. (2004). "Progressive Analysis Procedure for Progressive Collapse." *Journal of Performance of Constructed Facilities*, 18(2), 79–85.

Mueller, J., Stewart, M. G., and Hayes, W. (2011). *Terror, security, and money: Balancing the risks, benefits, and costs of homeland security*. New York.

Parisi, F., and Augenti, N. (2012). "Influence of seismic design criteria on blast resistance of RC framed buildings: A case study." *Engineering Structures*, Elsevier, 44, 78–93.

Paulay, T., and Priestley, M. (1992). *Seismic design of reinforced concrete and masonry buildings*. Wiley, New York.

Porto, F., Mosele, F., and Modena, C. (2010). "Experimental testing of tall reinforced masonry walls under out-of-plane actions." *Construction and Building Materials*, Elsevier Ltd, 24(12), 2559–2571.

Priestley, M. J. N. M. N., Calvi, G. M., Kowalsky, M. J., and Park, T. (2007). *Displacement-based seismic design of structures*. IUSS Press, Pavia, Italy.

Seif ElDin, H. M., and Galal, K. (2017). "In-Plane Seismic Performance of Fully Grouted Reinforced Masonry Shear Walls." *Journal of Structural Engineering*, 143(7), 4017054.

Shedid, M. T., Drysdale, R. G., and El-Dakhakhni, W. W. (2008). "Behavior of Fully Grouted Reinforced Concrete Masonry Shear Walls Failing in Flexure: Experimental Results." *Journal of Structural Engineering*, American Society of Civil Engineers, 134(11), 1754–1767.

Shedid, M. T., and El-Dakhakhni, W. W. (2014). "Plastic Hinge Model and Displacement-Based Seismic Design Parameter Quantifications for Reinforced Concrete Block Structural Walls." *Journal of Structural Engineering*, 140(4), 4013090.

Siam, A. S., Hussein, W. M., and El-Dakhakhni, W. W. (2017). "Scoring models for reinforced masonry shear wall maximum displacement prediction under seismic loads." *Engineering Structures*, 136, 511–522.

Siyam, M. A., El-Dakhakhni, W. W., Shedid, M. T., and Drysdale, R. G. (2016). "Seismic Response Evaluation of Ductile Reinforced Concrete Block Structural Walls. I: Experimental Results and Force-Based Design Parameters." *Journal of Performance of Constructed Facilities*, 30(4), 4015066.

Smith, N. L., Tait, M. J., El-Dakhakhni, W. W., and Mekky, W. F. (2016). "Response Analysis of Reinforced Concrete Block Infill Panels under Blast." *Journal of Performance of Constructed Facilities*, 30(6), 4016059.

The Masonry Society (TMS). (2016). *Building Code Requirements for Masonry Structures*. TMS 402-16/ACI 530-16/ASCE 5-16, Detroit, MI.

Thiagarajan, G., Rahimzadeh, R., and Kundu, A. (2013). "Study of Pressure-Impulse Diagrams for Reinforced Concrete Columns Using Finite Element Analysis." *International Journal of Protective Structures*, 4(4), 485–504.

Tichy, M., and Rakosnik, J. (1977). *Plastic Analysis of Concrete Frames with particular refrence to limit states design*. Collet's.

USACE, U. A. C. of E. (2008). *User's Guide for the Single-Degree-of-Freedom Blast Effects Design Spreadsheets (SBEDS)*. USACE, ACE Protective Design Centre, USA, PDC TR-06-01 Rev 1, Omaha, NE., NE.

USDOD, (U.S. Department of Defense). (2014). *Structures to Resist the Effects of Accidental Explosions*. *Unified Facilities Criteria 3-340-02*, Washington D.C.

Vasconcelos, G., and Lourenço, P. B. (2009). "In-Plane Experimental Behavior of Stone Masonry Walls under Cyclic Loading." *Journal of Structural Engineering*, 135(10), 1269–1277.

Zareian, F., and Kanvinde, A. (2013). "Effect of Column-Base Flexibility on the Seismic Response and Safety of Steel Moment-Resisting Frames." *Earthquake Spectra*, Earthquake Engineering Research Institute, 29(4), 1537–1559.

Zhang, X. (David), Singh, S., Bull, D. K., and Cooke, N. (2001). "Out-of-Plane Performance of Reinforced Masonry Walls with Openings." *Journal of Structural Engineering*, 127(1), 51–57.

Zhao, J., and Sritharan, S. (2007). "Modeling of Strain Penetration Effects in Fiber-Based Analysis of Reinforced Concrete StructuresConcrete Structures." *ACI Structural Journal*, 104(2), 133–141.

Table 2.1: Details of the test matrix

Wall	Vertical reinforcement		Horizontal reinforcement		TMS (2016)	Out-of-plane classification	$P_A/A_g f_m$ * (%)
	Number and size	ρ_v (%)	Size and spacing	ρ_h (%)			
L-00	6 # 3 (6 x 71 mm^2)	0.33	D4 every other course (25mm^2 @ 200mm)	0.14	Special	Under-reinforced	0.0
L-10	6 # 3 (6 x 71 mm^2)	0.33	D4 every other course (25mm^2 @ 200mm)	0.14	Special	Under-reinforced	10.0
M-00	6 # 4 (6 x 129 mm^2)	0.61	D4 every other course (25mm^2 @ 200mm)	0.14	Special	Under-reinforced	0.0
M-05	6 # 4 (6 x 129 mm^2)	0.61	D4 every other course (25mm^2 @ 200mm)	0.14	Intermediate	Under-reinforced	5.0
M-10	6 # 4 (6 x 129 mm^2)	0.61	D4 every other course (25mm^2 @ 200mm)	0.14	Intermediate	Balanced	10.0
M-15	6 # 4 (6 x 129 mm^2)	0.61	D4 every other course (25mm^2 @ 200mm)	0.14	Ordinary	Over-reinforced	15.0
H-10	15 # 3 (15 x 129 mm^2)	0.83	D4 every course (25mm^2 @ 100mm)	0.28	Ordinary	Over-reinforced	10.0

* A_g is the gross cross sectional area of the RMSW (127,800 mm^2)

Table 2.2: Percentage differences between the USACE (2008) / USDOD (2014) and the proposed model relative to the experimental results

Wall	At Δ_e (%)		At Δ_{ep} (%)		At Δ_u *(%)		$P_{u,exp} / P_{u,ana}$
	USACE /USDOD	Proposed model	USACE /USDOD	Proposed model	USACE /USDOD	Proposed model	
L-00	59	24	18	4	-10	-9	12
L-10	31	6	13	12	-38	-15	-10
M-00	64	38	14	12	-12	-11	11
M-05	52	-2	5	-5	-19	-2	5
M-10	43	10	8	7	29	3	-4
M-15	39	-6	0	0	-16	0	1
Average	48	12	10	5	-11	-6	2

* Calculated at 20% strength degradation

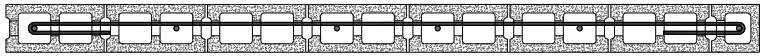

Vertical reinforcement: 6#3,
Horizontal reinforcement: D4 every other course
(Walls L-00 and L-10)

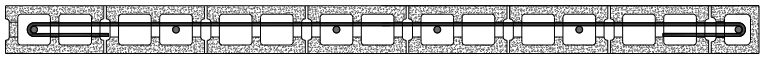

Vertical reinforcement: 6#4,
Horizontal reinforcement: D4 every other course
(Walls M-00, M-05, M-10 and M15)

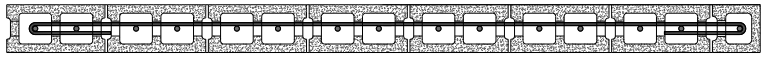

Vertical reinforcement: 15#3,
Horizontal reinforcement: D4 every course
(Wall H-10)

(a)

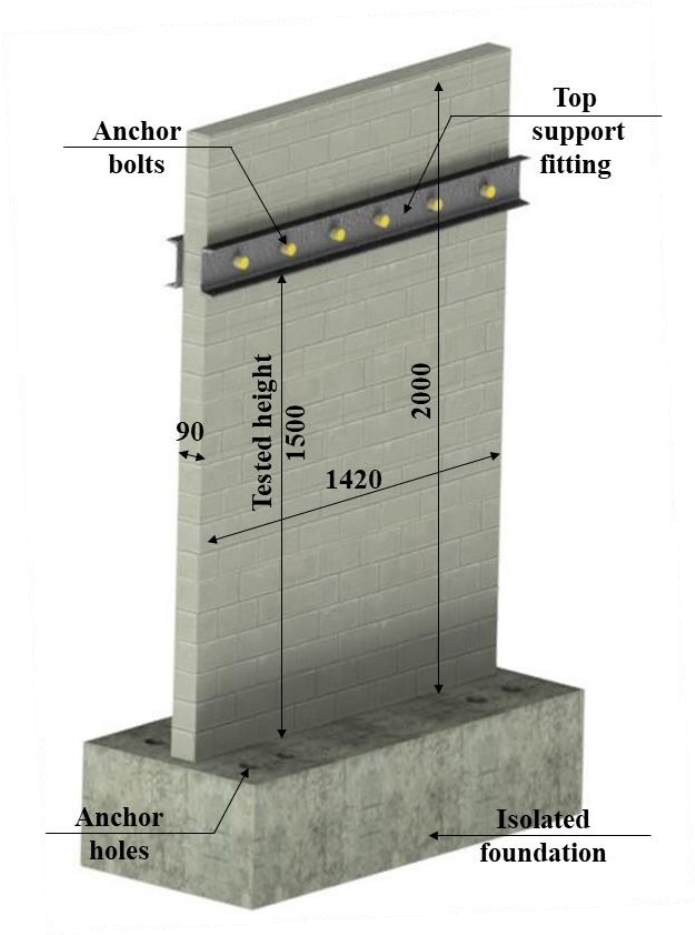

(b)

Figure 2.1: Tested walls: (a) Typical cross sections; (b) 3D view for a typical wall (all dimensions are in mm)

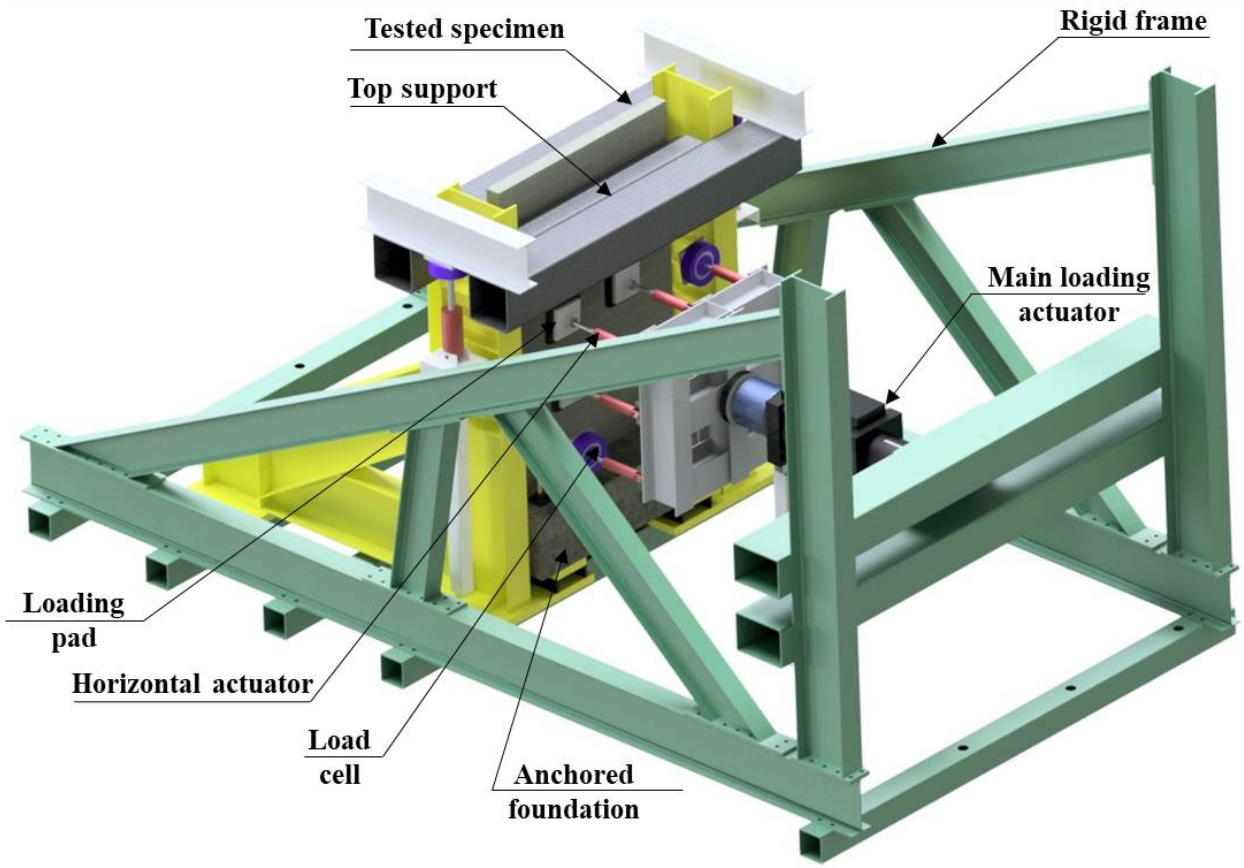
Tested specimen
Top support
Rigid frame
Main loading actuator
Loading pad
Horizontal actuator
Load cell
Anchored foundation

(a)

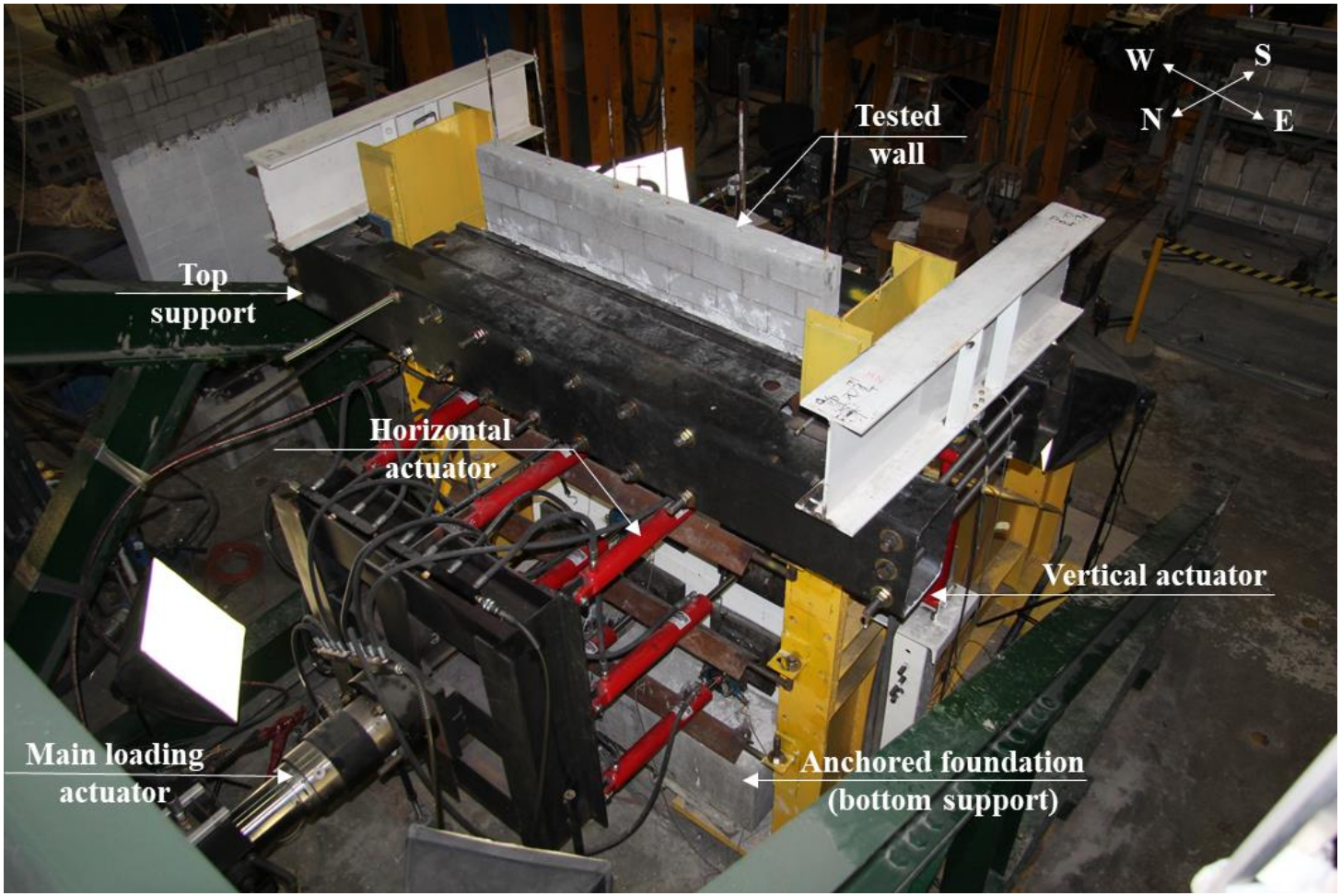

(b)

Figure 2.2: (a) 3D view for the test setup; (b) 3D view for the test setup

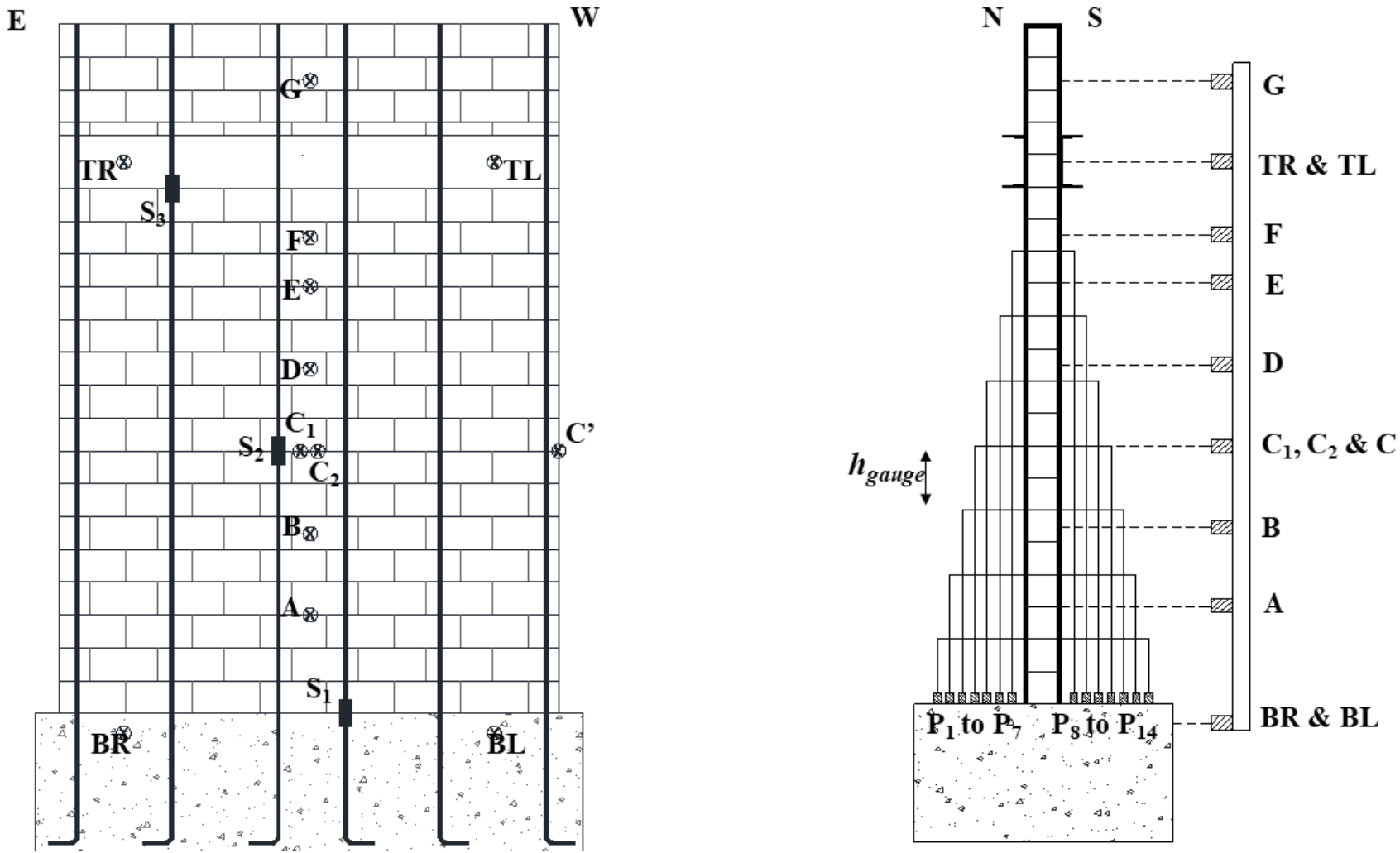

Figure 2.3: Typical instrumentation for the tested walls

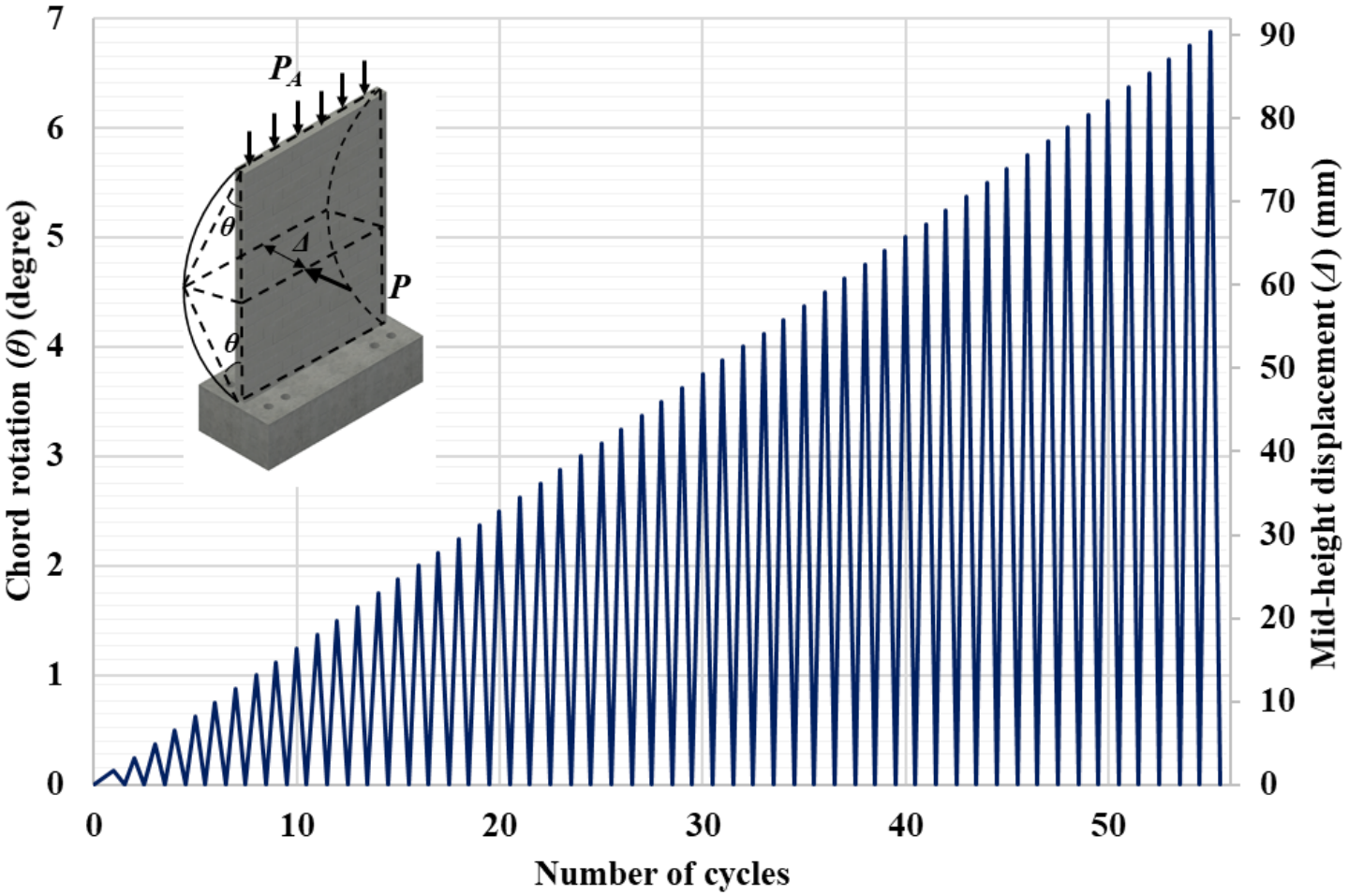

Figure 2.4: Loading protocol

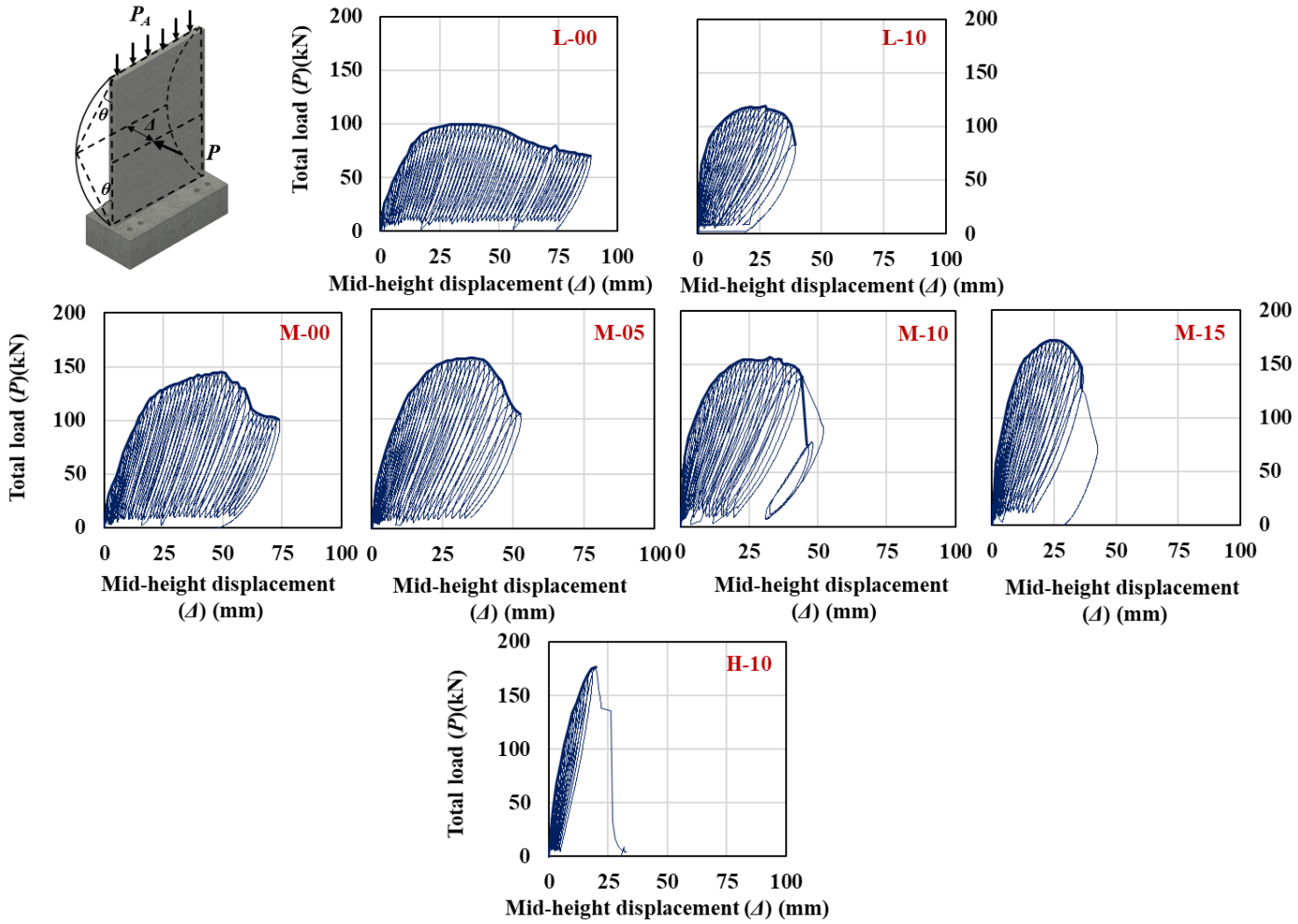

Figure 2.5: Load-displacement hysteric relationship

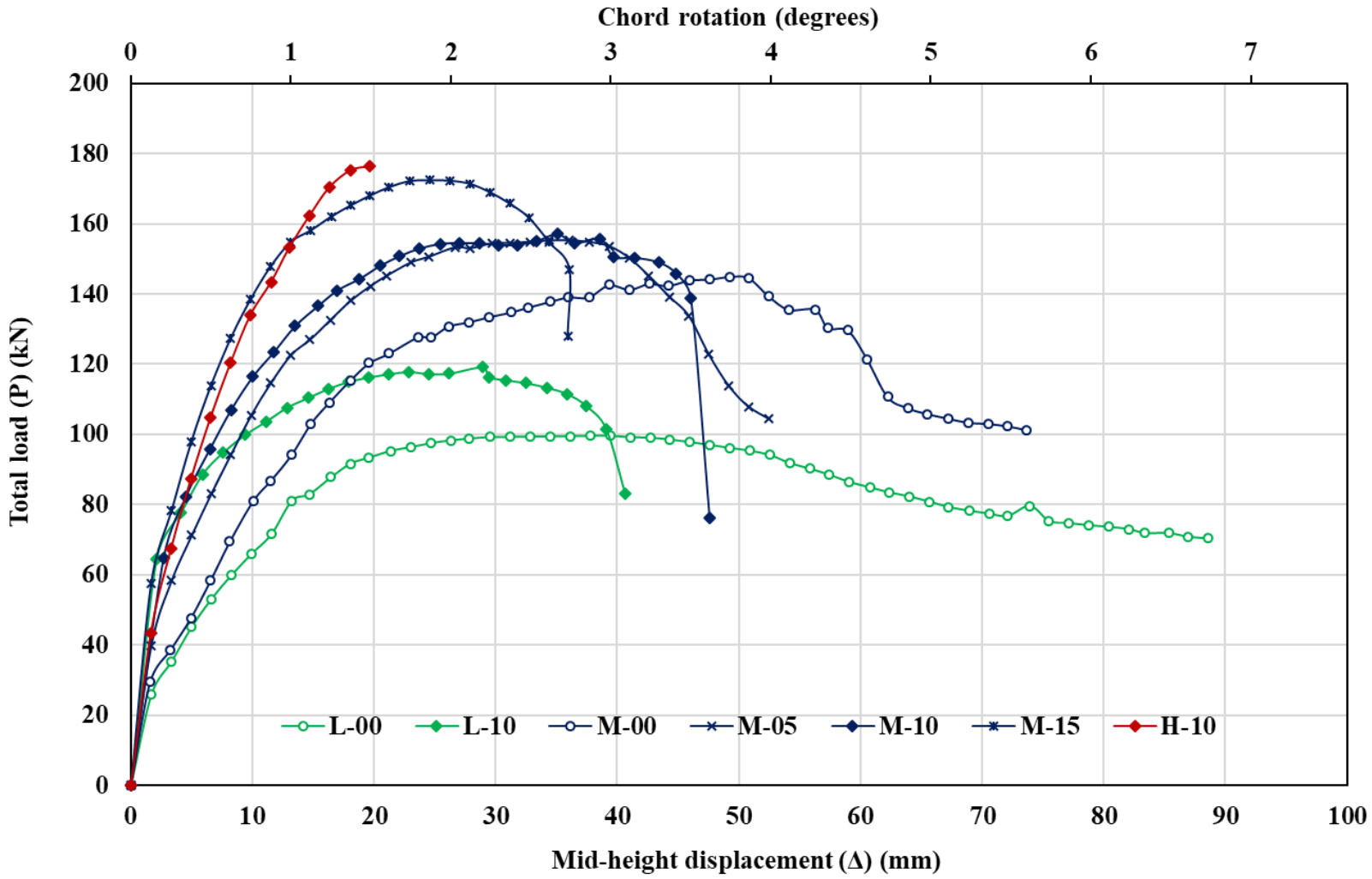

Figure 2.6: Resistance functions for the tested walls

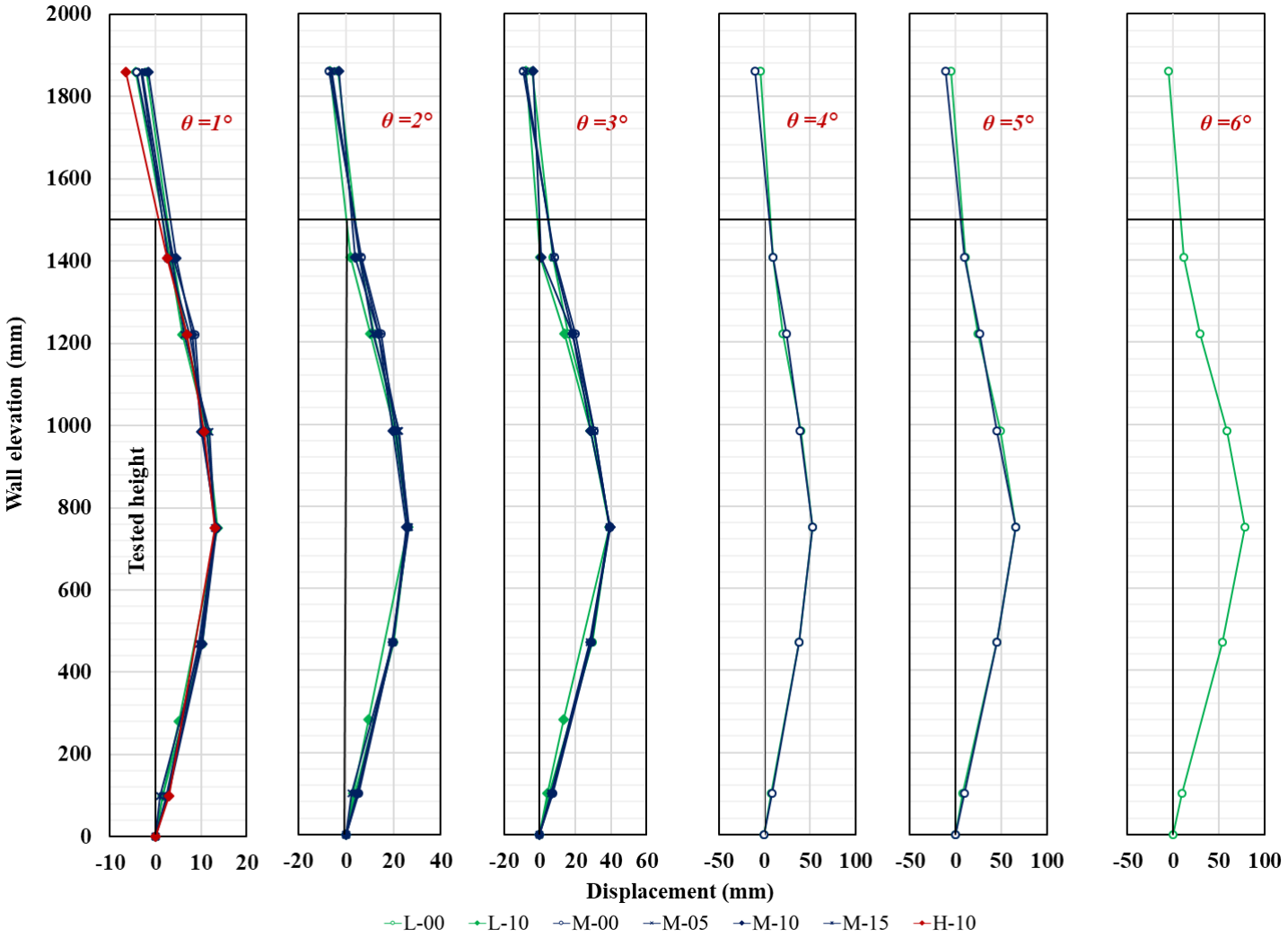

Figure 2.7: Displacement profile for the tested walls along their heights

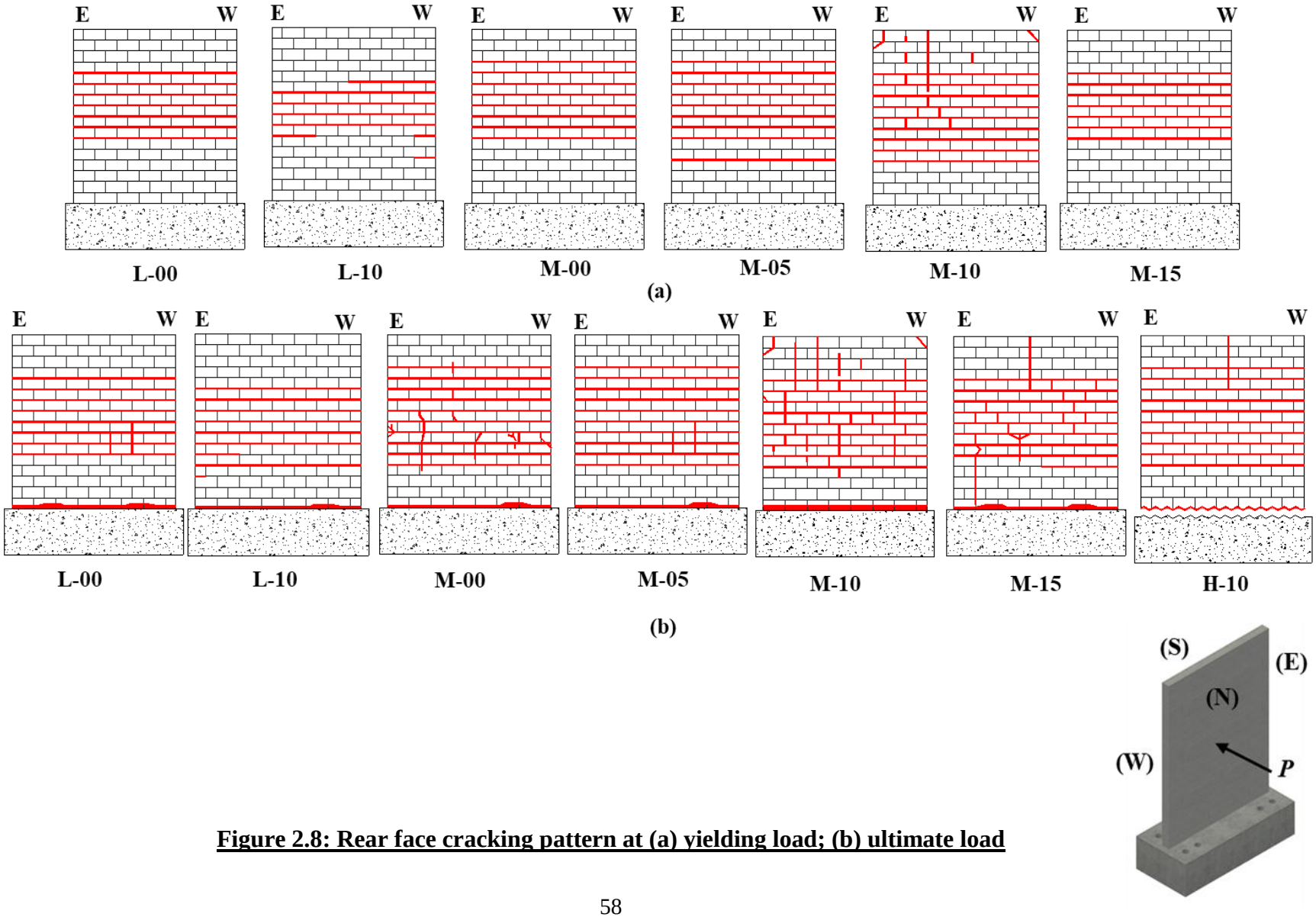

Figure 2.8: Rear face cracking pattern at (a) yielding load; (b) ultimate load

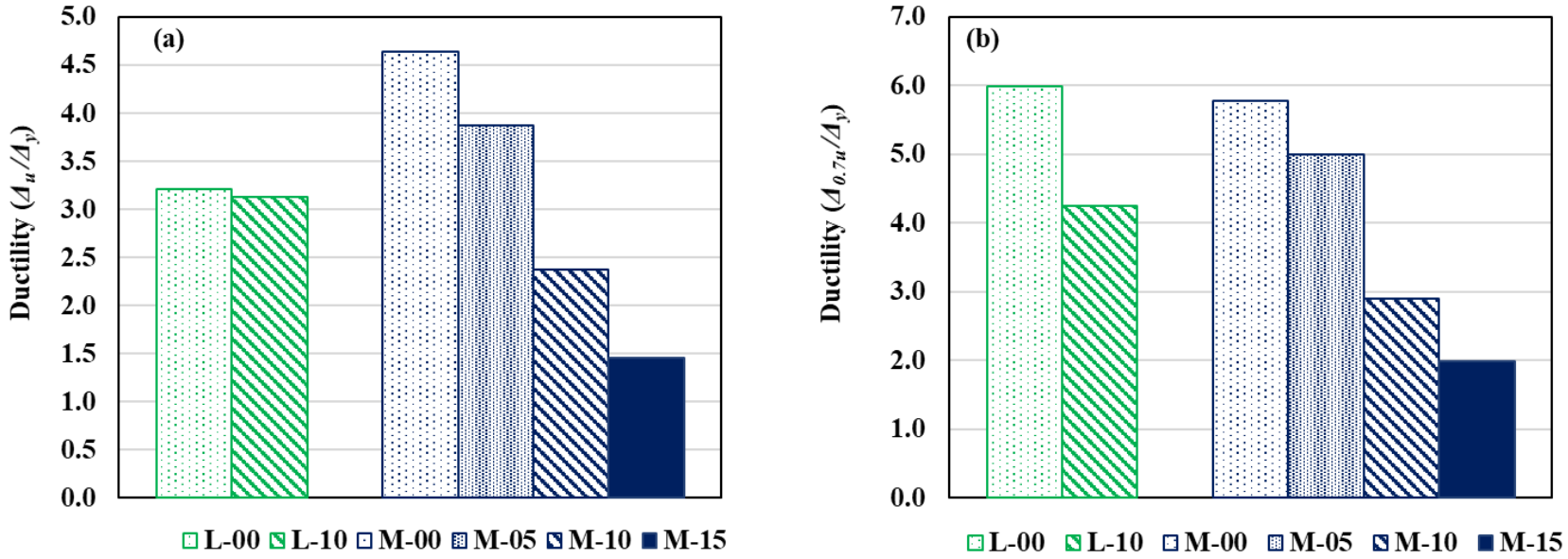

Figure 2.9: Displacement ductility using; (a) Δu; (b) Δ0.7u

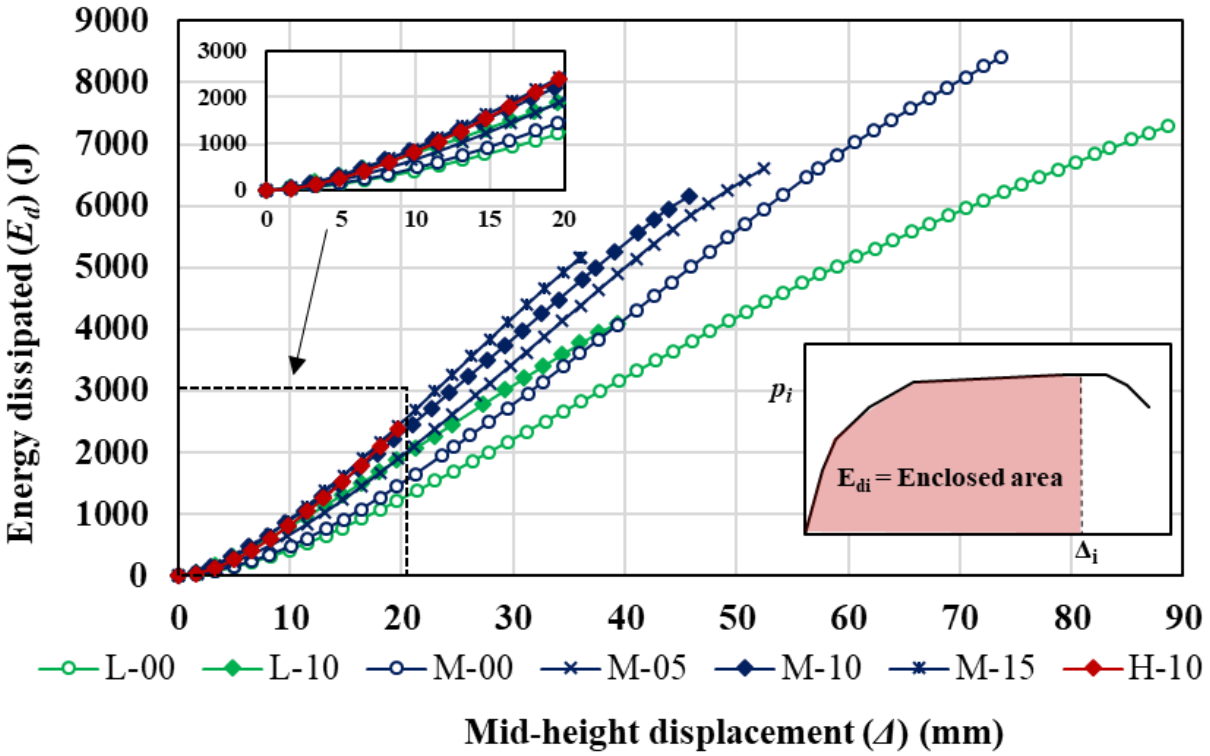

Figure 2.10: Energy dissipation propagation with respect to the mid-height displacement

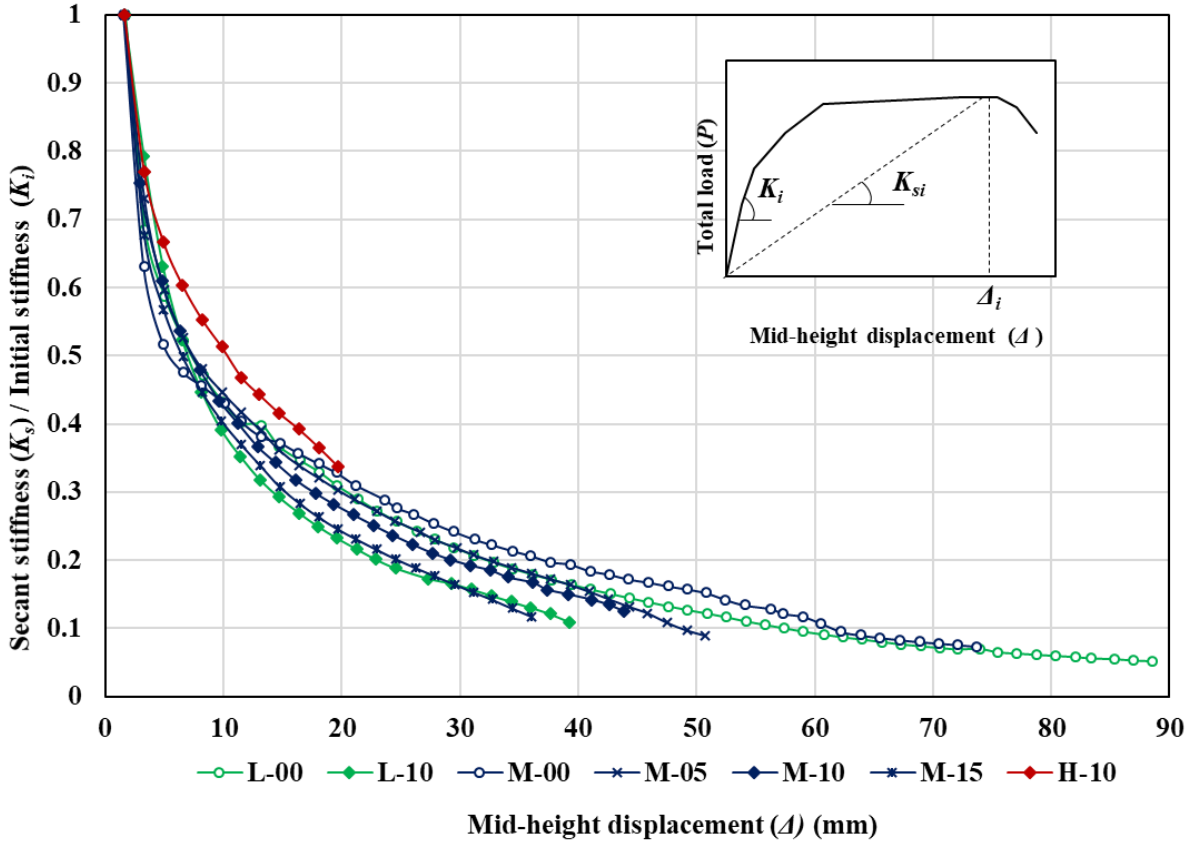

Figure 2.11: Secant stiffness degradation

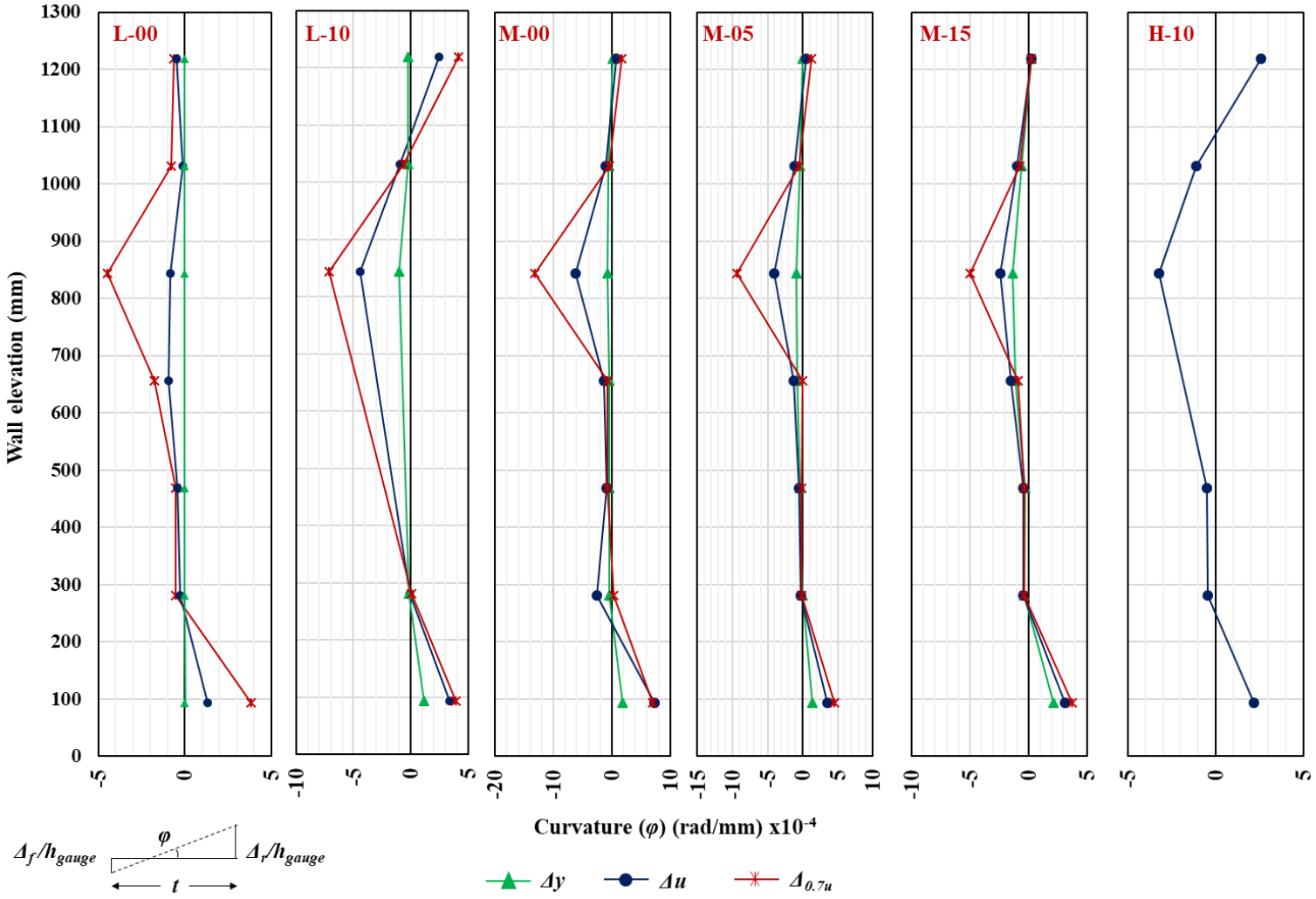

Figure 2.12: Cross-sectional curvature profile along the tested walls

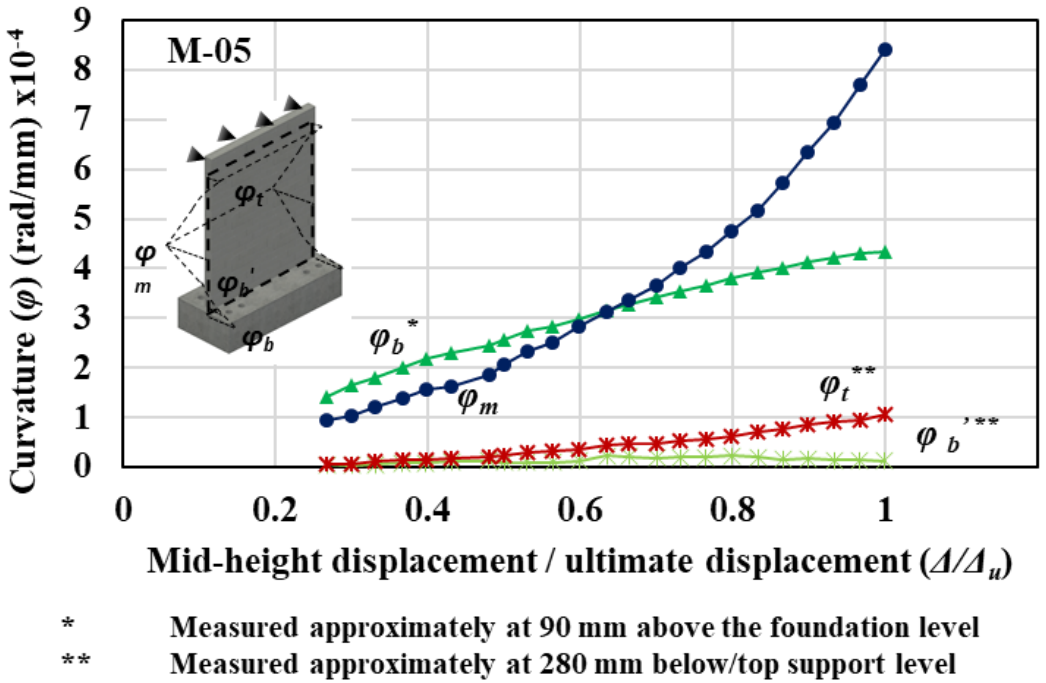

Figure 2.13: Typical cross-sectional curvature propagation at the critical locations

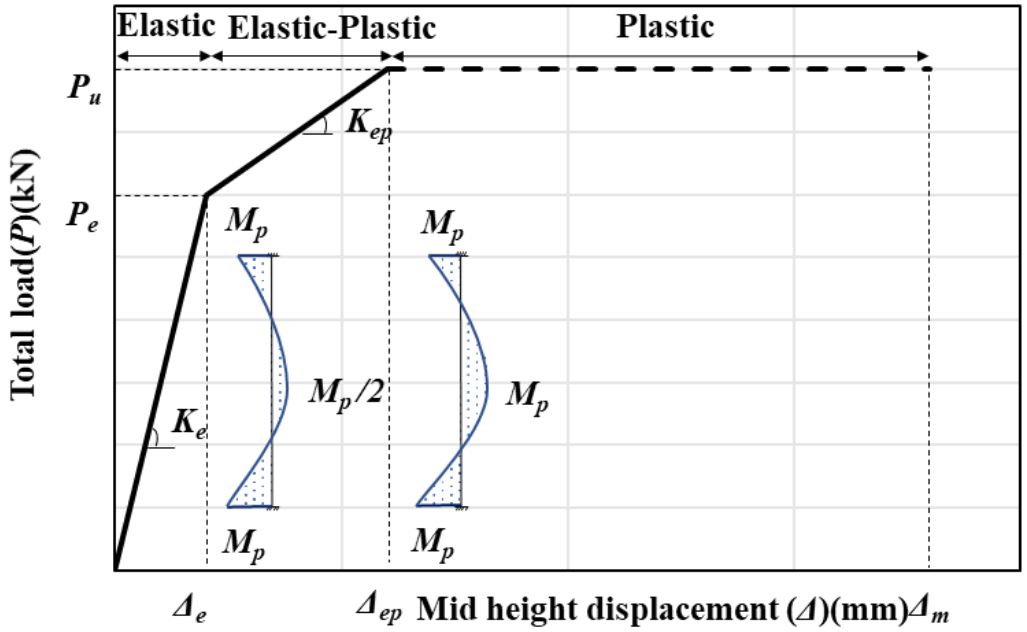

Figure 2.14: Idealized resistance function of the USACE (2008)/USDOD (2014)

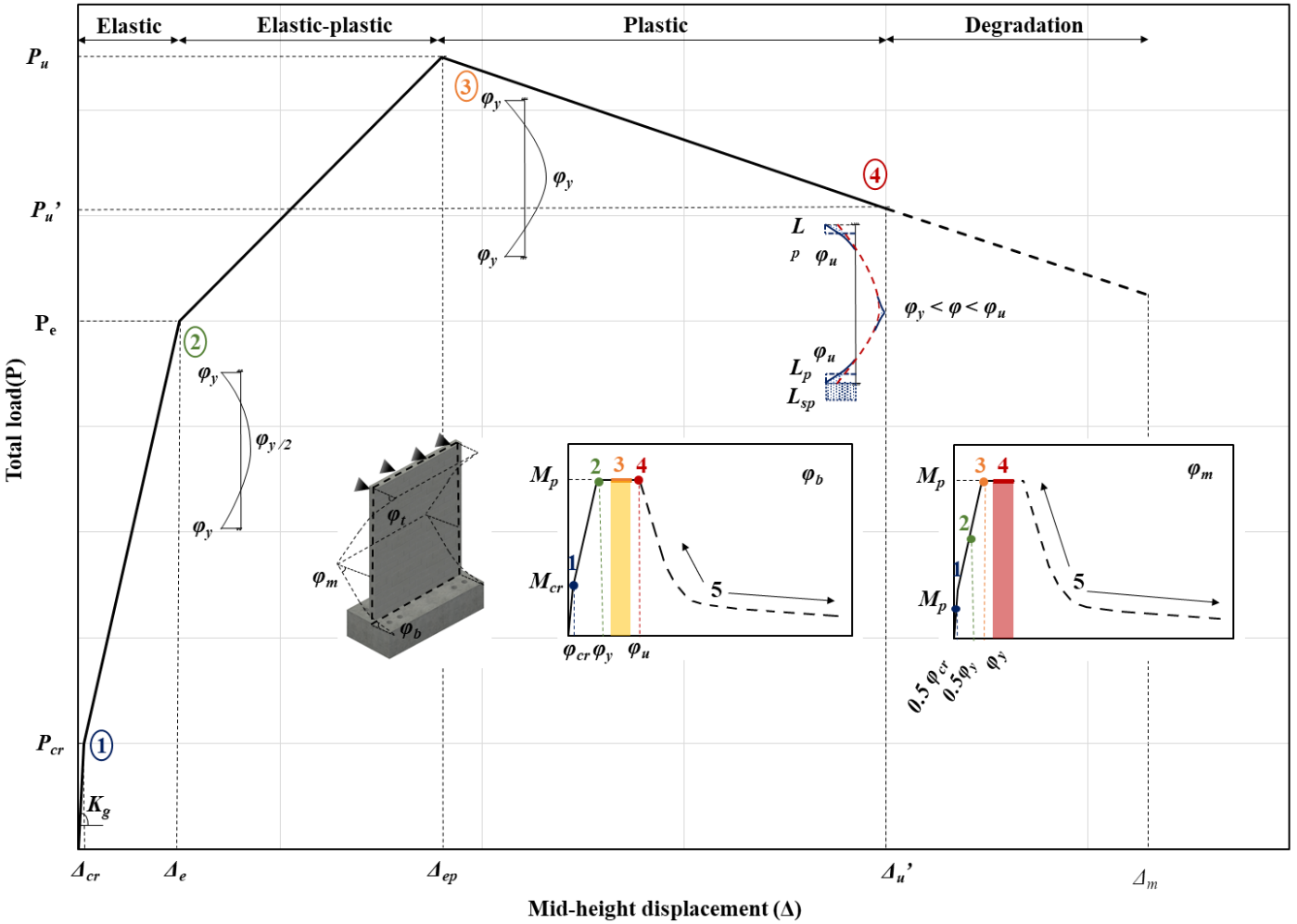

Figure 2.15: Proposed resistance function

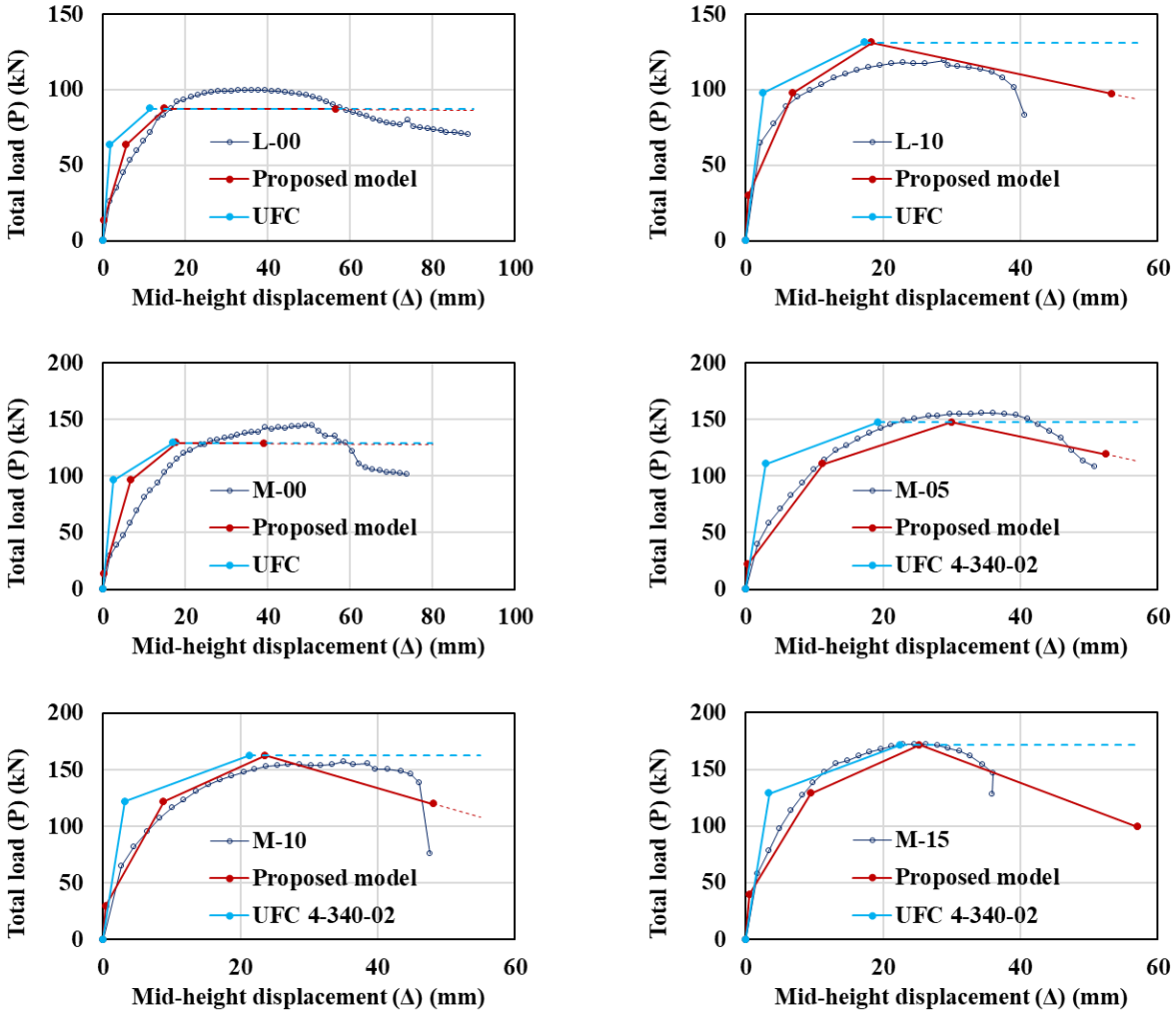

Figure 2.16: Experimental and analytical resistance functions

Chapter 3

BLAST FRAGILITY ASSESSMENT FOR LOAD-BEARING REINFORCED MASONRY SHEAR WALLS

3.1 ABSTRACT:

Reinforced masonry shear wall (RMSW) systems are widely used within the current North American construction practices. Although limited research has been carried out on the performance of load-bearing RMSWs under blast loading due to economic and technical constraints, these walls are perceived to be very vulnerable to blast loading. As such, the current study focuses on evaluating the blast performance of load-bearing RMSWs considering the blast wavefront parameter uncertainty. In this respect, a concentrated plasticity model is developed using the OpenSees code to simulate the out-of-plane response of load-bearing RMSWs. This model is first validated both statically and dynamically against different experimental datasets. Afterwards, the model is utilized within an iterative framework to track the different material strain rates in order to subsequently implement the corresponding dynamic increase factors to facilitate reliable blast response predictions. Finally, the model is used to assess the influence of the expected variability/uncertainty associated within several blast wavefront parameters on the response of RMSWs, when different axial stress levels and reinforcement ratios are present. The proposed framework is expected to open the gate for a new blast simulation tool that can be implemented within the context of blast design standards.

3.2 INTRODUCTION

The interest in blast-resistant construction has escalated over the past decade due to the increased frequency of terrorist attack threats and events (Marjanishvili 2004 ; Parisi and Augenti 2012). Generally, improvised explosive devices (IEDs) attacks can be categorized into suicidal, vehicle-born, or military (MIED) (LaFree and Legault 2009). According to the Global Terrorism database (START 2016), both suicidal and vehicle born improvised explosive devices attacks have been showing an increasing trend in terms of frequency and impact magnitude (i.e. fatalities). Subsequently, several studies have been conducted to develop mitigation measures through either minimizing the structural vulnerability (i.e. blast-resistant hardening schemes) and/or reducing the hazard intensity (i.e. augmenting the standoff distance or increasing the building envelope security) (ASCE 2011; CSA 2012; FEMA-426 2011). However, such measures impose economic constraints as they may constitute up to 30% of the facility construction cost (Campidelli et al. 2015b; Mueller et al. 2011). As such, these challenges require an optimized allocation for the blast-mitigation measures.

Although terrorism-induced risks are considered among the most difficult anthropogenic hazard-induced risks to be predicted (Ezell et al. 2010), current blast design standards (e.g. ASCE 2011; CSA 2012; USACE 2008; USDOD 2014) are still anchored on *deterministic* design-based threats (DBTs) with only few recommendations pertaining to considering the uncertain nature of the blast hazard, response, performance, cost and risk (Salem et al. 2017a). IEDs terrorist attacks are typically characterized by their high uncertainties at the DBT-level (i.e. charge weight and its stand-off distance) and the corresponding induced shock wave parameters. Within this context, thorough reliability analyses for a blast hazard are recommended (National Research Council 2010), where the consideration of blast uncertainty within a DBT can yield an effective comparison tool to assess the different blast protective measures (Stewart and Netherton 2008). To address this,

different researchers attempted to include the blast risk uncertainty in the context of a probabilistic risk assessment (PRA). For example, Stewart (2010) proposed a risk-informed framework to probabilistically evaluate the economic value of different mitigation measures. This framework was utilized later to quantify the risk in terms of casualties per building per year (Grant and Stewart 2012, 2015). Another PRA frameworks were introduced to probabilistically optimize the application of the blast mitigation measures (Stewart et al. 2006; Stewart and Netherton 2008; ElSayed et al. 2015a). These frameworks were capable of considering different sources of blast uncertainties, namely epistemic and aleatory uncertainties (Stewart and Netherton 2008). The epistemic uncertainty included the loading (i.e. detonation charge, stand-off distance, etc.) and the model (i.e. accuracy of predictive models) uncertainties, while aleatory uncertainty contained the inherent variability (weather, blast environment, etc.) (Stewart et al. 2006).

Several researchers accounted for different blast uncertainty sources through the assessment of structural and non-structural components. Most of the available literature integrated blast uncertainties in the form of fragility curves (Al-Habahbeh and Stewart 2015; Campidelli et al. 2016a; ElSayed et al. 2015a; Karlos et al. 2017; Olmati et al. 2014, 2016; Salem et al. 2017b; Stewart 2008). These fragility curves represent the probability of reaching a pre-defined performance against an intensity measure. In general, there are two intensity measures that can control the dynamic response of blast-resistant components, namely the reflected peak pressure and the impulse, as shown in Fig. 3.1 (Thiagarajan et al. 2013). Most of the available blast fragility curves are based only on a single intensity measure, impulse at a constant pressure demand (Campidelli et al. 2016b, 2017; Olmati et al. 2016; Parisi 2015). Although this can be valid for components responding within the impulsive regime (i.e. when the blast pressure magnitude does not significantly affect the component response) (Olmati et al. 2016), this may not be applicable to components responding within the dynamic or the quasi-static regime (i.e. when the component

response is highly influenced by the blast load pulse shape and its pressure magnitude) (Hayman 2014; Olmati et al. 2016). As such, the *fragility surface* concept was recently introduced to simultaneously account for reflected peak pressure and impulse measures (Olmati et al. 2016). In this respect, a very limited number of research studies have adopted the fragility surface concept within the blast performance prediction of different structural- (Parisi 2015) and non-structural (BIPS-05 2011; Smilowitz 2013) components.

Masonry façade/walls are often selected by architects/designers due to their aesthetic appearance and ease of construction (Salem et al. 2016). Furthermore, from a structural perspective, reinforced masonry shear walls (RMSWs) showed high ductility capacities in the in-plane direction when properly detailed (Shedid et al. 2008). Conversely, these walls have been found to exhibit low out-of-plane ductility capacities due to the standard mid-cell reinforcement placement practice (ElSayed et al. 2016). As such, these walls might be vulnerable to out-of-plane loading scenarios, like blast, (Browning et al. 2014; Campidelli et al. 2016a; Hoemann et al. 2015; Mayrhofer 2002; Oesterle et al. 2009; Smith et al. 2016). However, available studies were limited only to non-load bearing (i.e. no axial loads) RMSWs with several boundary conditions that do not represent well the typical RMSWs used in the current construction practices. This limited research is attributed to the unaffordable nature of blast field testing (El-Dakhakhni et al. 2010). Consequently, a reliable computational tool is needed to assess the blast performance of load-bearing RMSWs. Furthermore, this tool should account for the multiple sources of blast-related uncertainty as it may propagate into significant variability of the structural response (Campidelli et al. 2015a).

The objective of the current study is to investigate the influence of the variability/uncertainty associated with different blast wavefront parameters (i.e. the peak reflected pressure (P_r) and the positive specific impulse (I_s)) on the response of fully grouted RMSWs. These two wavefront parameters were selected in the current study as they are typically used to estimate

the blast performance, as mentioned earlier (Shin et al. 2015). In this respect, the study first develops a numerical model to predict the out-of-plane response of RMSWs using the OpenSees code (McKenna et al. 2000). The developed model is validated against experimental static results adapted from previous test programs. Following the static model validation, the model is used for blast response predictions utilizing the dynamic increase factors (DIFs) recommended by the USACE (2008), and USDOD (2014). The developed model is also compared to a simple single-degree-of-freedom model that is widely accepted by the current blast standards (ASCE 2011; CSA 2012; USACE 2008; USDOD 2014)). Afterwards, a generic framework, namely Blast OpenSees Simulation (BOSS) toolbox, is proposed and validated to assess the impact of several DIF models on the blast response of RMSWs. The BOSS toolbox is also used to probabilistically investigate the influence of the blast wavefront variability/uncertainty through fragility surfaces. Finally, the BOSS is applied (to some of the statically validated walls) to interrogate the probabilistic influence of different axial stress levels on the corresponding wall fragility curves.

3.3 MODEL DEVELOPMENT

According to the current North American blast standards, the dynamic behavior of different structural/non-structural components can be validated through analytical or numerical simulation techniques (ASCE 2011; CSA 2012). Analytical modeling techniques range from simplified elastic single-degree-of-freedom (SDOF) to non-linear multi-degree-of-freedom models (El-Dakhakhni et al. 2009). This modeling approach can capture the first few vibration modes without reverting to any detailed representation level. On the other hand, and although the finite element modeling technique can sometimes be more reliable than its analytical counterpart, it would require extensive computational resources because more detailed input parameters are typically used (El-Dakhakhni et al. 2009). As such, a reliable simple model is still required to facilitate a robust probabilistic blast assessment that can be used for different structural components.

The efficiency of the concentrated plasticity modeling approach has been demonstrated in nonlinear dynamic simulations (Dides and de la Llera 2005). The concentrated plasticity approach or the plastic hinge approach is based mainly on lumping all sources of nonlinearity at the expected plastic hinge locations (Papadopoulos and Fragiadakis 2015). This approach has been validated earlier in terms of predicting the in-plane response of RMSWs (Ezzeldin et al. 2014, 2016, 2018). Subsequently, within the context of predicting the out-of-plane response, this approach facilitates monitoring the time history response of the assumed plastic hinges and subsequently predicting the modified hinge behavior (i.e. moment-curvature) resulting from the DIF (Park et al. 2017), as will be discussed later in the current study.

3.3.1 Geometrical Model

As mentioned earlier, the developed model is based on the concentrated plasticity modeling approach using OpenSees (McKenna et al. 2000). As can be seen in Fig. 3.2, the model comprises three zero-length inelastic rotational springs connected with two elastic beam-column elements. These rotational springs are utilized to simulate the nonlinear behavior of RMSWs, through a bilinear elastic-perfect-plastic relationship representing the out-of-plane moment-curvature of the wall cross-section, defined only by two yielding parameters (i.e. M_y and φ_y). This assumption is considered acceptable due to the negligible hardening in the out-of-plane behavior of RMSWs (Browning et al. 2011; ElSayed et al. 2016). In the current study, only the yielding parameters were extracted from an incremental fiber analysis (i.e. strain increments) accounting for both internal and external stresses. The fiber stresses were based on the average strain of each fiber section using the corresponding material response. The concrete masonry grout/units were modeled using an unconfined concrete model, while the reinforcement was modeled using a monotonic stress-strain relationship (Chang and Mander 1994).

The elastic beam-column elements were modeled using the effective cross-sectional area (A_e) and the effective moment of inertia (I_e), as presented in Eq. (1) (Paulay and Priestley 1992). Where α is a stiffness reduction factor, P_A is the axial load, f_y is the vertical reinforcement yield strength, and f_m' is the masonry average compressive strength.

$$A_e = \alpha A_g \;;\; I_e = \alpha I_g \;;\; \alpha = \left(\frac{100}{f_y} + \frac{P_A}{f_m' A_g} \right) \tag{1}$$

3.3.2 Model Validation under Static Loading

The developed model is validated against the experimental results of seven fully grouted (i.e. four load-bearing and three non-load bearing) RMSWs tested in the out-of-plane direction in previous studies (Browning et al. 2011, 2014; Salem et al. 2018). These walls were subjected to a distributed loading pattern with different boundary conditions. One of these walls, reported by Browning et al. 2011, 2014, was a full-scale non-load bearing RMSW loaded using a vacuum chamber. This wall was simply supported by providing a clearance at the supports. The other six walls were subjected to nine distributed loading patches in the out-of-plane direction (Salem et al. 2018). These walls were half-scale walls tested a with fixed-fixed boundary condition, four of which were axially loaded while the remaining two walls were not axially loaded throughout the test, only the walls flexurally dominated walls were selected. Table 3.1 presents a summary of the wall geometrical and material properties, the corresponding boundary conditions and the axial load levels. The walls in the current study were identified with two letters and a number. The first letter (S or F) represents the wall boundary condition (i.e. simple or fixed), while the second letter (L, M, or H) refers to the relative vertical reinforcement ratio (i.e. low, moderate, or high). The number (0, 10, or 15) represents also the axial stress ratio (based on the gross cross-sectional area). For example, Wall

FH-10 is a fixed-fixed wall with the highest vertical reinforcement ratio (ρ_v = 0.61%) and an axial stress ratio of 10%.

Figure 3.3 compares the results of the developed model to those from the experimental tests. The figure shows that the model is capable of identifying the key out-of-plane response points (i.e. elastic and ultimate), as defined by the USACE (2008) and the USDOD (2014). These key response points are attributed to the yielding of the concentrated plastic hinges, which is also confirmed through the spring's recorded history. In this context, the simple supported wall had only one key point (i.e. ultimate), while the other six fixed walls had two key points which allowed the moment redistribution between the support and middle springs. This behavior is consistent with the explanation reported by Salem et al. (2018).

3.3.3 Model Validation under Dynamic Loading

Based on literature, most of the previous studies have used their validated concentrated plasticity *static* models directly through *dynamic* seismic analysis (Bozer 2017; Ezzeldin et al. 2016, 2018). However, the static model cannot be adopted directly for blast loading, due to the strain rate effects. This is because, during blast loading, different materials (concrete, masonry, and steel, etc.) within the wall exhibit significant strength increase due to the high strain-rate effect, that in turn enhances the wall blast performance (El-Dakhakhni et al. 2009; Rafsanjani et al. 2015b). This strain-rate effect is considered through either a failure envelope (i.e. using Mohr's circle) (Eamon et al. 2004; Rafsanjani et al. 2015a; Wei and Hao 2009) or a simplified dynamic-increase factor (DIF) approach (USACE 2008; USDOD 2014). The failure envelop approach can be used within the finite element modeling technique which may not be appropriate during early design stages due to the corresponding computational complexity (El-Dakhakhni et al. 2009). Conversely, DIF approach is widely adopted for simplified macro (Browning et al. 2011; Campidelli et al. 2016c; El-Dakhakhni et al. 2010; Olmati et al. 2014; Park et al. 2017; Shi and Stewart 2015) and finite element (Cui et

al. 2015; Thiagarajan et al. 2013) models. Subsequently, the developed concentrated plasticity model in the current study adopts the DIF approach to consider the strain-rate effect in the properties of the concentrated springs and the elastic beam-column elements. The DIF is the ratio of the dynamic stress to the elastic stress based on the material strain rate (USDOD 2014). For simplicity, the current blast design standards calculate the average strain rate using the time required by the material to reach its assumed plastic (yielding/ultimate) capacity (based on the material), as illustrated in Eq. (2) (USACE 2008; USDOD 2014).

$$\varepsilon' = \frac{\varepsilon_p}{t_p} \tag{2}$$

Where ε' is the average strain rate of the material (s^{-1}), while t_p (s) is the time required by this material to reach the plastic stain (ε_p). Furthermore, the current blast standards estimate approximate DIFs for different materials subjected to different kinds of stresses (i.e. flexural, axial, shear, bond), under different blast wave environments (i.e. far or near field) (ASCE 2011; CSA 2012; USACE 2008; USDOD 2014). Subsequently, the DIFs were applied to the developed model by increasing the mechanical properties of the materials used within the blast loading context. These mechanical properties influence both the spring (strength and stiffness) and the elastic beam-column elements.

The developed blast model was validated against the experimental results of six third-scale RMSWs subjected to a far-field explosion ($Z \geq 1.6$) (Campidelli et al. 2016c; Hayman 2014), where Z is the scaled distance, calculated using the *Hopkinson-Cranz Law*, as presented in Eq. 3.

$$Z = \frac{R}{\sqrt[3]{W}} \tag{3}$$

Where *R* (m) is the standoff distance measured from the center of the explosive charge to the investigated point, while *W* is the equivalent charge weight (in *TNT* equivalent) (*kg*). The six walls were 1000 × 1000 × 63.3 mm constructed using a third scale concrete masonry unit (CMU) with an average compressive strength of 20.8 *MPa*. These walls consisted of two groups (i.e. low and high ρ_v) subjected to three different blast scenarios with the same standoff distance (i.e. 5.0 *m*), as presented in Table 3.2. As such, all walls were identified using a letter and a number. The letter "L or H" represents the ρ_v (i.e. Low or High), while the number refers to the *TNT* equivalent weight in kg (i.e. 6, 12, or 30). For example, Wall H-12 denotes for a high vertical reinforcement ratio (ρ_v = 1.07%) tested using a *TNT eqv.* of 12 *kg* with a standoff distance of 5.0 *m* (*Z*=2.18 $m/kg^{1/3}$). All the vertical reinforcements of the tested walls were welded to structural C-channels at the top and the bottom ends on the walls. Each C-channel was in contact with a fixed solid bar welded to a steel bunker in order to provide simply supported boundary conditions (Campidelli et al. 2016c).

Each bunker was instrumented with three pressure transducers to record the reflected pressure history. The measured blast signals were fitted to the Friedlander exponential profile as illustrated in Fig. 3.4 and derived using Eq. 4.

$$P(t) = P_{\max}\left(1-\frac{t-t_a}{t_d}\right)^{e^{-\gamma(t-t_a)/t_d}} \tag{4}$$

Where *P* is the pressure at time *t*, P_{max} is considered as the peak reflected pressure, P_r, t_a (*ms*) is the arrival time, t_d (*ms*) is the positive phase loading duration, while γ is the waveform coefficient which determines the rate of pressure decay. Moreover, the positive specific impulse, I_s, is evaluated through the integration of the pressure through the loading duration evaluated using Eq. 5. I_s is considered another influential parameter affecting the post-blast performance.

$$I_s = \int_{t_a}^{t_t+t_o} P(t)dt = P_{\max} t_0 \left(\frac{e^{-\gamma} + \gamma - 1}{\gamma^2} \right) \quad (5)$$

The wavefront parameters (P_r, I_s, t_d, γ) were calculated using the least-squares error through several strategies reported by Campidelli et al. (Campidelli et al. 2015b); however, P_r, and I_s are only reported in the current study, as presented in Table 3.3.

To validate the assumed experimental boundary conditions, an analytical SDOF model was used to predict the dynamic response of the six tested walls using different boundary conditions (i.e. simple-simple and fixed-fixed). To facilitate a direct comparison, the resistance functions of all the walls were derived based on the DIFs suggested by the USDOD (USDOD 2014). The DIF of the concrete compressive (used in the CMU) and reinforcement yielding strengths were taken as 1.19 and 1.17, respectively. The SDOF models were excited using an idealized linear wave simulating the recorded P_r and I_s, where t_d was calculated using Eq. (6).

$$t_d = \frac{2I_s}{P_r} \quad (6)$$

For the different boundary conditions, the SDOF model used the corresponding resistance functions as well as transformation factors (load-mass factors) (Biggs 1964). The load-mass factors (K_{LM}) were utilized to rigorously simplify the distributed mass and load/resistance into a SDOF model. Eq. 7 presents the equation of motion for the used SDOF model (Biggs 1964).

$$K_{LM} m\ddot{\Delta} + k\Delta = P(t) \quad (7)$$

Where m is the lumped mass and k is the wall stiffness, while $\ddot{\Delta}$ and Δ are the acceleration and displacement of the control point. Subsequently, the SDOF natural period (T) is calculated using Eq. 8.

$$T = 2\pi\sqrt{\frac{K_{LM}m}{k}} \tag{8}$$

Table 3.3 summarizes the predicted response of the SDOF for both boundary conditions (i.e. simple-simple and fixed-fixed). The SDOF hinged boundary condition predictions showed an average deviation of 1118% from the experimental results, while the fixed counterpart showed an average deviation of 114% . These results confirm that the walls were at least not purely-hinged as assumed while testing. As such, a fixed-fixed boundary condition was considered within the following analysis.

To allow for a direct comparison with the SDOF model, the developed concentrated plasticity model used the same DIFs as the SDOF while assuming linear blast waves, as shown in Fig. 3.4. The blast load was applied as a distributed load on the elastic beam-column elements following the fitted exponential time series. However, the masses of the RMSWs were lumped at the wall's center of gravity (i.e. at the middle node). As can be seen in Table 3.3, the developed model showed an average deviation of 123% from the experimental results. This entails the predictions proximity of the developed model with respect to the SDOF analytical model that is currently accepted by the blast design standards (USACE 2008; USDOD 2014).

3.4 PROPOSED ITERATIVE DYNAMIC MODEL

This section presents a sensitivity investigation for the influence of the DIFs on the response of the developed model. The DIFs for both the concrete and reinforcement were calculated based on the average strain rate, as shown in Eq. 2. Where (ε_p) for concrete is the concrete strain at the peak stress (concrete maximum stress/ concrete young's modulus), while ε_p for the steel reinforcement is the yielding strain (reinforcement yielding stress/ steel young's modulus). The t_p for both materials are assumed to be the time required by the concentrated rotational spring to reach the

yielding capacity (h_y). As such, to calculate the average strain rate of the concrete (ε'_c) and the reinforcement (ε'_{rft}) in the developed model, Eq. 2 can be rewritten as:

$$\varepsilon'_c = \frac{\varepsilon_c}{h_y} = \frac{f'_m / E_c}{h_y} \tag{9.a}$$

$$\varepsilon'_{rft} = \frac{\varepsilon_y}{h_y} = \frac{f_y / E_s}{h_y} \tag{9.b}$$

Where E_c and E_s are the concrete and reinforcement Young's modulus, respectively. The DIFs for both materials were applied in an iterative process through calculating the h_y, followed by updating the model elements (i.e. three springs and two elastic beam-column elements). This iterative process was performed using a proposed framework with an iterative subroutine, as shown in Fig. 3.5 (a, b). The framework started with the static properties of the tested component while ignoring the DIFs. More specifically, the initial spring properties were determined through a sectional fiber analysis as discussed earlier in the static model, while DIFs were assumed to be equal to 1.0. The performance of the concentrated spring was then monitored to check its yielding and also determine the h_y if applicable. Subsequently, the DIFs were calculated (i.e. using the relevant DIF models for the used materials), and then the spring properties were updated using the corresponding DIFs. Afterwards, dynamic analyses were performed using the updated springs in a loop manner using the proposed subroutine shown in Fig. 3.5b until the predefined number of iterations (n) was reached. Where n was selected to ensure the convergence/ stabilization of the calculated DIFs. Figure 3.6 illustrates the behavior wall L12 using the iterative framework (using the graphical DIF recommended by the *UFC 3-340*). Where the concrete compression DIF model was applied to the CMU, while the DIF model for Grade 60 yield reinforcement was used for the

vertical reinforcement. Figures 3.6 (a and b) demonstrate the behavior of the spring parameters (M_y, φ_y) at different iterations till convergence occurred, while Fig. 3.6(c) illustrates the spring yielding time (h_y). Figure 3.6(d) also shows the variation of the mid-height displacement during different iterations. At the first iteration, using the initial springs properties (i.e. no DIFs) (M_y = 5.14 kN.m and φ_y = 0.0024 rad/mm), the mid-height displacement was 99.5mm that led to spring yielding time of 1 $\times 10^{-6}$ s. Consequently, the spring properties were modified (M_y = 9.1 kN.m and φ_y = 0.0039 rad/mm) using the proposed subroutine that resulted in a smaller mid-height displacement of 52.5mm with subsequent spring yielding time of 3 $\times 10^{-6}$ s. Accordingly, the springs properties were modified (M_y = 8.8 kN.m and φ_y = 0.0049 rad/mm), while the spring yielding time was stabilized at 3 $\times 10^{-6}$ s with a corresponding mid-height displacement of 55.4mm, as shown in Fig. 6d.

3.4.1 Wall Blast Response Sensitivity to DIF

Although several studies have investigated the DIFs of the CMUs, presently, there is no consensus regarding the formulation used to evaluate such factors. Multiple researchers have applied the concrete DIF recommended by the CEB-FIP Model Code 1990 (Comite Euro-International du Beton) within the context of blast response prediction for RMSWs (Campidelli et al. 2016b; c; ElSayed et al. 2016; Smith et al. 2016). This is mainly due to the lack of literature on the DIFs of CMU prisms (Campidelli et al. 2016c). The CEB DIFs for both the average compressive strength ($DIF_{m\sigma}$) and concrete young's modulus (DIF_{mE}) are illustrated in Eqs. 10 (a and b) and Eq.11, respectively.

$$DIF_{m\sigma} = \left(\frac{\varepsilon'}{3\times10^{-6}} \right)^{1.016\delta_s}, \quad \varepsilon' \le 30 \tag{10.a}$$

$$DIF_{m\sigma} = \beta_s \left(\frac{\varepsilon'}{3\times10^{-6}} \right)^{1/3}, \quad \varepsilon' > 30 \tag{10.b}$$

Where

$$\beta_s = 10^{7.112\delta_s - 2.33} \; ; \quad \delta_s = \frac{1}{10 + 6\, f_m^{'} / 10}$$

$$DIF_{mE} = \left(\frac{\varepsilon^{'}}{3 \times 10^{-6}} \right)^{0.026} \tag{11}$$

However, the use of the concrete DIF disregards the interaction between the masonry components (i.e. masonry units and mortar) and subsequently ignores the orthotropic nature of masonry walls (Wu and Hao 2006). As such different studies accounted for the masonry orthotropic nature through considering both the masonry units and mortar (Rafsanjani et al. 2015b; Wei and Hao 2009; Zucchini and Lourenço 2004). In this context, Wei and Hao 2009 proposed a homogenized formulation for the masonry DIF through considering both the masonry units/mortar and their subsequent interaction as shown in Eqs. 12 (a and b). Where Eq. 12 represents the homogenized $DIF_{m\sigma}$ (normal to the bed joint), while Eq. 13 (a and b) are for the DIF_{mE} considering the same direction of the continuous approach (Wei and Hao 2009).

$$DIF_{m\sigma} = 1.114 + 0.038 \log_{10}(\varepsilon'), \qquad \varepsilon \le 3.55 \tag{12.a}$$

$$DIF_{m\sigma} = 1.1338 - 0.3417 \log_{10}(\varepsilon') + 0.6247 \left(\log_{10}(\varepsilon') \right)^2, \qquad \varepsilon > 3.55$$

(12.b)

$$DIF_{mE} = 1.01 + 0.0033 \log_{10}(\varepsilon'), \qquad \varepsilon \le 3.08 \tag{13.a}$$

$$DIF_{mE} = 1.0266 - 0.2196\log_{10}(\varepsilon') + 0.3854\left(\log_{10}(\varepsilon')\right)^2, \qquad \varepsilon > 3.08$$

(13.b)

In this respect, the developed framework including the proposed subroutine evaluated the response of wall L12 using different CMU DIFs. The iterative model adopted the concrete DIF recommended by the CEB and the homogenized masonry DIF proposed by Wei and Hao (Béton 1990; Wei and Hao 2009). On the other side, the DIF for the reinforcement steel, proposed by Malvar (Eq. 14), was used in both scenarios due to its wide range of applications (El-Dakhakhni et al. 2009; Malvar 1998). The steel DIFs were applied to the yield (DIF_{fy}) and ultimate (DIF_{fu}) strengths based on the corresponding power used, as presented in Eq. 15 (a and b).

$$DIF_{fx} = \left(\frac{\varepsilon'}{10^{-4}}\right)^{\alpha_x} \tag{14}$$

$$\alpha_y = 0.074 - 0.04\frac{f_y}{414} \tag{15.a}$$

$$\alpha_u = 0.019 - 0.009\frac{f_y}{414} \tag{15.b}$$

The sensitivity assessment was performed based on a triangular blast wave through a constant impulse but different peak pressure demands. The sensitivity criterion, constant I_s with a variable P_r, was selected to conceptualize the influence of loading duration variability as it has been claimed to significantly influence the DIF (USDOD 2014). The I_s was selected to match the observed impulse in the field test for wall L12 (699 kPa.ms). Figure 3.7 demonstrates the sensitivity of Wall L12 response using the developed and SDOF models with fixed DIFs recommended by the

blast standards (USDOD 2014), ($DIF_{m\sigma}$ = 1.19; DIF_{fy} = 1.17). The figure also shows the dynamic response of Wall L12 using the iterative models while adopting the CEB (Béton 1990) and Wei and Hao (2009) DIFs. As can be seen in the figure, all the models overestimated the mid-height displacement of wall L12 at P_r = 866 kPa; however, both iterative models (using the CEB and Wei and Hao DIFs) showed better predictions than that using fixed DIFs, which is also numerically illustrated in Table 3.3.

Figure 3.7 illustrates that both iterative models are sensitive to P_r before the wall response plateaus at high P_r demands (i.e. approximately 400 kPa). This behavior is mainly attributed to the different loading regimes (i.e. impulsive, dynamic, and quasi-static). Where at low P_r demands, longer loading duration (i.e. given a constant I_s), the wall response tends towards the quasi-static regime which is influenced only by the P_r. On the other side, at higher P_r demands, shorter loading duration (i.e. given a constant I_s), the wall response plateaus as being a function solely in I_s (representing the impulsive region). On the contrary, both fixed DIF models are not able to capture the influence of the loading duration on the wall response through the different loading regimes, as can be seen from the monotonic response increase in Fig. 3.7.

It is worth mentioning that the variation of the CMU DIFs at different ε' values (i.e. Eqs. 10 to 13) influenced both iterative models. As can be seen in Fig. 3.7, at low P_r demands, large h_y values were recorded (i.e. longer time to reach spring yield) and thus small ε'. This small ε' resulted in relatively small DIFs (i.e. Eqs 10.a; 12a; and 13a) and thus the wall displacements increased with the corresponding increase of P_r. At higher P_r demands, the h_y values decreased significantly leading to large ε', which abruptly increased the DIFs (i.e. Eqs 10.b; 12b; and 13b). Subsequently, the wall stiffness increased and the corresponding displacements decreased before plateauing trend occurred, as shown in Fig. 3.7.

The proposed iterative model through Wei and Hao DIFs (Wei and Hao 2009) was used in the current study to validate the tested six walls (blast database) using the recorded P_r and I_s. The blast waves were applied using both the idealized linear path and the exponential Friedlander (while accounting for the measured t_d as well) to investigate the influence of the wave shape on the dynamic response of the tested RMSWs. Table 3.3 summarizes the iterative model deviation from the experimental results for both wave shapes. The iterative model using a linear path showed an average deviation of 39% (c.o.v. = 6%), while the exponential Friedlander wave showed an average deviation of 29% (c.o.v. = 5%). As can be seen in Table 3.3, these results can be considered acceptable compared to those form the simplified SDOF accepted by the current blast standards (ASCE 2011; CSA 2012; USDOD 2014).

3.4.2 Blast Wavefront Uncertainty Influence on Wall Response

This section investigates the influence of the uncertainty/variability associated with P_r and I_s on the blast response of RMSWs while accounting for the uncertainty in P_r and I_s. The investigation was achieved using a pseudo-random sample through a Monte Carlo simulation using the proposed iterative model (using Wei and Hao (2009) DIFs). As such, a blast wave simplification (i.e. linear path) was assumed for comparison to facilitate the probabilistic assessment. The uncertainties associated with P_r and I_s were derived through applying the method of moments to fit the wavefront uncertainty parameters from the literature (Campidelli et al. 2015b). Where the P_r was fitted for a gamma distribution with a mean of 0.99 and a c.o.v. of 0.18, while the I_s was fitted to a normal distribution of a mean of 1.01 and a c.o.v. of 0.19 (Campidelli et al. 2015b). Figures 3.8 (a and b) show the influence of changing P_r and I_s, respectively, while considering their associated uncertainties. Figure 3.8a presents the influence of changing the mean P_r from 50 to 500 kPa while maintaining the mean I_s to 1000 kPa.ms. Figure 3.8a shows a similar trend as Fig. 3.7, where the wall response is sensitive to P_r at low P_r values (i.e. till 250 kPa) before it plateaus at higher pressure

values. Figure 3.8b represents the influence of changing the I_s (ranging from 200-1000 kPa.ms), while holding P_r to 500 kPa. Figure 3.8b demonstrates the unlimited propagation of wall's response when I_s is increased. This is attributed to high interdependency between the structural response and the load impulse loaded within the impulsive regime that is proven within the fundamentals of dynamics (Chopra 2016). As can be seen in tables. 3.8 (a and b), it is clear that both P_r and I_s parameters influence the probabilistic blast response of RMSWs. As such, a fragility surface that represents the probability of reaching a specific damage state while accounting for both P_r and I_s, as presented in Eq. 16 (Parisi 2015), will be presented.

$$P_f = \mathrm{P}_r\left[G(X) < DS \mid I_s, P_r\right] \tag{16}$$

Where *G(X)* is the blast response of the tested component. Figure 3.9a shows the fragility surface of Wall L12 considering the moderate damage state (DS2) (chord rotation "θ" =2°) (ASCE 2011; CSA 2012), while Figures 3.9 (b, c, and d) present the three projections (i.e. elevation, side view and plan) for the same wall fragility surface. From these figures, the fragility surface can be considered the natural extension of the deterministic-based P-I diagrams that can facilitate probabilistic blast risk assessment. More specifically, Figs. 3.9 (b and c) show the probabilistic envelope for Wall L12 through the variation of P_r and I_s, respectively. Both figures also illustrate the unsymmetrical probabilistic blast performance that clearly highlights the importance of considering both P_r and I_s. Furthermore, Fig. 3.9d shows the influence of P_r and I_s on the probabilistic blast performance of Wall L12, where this figure reveals a new dimension to the typical P-I diagrams through the probability contour lines. For example, the probability of exceeding the moderate damage state (DS2) at P_r of 150 kPa and I_s of 500 kPa.ms is 57%. Such probability cannot be established by typical P-I diagrams due to their deterministic nature (e.g. either exceeding the considered DS or not).

3.4.3 Axial Load Effect on Wall Response

As mentioned earlier, the current study aims to investigate the influence of the axial stress levels on the blast performance of RMSWs with different vertical reinforcement ratios. The lack of studies investigating the axial stress in literature has resulted from the difficulty of applying a constant axial stress simultaneously while subjecting a wall to blast loading (ElSayed et al. 2015b). Reinforcement ratio is important to investigate due to its expected influence on the walls' out-of-plane dynamic response (ElSayed et al. 2016). The investigation is demonstrated through developing fragility curves for the tested walls (i.e. used earlier in the static validation section), considering DS2 only. The fragility curves are presented using I_s as the main intensity measure at different P_r values, as shown in Figs. 10 (a to d). The fragility curves were selected in the current section rather than fragility surfaces to visually clarify the influence of the tested parameters. Figures 3.10 (a to d) show similar trends, where the axial stress level is inversely proportional to the probability of exceeding DS2. For example, at I_s =800 kPa.ms, the probabilities of exceeding DS2 for Wall FH-15 are 0.85 and 0.36 at P_r= 250 kPa and 2,000 kPa, respectively, while these probabilities for Wall FH-00 are 0.90 and 0.87. The higher probabilities at low pressure values are attributed to the low stiffness of the wall due to the small DIFs, as explained earlier. Furthermore, similar observations can also be depicted for different reinforcement ratios, as illustrated by comparing Walls FM-00 and FM-10. It is also worth mentioning that the probability of exceeding DS2 is inversely proportional to the vertical reinforcement ratio. For example, the probability of exceeding DS2 is reduced by 60% when the vertical reinforcement ratio is increased from 0.62 to 1.07 (i.e. comparing Wall FM-00 to Wall FH-00) at P_r =500 kPa and I_s =700 kPa.ms. It should be noted that these conclusions are limited to the tested parameters range (i.e. axial load and vertical reinforcement ratio), which covers the flexurally dominated out-of-plane RMSWs performance.

3.5 CONCLUSION

The current study focused on evaluating the blast performance of load-bearing reinforced masonry shear walls (RMSWs) in order to subsequently assess the influence of wavefront parameters uncertainty on these walls. As such, a concentrated plasticity model was developed and first statically validated using previous experimental results considering different boundary conditions, axial load levels, and vertical reinforcement ratios. The model was capable of reasonably well mimicking the wall's out-of-plane key points (i.e. elastic and ultimate), with an average deviation of 11% from the reported results.

The developed model was then validated to simulate the blast response of RMSWs by using dynamic increase factors (DIFs). Comparing the model predictions to the results of experimentally tested RMSWs subjected to far-field explosions and to an analytical single degree of freedom model, showed a good agreement. Moreover, a blast OpenSees simulation (BOSS) framework was proposed to include a computational subroutine to facilitate the iterative calculations of the DIFs. The proposed framework was used to assess the influence of the blast wavefront parameters variability on the response of the RMSWs. The model was also applied to evaluate the influence of the wave shape idealization using an exponential Friedlander wave and a linear wave path. The exponential wave showed better predictions with an average deviation of 29%, compared to 39%, when the linear wave path was adopted. Furthermore, the BOSS was also applied to investigate the sensitivity of RMSWs blast response to the wavefront parameters uncertainties. The relevant results were presented as fragility surfaces to visualize RMSWs probabilistic blast response at different loading regimes.

Finally, the influence of the axial stress level on the blast response of RMSWs with different vertical reinforcement rations was presented. The probabilistic assessment was presented through the fragility curves at different axial stress demands. The fragility curves showed similar trends for

the influence of the axial stress levels and the vertical reinforcement ratios on the blast performance of RMSWs. More specifically, the axial stress level and the vertical reinforcement ratio were found to be in an inverse relationship to the predicted deformations.

Although the current study presented an investigation for the influence of axial load level on RMSW blast response within a practical range, 0-15% of the compressive axial strength, additional investigations are still required to cover a wider range of axial load levels. Furthermore, additional parametric investigations, covering a wider geometric and strength spectrum, are still needed to provide a reliable database for RMSWs blast response which can be achieved using the comprehensively elaborated model.

3.6 ACKNOWLEDGMENTS

Financial support has been provided through a Collaborative Research and Development Grant funded by the Natural Sciences and Engineering Research Council (NSERC) of Canada. Industrial support has been provided by the Canadian Concrete Masonry Producers Association (CCMPA) and the Canada Masonry Design Centre (CMDC). Additional support has been provided through the McMaster University Institute for Multi-Hazard Systemic Risk Studies.

3.7 NOTATION

The following symbols are used in this paper:

$\Delta^{\cdot\cdot}$ = acceleration at the control point;

Δ = displacement at the control point;

A_e = effective cross section area;

A_g = gross cross section area;

DIF_{fu} = dynamic increase factor for the reinforcement steel ultimate strength;

DIF_{fy} = dynamic increase factor for the reinforcement steel yielding strength;

DIF_{mE} = dynamic increase factor for the compressive young's modulus;

$DIF_{m\sigma}$ = dynamic increase factor for the average compressive strength;

E_c = concrete young's modulus;

E_s = reinforcement steel young's modulus;

f_m' = masonry average compressive strength;

f_y = vertical reinforcement yield strength;

h_y = time required by the concentrated hinge to yield;

I_e = effective moment of inertia;

I_g = gross moment of inertia;

I_s = positive specific impulse;

k = wall stiffness;

K_{LM} = load-mass factor;

m = lumped mass;

M_y = concentrated spring yielding capacity;

$P(t)$ = pressure at time t;

P_A = axial load;

P_{max} = maximum pressure;

P_r = positive reflected pressure;

R = standoff distance;

T = natural period;

t_a = arrival time;

t_d = positive phase loading duration;

t_p = time required by the material to reach the plastic stain;

W = equivalent charge weight;

Z = scaled distance;

α = reduction factor;

γ = waveform coefficient;

ε' = average strain rate;

$\dot{\varepsilon}_c$ = concrete average strain rate;

$\dot{\varepsilon}_{rft}$ = reinforcement steel average strain rate;

ε_p = plastic strain; and

φ_y = concentrated spring curvature capacity.

3.8 REFERENCES

Al-Habahbeh, O., and Stewart, M. (2015). "Stochastic reliability of unreinforced masonry walls subjected to blast." *The Sixth Jordanian International Civil Engineering Conference*, Amman, Jordan.

ASCE. (2011). *Blast Protection of Buildings*. *ASCE 59-11*, (American Society of Civil Engineers, ed.), American Society of Civil Engineers, Reston, VA, VA.

Béton, C. E.-I. du. (1990). "CEB-FIP model code 1990.pdf."

Biggs, J. (1964). *Introduction to structural dynamics*. McGraw-Hill College, New York.

BIPS-05. (2011). *Preventing Structures from Collapsing to Limit Damage to Adjacent Structures and Additional Loss of Life when Explosives Devices Impact Highly Populated Urban Centers*.

Bozer, A. (2017). "Effect of modelling parameters on non-linear seismic response of concrete structures." *Proceedings of the Institution of Civil Engineers - Structures and Buildings*, Thomas Telford Ltd, 170(12), 901–916.

Browning, R. S., Dinan, R. J., and Davidson, J. S. (2014). "Blast Resistance of Fully Grouted Reinforced Concrete Masonry Veneer Walls." *Journal of Performance of Constructed Facilities*, 28(2), 228–241.

Browning, R. S., Hoemann, J. M., and Davidson, J. S. (2011). "Large-Deflection Response of Fully Grouted Reinforced Masonry Walls to Static and Dynamic Out-of-Plane Pressure." *ACI special publication*, 281, 1–20.

Campidelli, M., El-Dakhakhni, W., Tait, M., and Mekky, W. (2016a). "Probabilistic risk assessment of masonry buildings exposed to improvised explosive devices." *Brick and*

Block Masonry, CRC Press, 959–966.

Campidelli, M., El-Dakhakhni, W., Tait, M., and Mekky, W. (2016b). "Risk– driven fragility evaluation of reinforced concrete block walls subjected to blast hazard." *Brick and Block Masonry*, CRC Press, 967–975.

Campidelli, M., El-Dakhakhni, W. W., Tait, M. J., and Mekky, W. (2015a). "Blast Design-Basis Threat Uncertainty and Its Effects on Probabilistic Risk Assessment." *ASCE-ASME Journal of Risk and Uncertainty in Engineering Systems, Part A: Civil Engineering*, 1(4), 04015012.

Campidelli, M., El-Dakhakhni, W. W., Tait, M. J., and Mekky, W. (2017). "Resilience of Masonry Systems in Nuclear Power Plants Under Blast Risk." *Volume 4: Fluid-Structure Interaction*, ASME, Waikoloa, Hawaii, V004T04A020.

Campidelli, M., Tait, M. J., El-Dakhakhni, W. W., and Mekky, W. (2015b). "Inference of Blast Wavefront Parameter Uncertainty for Probabilistic Risk Assessment." *Journal of Structural Engineering*, 141(12), 04015062.

Campidelli, M., Tait, M. J., El-Dakhakhni, W. W., and Mekky, W. (2016c). "Numerical strategies for damage assessment of reinforced concrete block walls subjected to blast risk." *Engineering Structures*, 127, 559–582.

Chang, G., and Mander, J. (1994). "Seismic Energy Based Fatigue Damage Analysis of Bridge Columns: Part I - Evaluation of Seismic Capacity." *(NCEER) Technical Report 94-0006*.

Chopra, A. K. (2016). *Dynamics of Structures*. Pearson.

CSA. (2012). *CSA S850-12 Design and assessment of buildings subjected to blast loads*. Canadian Standards Association, Mississauga, ON, Canada.

Cui, J., Shi, Y., Li, Z., and Chen, L. (2015). "Failure Analysis and Damage Assessment of RC Columns under Close-In Explosions." *Journal of Performance of Constructed Facilities*, 29(5), B4015003.

Dides, M. A., and de la Llera, J. C. (2005). "A comparative study of concentrated plasticity models in dynamic analysis of building structures." *Earthquake Engineering & Structural Dynamics*, 34(8), 1005–1026.

Eamon, C. D., Baylot, J. T., and O'Daniel, J. L. (2004). "Modeling Concrete Masonry Walls Subjected to Explosive Loads." *Journal of Engineering Mechanics*, 130(9), 1098–1106.

El-Dakhakhni, W. W., Changiz Rezaei, S. H., Mekky, W. F., and Razaqpur, A. G. (2009). "Response sensitivity of blast-loaded reinforced concrete structures to the number of degrees of freedomThis article is one of a selection of papers published in the Special Issue on Blast Engineering." *Canadian Journal of Civil Engineering*, 36(8), 1305–1320.

El-Dakhakhni, W. W., Mekky, W. F., and Rezaei, S. H. C. (2010). "Validity of SDOF Models for Analyzing Two-Way Reinforced Concrete Panels under Blast Loading." *Journal of Performance of Constructed Facilities*, 24(4), 311–325.

ElSayed, M., Campidelli, M., El-Dakhakhni, W., and Tait, M. (2015a). "Simplified Framework for Blast-Risk-Based Cost-Benefit Analysis for Reinforced Concrete-Block Buildings." *Journal of Performance of Constructed Facilities*, 04015077(13), 04015077.

ElSayed, M., El-Dakhakhni, W., and Tait, M. (2015b). "Response Evaluation of Reinforced Concrete Block Structural Walls Subjected to Blast Loading." *Journal of Structural Engineering*, 141(11), 04015043.

ElSayed, M., El-Dakhakhni, W., and Tait, M. (2016). "Resilience Evaluation of Seismically

Detailed Reinforced Concrete-Block Shear Walls for Blast-Risk Assessment." *Journal of Performance of Constructed Facilities*, 30(4), 04015087.

Ezell, B. C., Bennett, S. P., von Winterfeldt, D., Sokolowski, J., and Collins, A. J. (2010). "Probabilistic Risk Analysis and Terrorism Risk." *Risk Analysis*, 30(4), 575–589.

Ezzeldin, M., El-Dakhakhni, W., and Wiebe, L. (2018). "Reinforced Masonry Building Seismic Response Models for ASCE/SEI-41." *Journal of Structural Engineering*, 144(1), 04017175.

Ezzeldin, M., Wiebe, L., and El-Dakhakhni, W. (2016). "Seismic Collapse Risk Assessment of Reinforced Masonry Walls with Boundary Elements Using the FEMA P695 Methodology." *Journal of Structural Engineering*, 142(11), 04016108.

Ezzeldin, M., Wiebe, L., Shedid, M., and El-Dakhakhni, W. (2014). "Numerical Modelling of Reinforced Concrete Block Structural Walls Under Seismic Loading." *9th International Masonry Conference*, Guimarães.

FEMA-426. (2011). *BIPS 06/FEMA 426: Reference Manual to Mitigate Potential Terrorist Attacks against Buildings*. U.S. Department of Homeland Security.

Grant, M., and Stewart, M. G. (2012). "A systems model for probabilistic risk assessment of improvised explosive device attacks." *International Journal of Intelligent Defence Support Systems*, 5(1), 75.

Grant, M., and Stewart, M. G. (2015). "Probabilistic Risk Assessment for Improvised Explosive Device Attacks That Cause Significant Building Damage." *Journal of Performance of Constructed Facilities*, 29(5), B4014009.

Hayman, M. (2014). "Response of one-way reinforced masonry flexural walls under blast loading." McMaster University, Hamilton, ON, Canada.

Hoemann, J. M., Shull, J. S., Salim, H. H., Bewick, B. T., and Davidson, J. S. (2015). "Performance of Partially Grouted, Minimally Reinforced CMU Cavity Walls against Blast Demands. II: Performance under Impulse Loads." *Journal of Performance of Constructed Facilities*, 29(4), 04014114.

Karlos, V., Solomos, G., and Larcher, M. (2017). "Probabilistic analysis of steel columns under blast induced loads." *EUROSTEEL*, Copenhagen, Denmark, 3960–3969.

LaFree, G., and Legault, R. (2009). *Developing An Empirical Understanding of Improvised Explosive Devices: A Social and Behavioral Science Perspective*. College Park, MD.

Malvar, L. J. (1998). "Review of static and dynamic properties of steel reinforcing bars." *ACI Materials Journal*, 95(5), 609–616.

Marjanishvili, S. M. (2004). "Progressive Analysis Procedure for Progressive Collapse." *Journal of Performance of Constructed Facilities*, 18(2), 79–85.

Mayrhofer, C. (2002). "Reinforced masonry walls under blast loading." *International Journal of Mechanical Sciences*, 44(6), 1067–1080.

McKenna, F., Fenves, G., and Scott, M. (2000). "Open System for Earthquake Engineering Simulation." University of California, Berkeley, CA.

Mueller, J., Stewart, M. G., and Hayes, W. (2011). *Terror, security, and money: Balancing the risks, benefits, and costs of homeland security*. New York.

National Research Council. (2010). *Review of the Department of Homeland Security's Approach to Risk Analysis*. National Academies Press, Washington, D.C.

Oesterle, M. G., Hegemier, G. A., and Morrill, K. B. (2009). "Response of Concrete Masonry

Walls to Simulated Blast Loads." *Structures Congress 2009*, American Society of Civil Engineers, Reston, VA, 1–10.

Olmati, P., Petrini, F., and Gkoumas, K. (2014). "Fragility analysis for the Performance-Based Design of cladding wall panels subjected to blast load." *Engineering Structures*, 78, 112–120.

Olmati, P., Petrini, F., Vamvatsikos, D., and Gantes, C. (2016). "Simplified fragility-based risk analysis for impulse governed blast loading scenarios." *Engineering Structures*, 117, 457–469.

Papadopoulos, V., and Fragiadakis, M. (2015). "Plastic Hinge and Plastic Zone Seismic Analysis of Frames." *Encyclopedia of Earthquake Engineering*, Springer Berlin Heidelberg, Berlin, Heidelberg, 1926–1933.

Parisi, F. (2015). "Blast fragility and performance-based pressure–impulse diagrams of European reinforced concrete columns." *Engineering Structures*, Elsevier, 103, 285–297.

Parisi, F., and Augenti, N. (2012). "Influence of seismic design criteria on blast resistance of RC framed buildings: A case study." *Engineering Structures*, Elsevier, 44, 78–93.

Park, G.-K., Kwak, H.-G., and Filippou, F. C. (2017). "Blast Analysis of RC Beams Based on Moment-Curvature Relationship Considering Fixed-End Rotation." *Journal of Structural Engineering*, 143(9), 04017104.

Paulay, T., and Priestley, M. (1992). *Seismic design of reinforced concrete and masonry buildings*. Wiley, New York.

Rafsanjani, S. H., Lourenço, P. B., and Peixinho, N. (2015a). "Dynamic interface model for masonry walls subjected to high strain rate out-of-plane loads." *International Journal of*

Impact Engineering, 76, 28–37.

Rafsanjani, S. H., Lourenço, P. B., and Peixinho, N. (2015b). "Implementation and validation of a strain rate dependent anisotropic continuum model for masonry." *International Journal of Mechanical Sciences*, Pergamon, 104, 24–43.

Salem, S., Campidelli, M., El-Dakhakhni, W. W., and Tait, M. J. (2017a). "Resilience-based design of urban centres: application to blast risk assessment." *Sustainable and Resilient Infrastructure*, 1–18.

Salem, S., Campidelli, M., Tait, M., and El-Dakhakhni, W. (2017b). "Probabilistic Resilience Framework for Blast Resistant Infrastructure." *Engineering Mechanics Institute Conference*, Y. Bazilevs and J. S. Chen, eds., San Diego, California, USA.

Salem, S., El-Dakhakhni, W., and Tait, M. (2016). "Resilience-based design of reinforced masonry wall buildings under blast loading." *Brick and Block Masonry: Trends, Innovations and Challenges - Proceedings of the 16th International Brick and Block Masonry Conference, IBMAC 2016*.

Salem, S., Ezzeldin, M., El-Dakhakhni, W., and Tait, M. (2018). "Out-of-Plane Behavior of Load-Bearing Reinforced Masonry Shear walls." *Journal of Structural Engineering*, Submitted.

Shedid, M. T., Drysdale, R. G., and El-Dakhakhni, W. W. (2008). "Behavior of Fully Grouted Reinforced Concrete Masonry Shear Walls Failing in Flexure: Experimental Results." *Journal of Structural Engineering*, American Society of Civil Engineers, 134(11), 1754–1767.

Shi, Y., and Stewart, M. G. (2015). "Damage and risk assessment for reinforced concrete wall

panels subjected to explosive blast loading." *International Journal of Impact Engineering*, Pergamon, 85, 5–19.

Shin, J., Whittaker, A. S., and Cormie, D. (2015). "Incident and Normally Reflected Overpressure and Impulse for Detonations of Spherical High Explosives in Free Air." *Journal of Structural Engineering*, 141(12), 04015057.

Smilowitz, R. (2013). "vulnerability assessment in urban streetscapes." *Safety, Reliability, Risk, Resilience and Sustainability of Structures and Infrastructure*, G. Deodatis, B. R. Ellingwood, and D. M. Frangopol, eds., Taylor & Ftancis Group, London, England, 2757–2760.

Smith, N. L., Tait, M. J., El-Dakhakhni, W. W., and Mekky, W. F. (2016). "Response Analysis of Reinforced Concrete Block Infill Panels under Blast." *Journal of Performance of Constructed Facilities*, 30(6), 04016059.

START. (2016). "Global Terrorism Database [Data file]." *National Consortium for the Study of Terrorism and Responses to Terrorism (START)*, <http://www.start.umd.edu/gtd/>.

Stewart, M. G. (2008). "Cost Effectiveness of Risk Mitigation Strategies for Protection of Buildings against Terrorist Attack." *Journal of Performance of Constructed Facilities*, 22(April), 115–120.

Stewart, M. G. (2010). "Risk-informed decision support for assessing the costs and benefits of counter-terrorism protective measures for infrastructure." *International Journal of Critical Infrastructure Protection*, Elsevier B.V., 3(1), 29–40.

Stewart, M. G., and Netherton, M. D. (2008). "Security risks and probabilistic risk assessment of glazing subject to explosive blast loading." *Reliability Engineering & System Safety*, 93(4),

627–638.

Stewart, M. G., Netherton, M. D., and Rosowsky, D. V. (2006). "Terrorism Risks and Blast Damage to Built Infrastructure." *Natural Hazards Review*, American Society of Civil Engineers, 7(3), 114–122.

Thiagarajan, G., Rahimzadeh, R., and Kundu, A. (2013). "Study of Pressure-Impulse Diagrams for Reinforced Concrete Columns Using Finite Element Analysis." *International Journal of Protective Structures*, 4(4), 485–504.

USACE, U. A. C. of E. (2008). *User's Guide for the Single-Degree-of-Freedom Blast Effects Design Spreadsheets (SBEDS)*. USACE, ACE Protective Design Centre, USA, PDC TR-06-01 Rev 1, Omaha, NE., NE.

USDOD, (U.S. Department of Defense). (2014). *Structures to Resist the Effects of Accidental Explosions*. *Unified Facilities Criteria 3-340-02*, Washington D.C.

Wei, X., and Hao, H. (2009). "Numerical derivation of homogenized dynamic masonry material properties with strain rate effects." *International Journal of Impact Engineering*, Pergamon, 36(3), 522–536.

Wu, C., and Hao, H. (2006). "Derivation of 3D masonry properties using numerical homogenization technique." *International Journal for Numerical Methods in Engineering*, Wiley-Blackwell, 66(11), 1717–1737.

Zucchini, A., and Lourenço, P. B. (2004). "A coupled homogenisation–damage model for masonry cracking." *Computers & Structures*, Pergamon, 82(11–12), 917–929.

Table 3.1: Details of the static database

Wall	Dimension (W x H x t) (mm)	Vertical reinforcement			Horizontal reinforcement		f_m' *(MPa)*	$P_A/A_g f_m'$ *(%)*	Boundary condition
		Number and size	ρ_v (%)	f_y *(MPa)*	Size and spacing	ρ_h (%)			
SL-00	3568 x 2946 x 200	4 # 5 (4x200 mm^2)	0.11	550	MW18 every other course (18mm^2 @ 400mm)	0.28	20.1	0.0	Simple-Simple
FM-00	1420 x 1500 x 90	6 # 3 (6x71 mm^2)	0.33	459	D4 every other course (25mm^2 @ 200mm)	0.14	13.5	0.0	Fixed-Fixed
FM-10	1420 x 1500 x 90	6 # 3 (6x71 mm^2)	0.33	459	D4 every other course (25mm^2 @ 200mm)	0.14	13.5	10.0	Fixed-Fixed
FH-00	1420 x 1500 x 90	6 # 4 (6x129 mm^2)	0.61	436	D4 every other course (25mm^2 @ 200mm)	0.14	13.5	0.0	Fixed-Fixed
FH-05	1420 x 1500 x 90	6 # 4 (6x129 mm^2)	0.61	436	D4 every other course (25mm^2 @ 200mm)	0.14	13.5	5.0	Fixed-Fixed
FH-10	1420 x 1500 x 90	6 # 4 (6x129 mm^2)	0.61	436	D4 every other course (25mm^2 @ 200mm)	0.14	13.5	10.0	Fixed-Fixed
FH-15	1420 x 1500 x 90	6 # 4 (6x129 mm^2)	0.61	436	D4 every other course (25mm^2 @ 200mm)	0.14	13.5	15.0	Fixed-Fixed

Table 3.2: Details of the walls tested under blast

Wall	Vertical reinforcement			Horizontal reinforcement		*Charge weight (TNT eqv.) (kg)*	Scaled distance Z ($m/kg^{1/3}$)	Δ_{exp} *(mm)*
	Number and size	ρ_v (%)	f_y *(MPa)*	Size and spacing	ρ_h (%)			
L6	15 D4 (15x26 mm^2)	0.62	476	W1.7 every course ($11mm^2$ @ 63.3mm)	0.26	6	2.75	16.0
L12	15 D4 (15x26 mm^2)	0.62	476	W1.7 every course ($11mm^2$ @ 63.3mm)	0. 26	12	2.18	37.4
L30	15 D4 (15x26 mm^2)	0.62	476	W1.7 every course ($11mm^2$ @ 63.3mm)	0. 26	30	1.61	173.9
H6	15 D7 (15x45 mm^2)	1.07	484	W1.7 every course ($11mm^2$ @ 63.3mm)	0. 26	6	2.75	14.3
H12	15 D7 (15x45 mm^2)	1.07	484	W1.7 every course ($11mm^2$ @ 63.3mm)	0. 26	12	2.18	18.0
H30	15 D7 (15x45 mm^2)	1.07	484	W1.7 every course ($11mm^2$ @ 63.3mm)	0. 26	30	1.61	50.5

Table 3.3: Wall Dynamic response predictions

Wall	Reflected pressure P_r (kPa)	Specific impulse *Is* (kPa.ms)	Δ_{exp}	$\Delta_{SDOF,\ hinged}$	$\Delta_{SDOF,\ fixed}$	$\Delta_{proposed,\ fixed\ DIF,\ linear\ wave}$	$\Delta_{proposed,\ linear\ wave}$	$\Delta_{proposed,\ Friedlander\ wave}$	Deviation from the experimental results (%)				
									$\Delta_{SDOF,hinged}$	$\Delta_{SDOF,\ fixed}$	$\Delta_{proposed,\ fixed\ DIF,\ linear\ wave}$	$\Delta_{proposed,\ linear\ wave}$	$\Delta_{proposed,\ Friedlander\ wave}$
L6	406	439	16.00	179.15	31.44	33.45	22.60	18.27	1,020	97	109	41	14
L12	866	699	37.40	467.10	79.92	84.3	52.50	50.65	1,149	114	125	40	35
L30	1922	1281	173.90	1588.16	268.42	304.51	186.00	182.30	813	54	75	7	5
H6	328	397	14.30	117.60	22.00	19.34	20.50	19.00	722	54	35	43	33
H12	687	579	18.00	255.05	45.90	43.51	25.80	24.10	1,317	155	142	43	34
H30	2785	1076	50.50	901.60	157.37	176.99	79.20	76.40	1,685	212	250	57	51
Average (%)									1,118	114	123	39	29
c.o.v.(%)									3,941	70	90	6	5

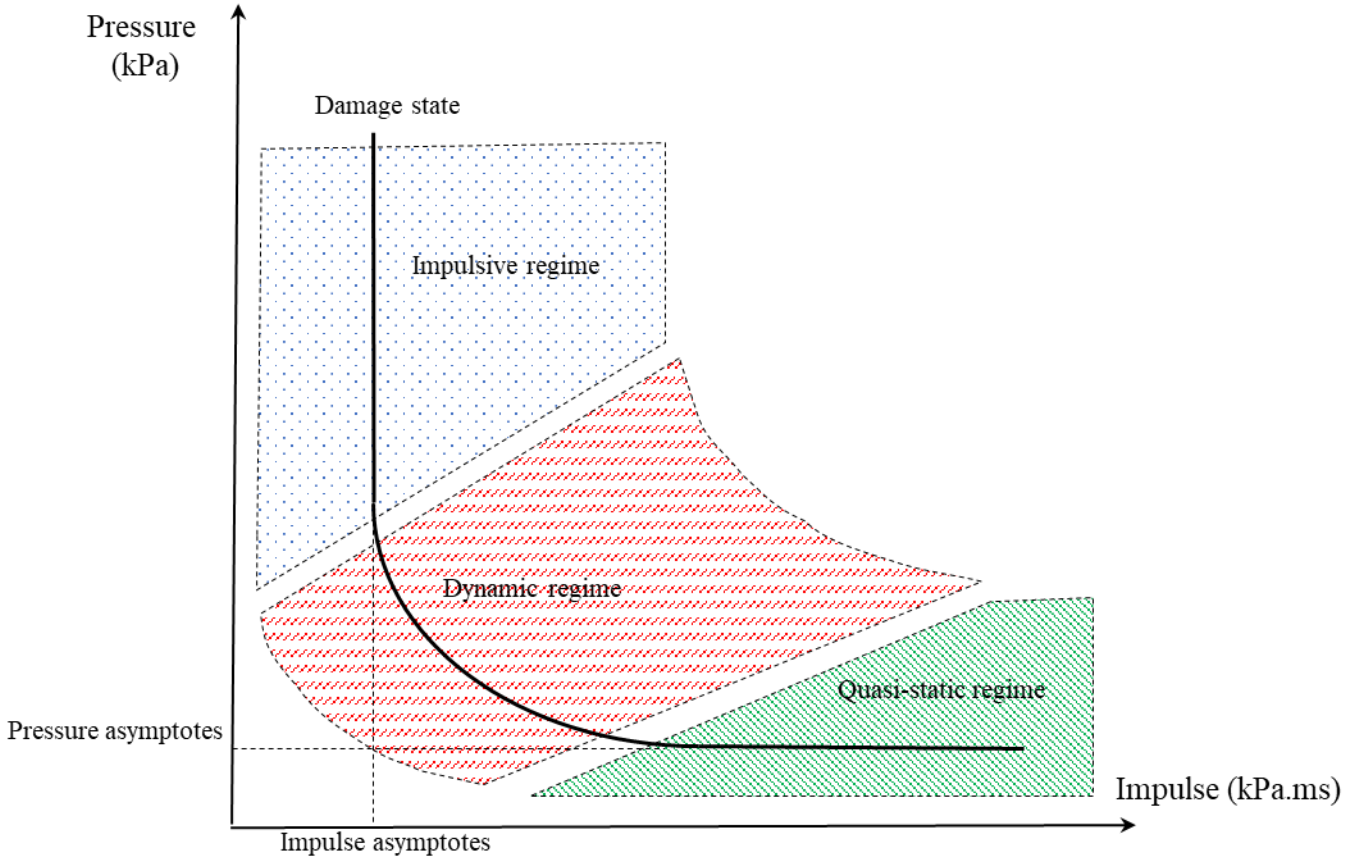

Figure 3.1: Pressure-Impulse diagram

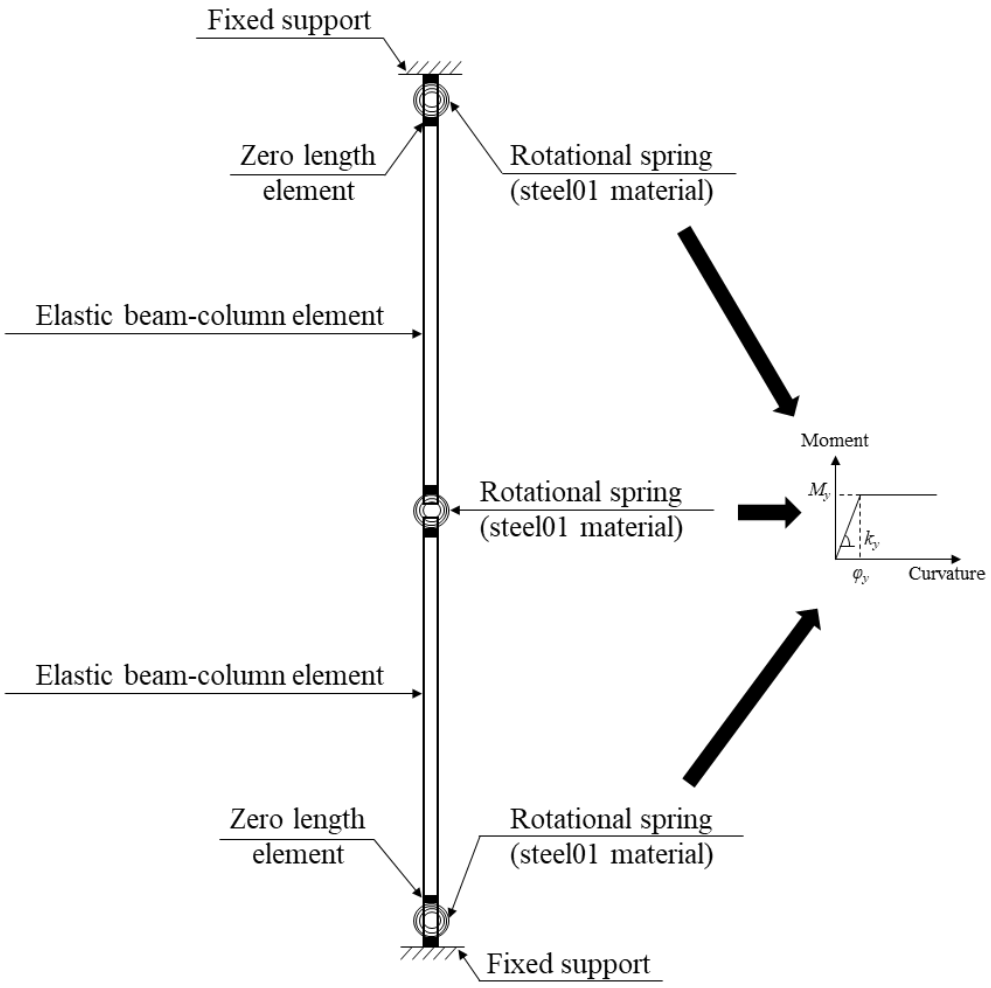

Figure 3.2: Schematic diagram of the model

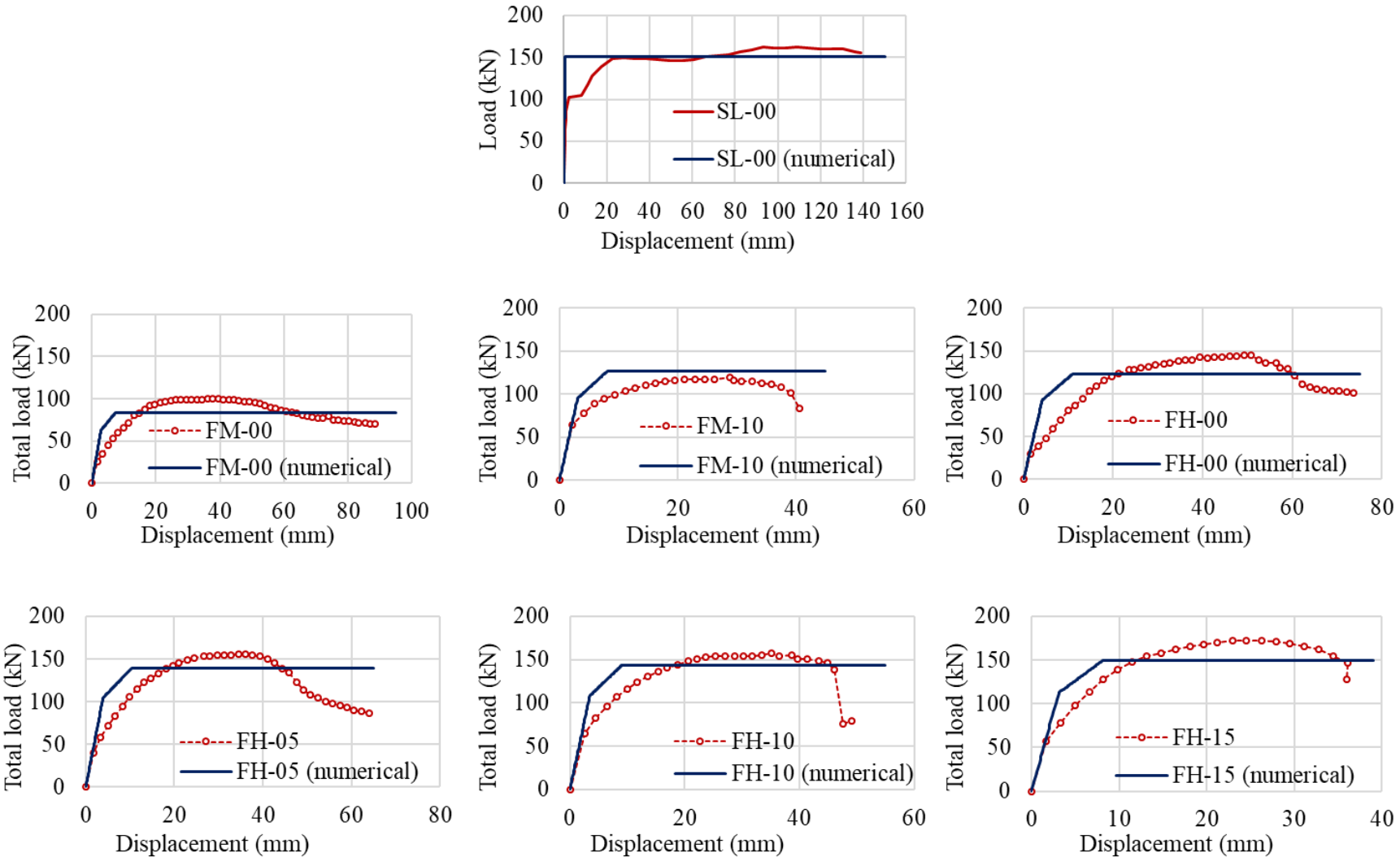

Figure 3.3: Static model validation for load bearing RMSWs

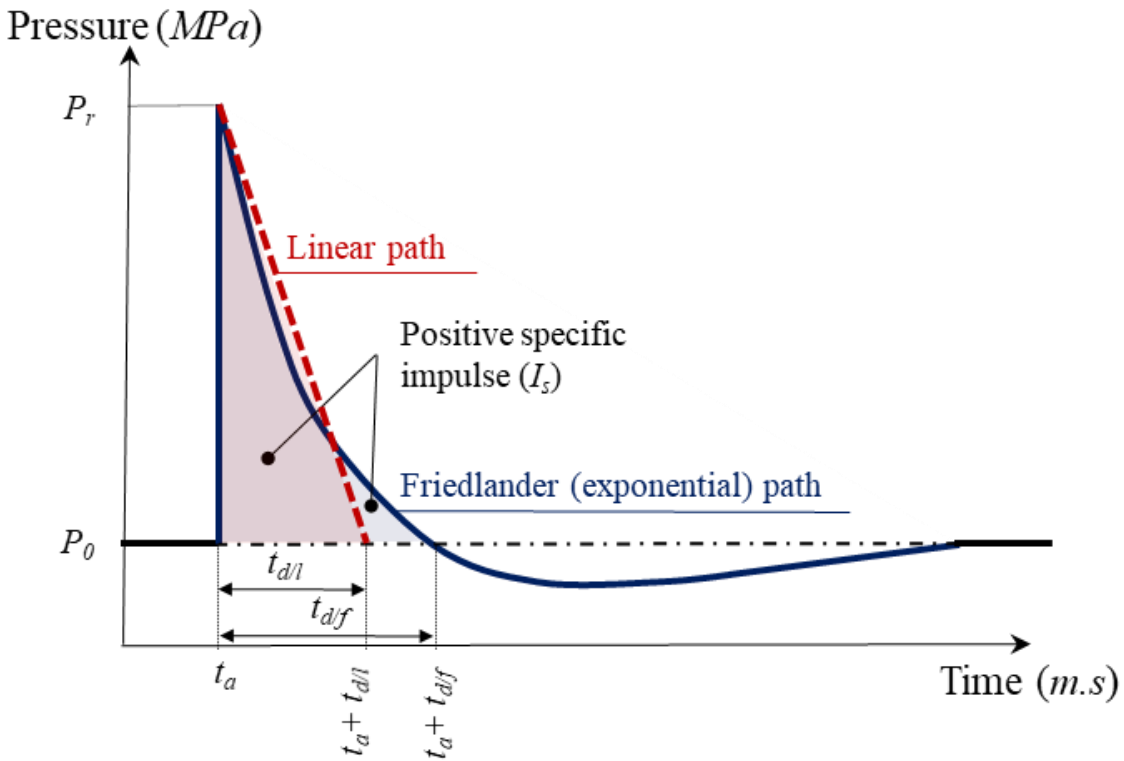

Figure 3.4: Friedlander and linear blast wave profiles

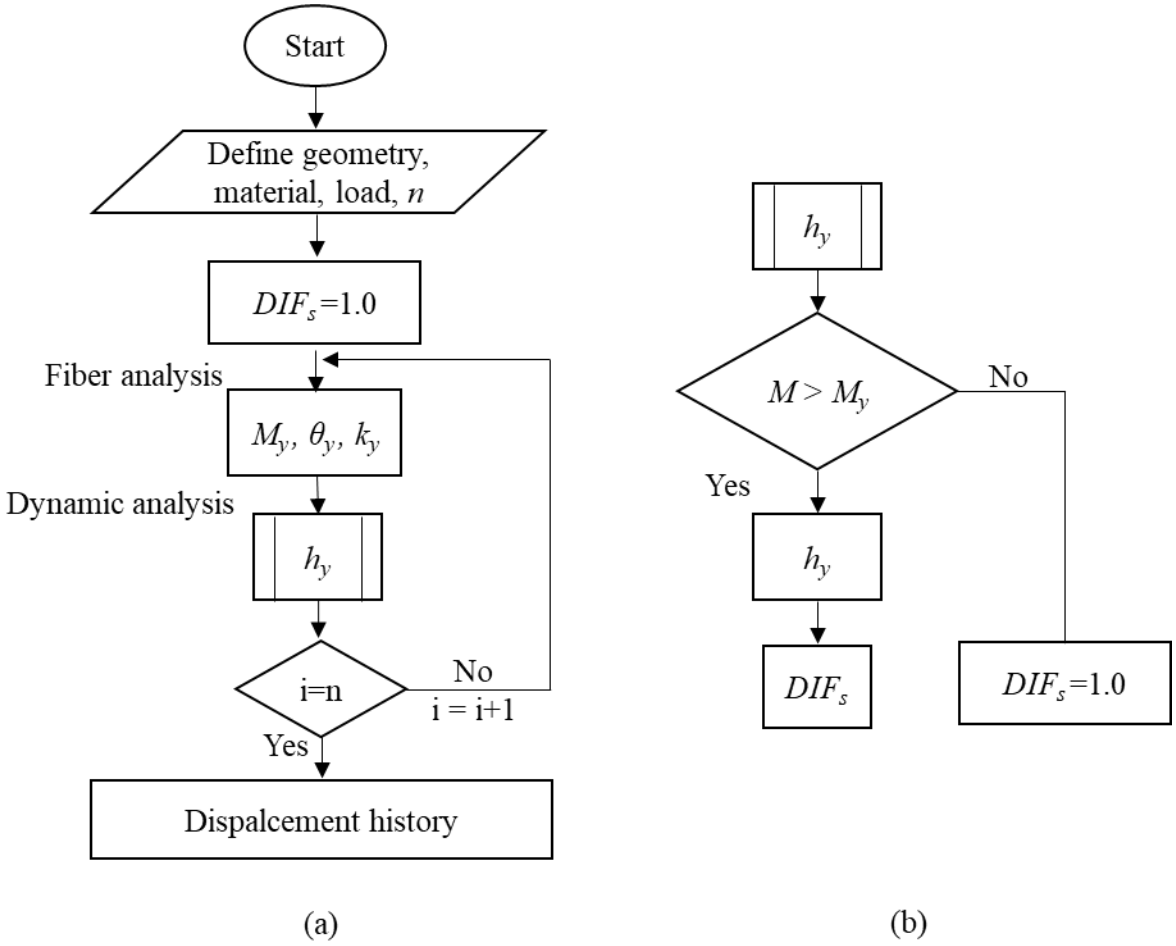

Figure 3.5: Iterative blast concentrated plasticity approach modelling: (a) framework; (b) iterative subroutine

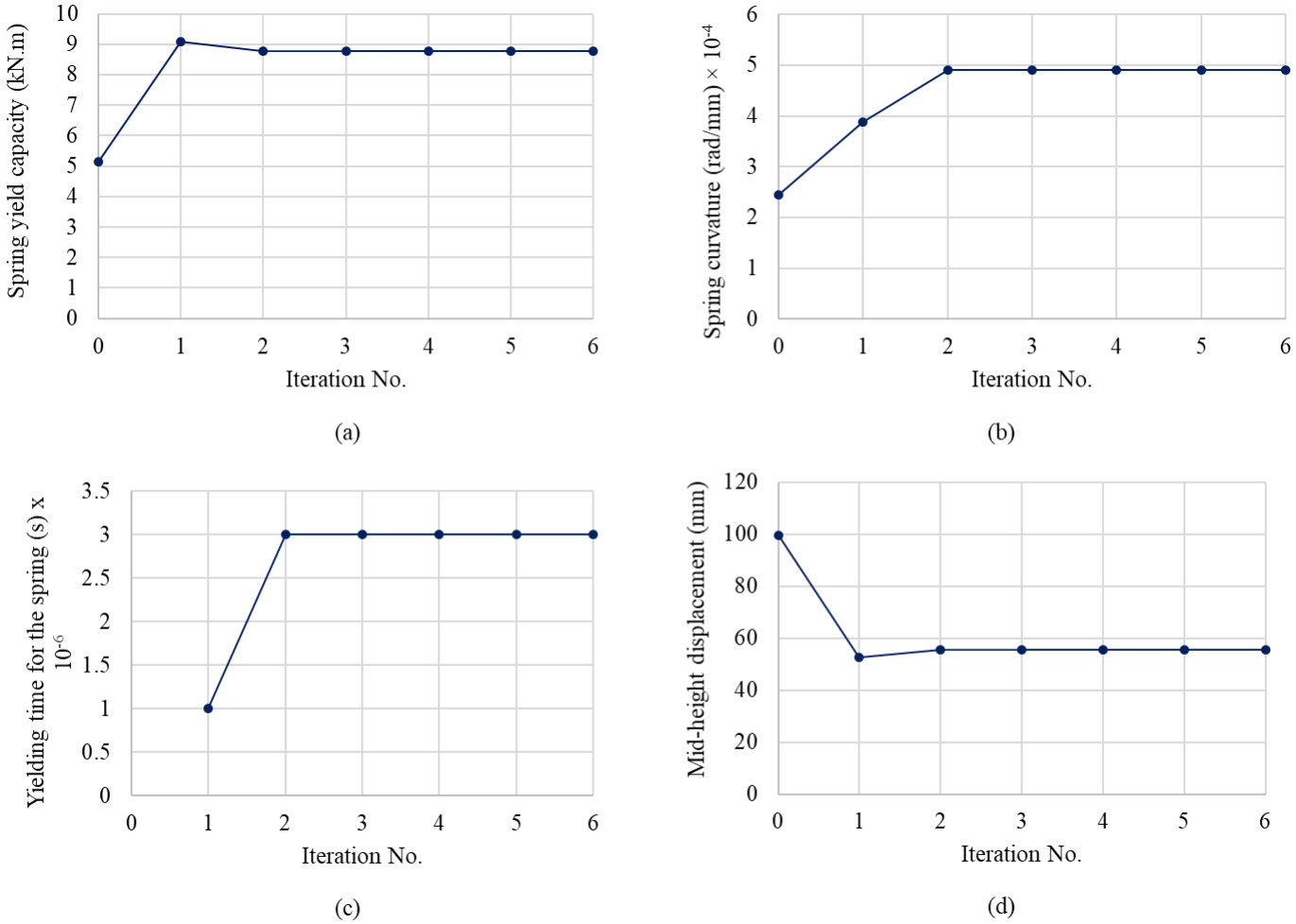

Figure 3.6: Convergence of wall L12: (a) spring yielding capacity; (b) spring yielding curvature; (c) spring yielding time; (d) mid-height displacement

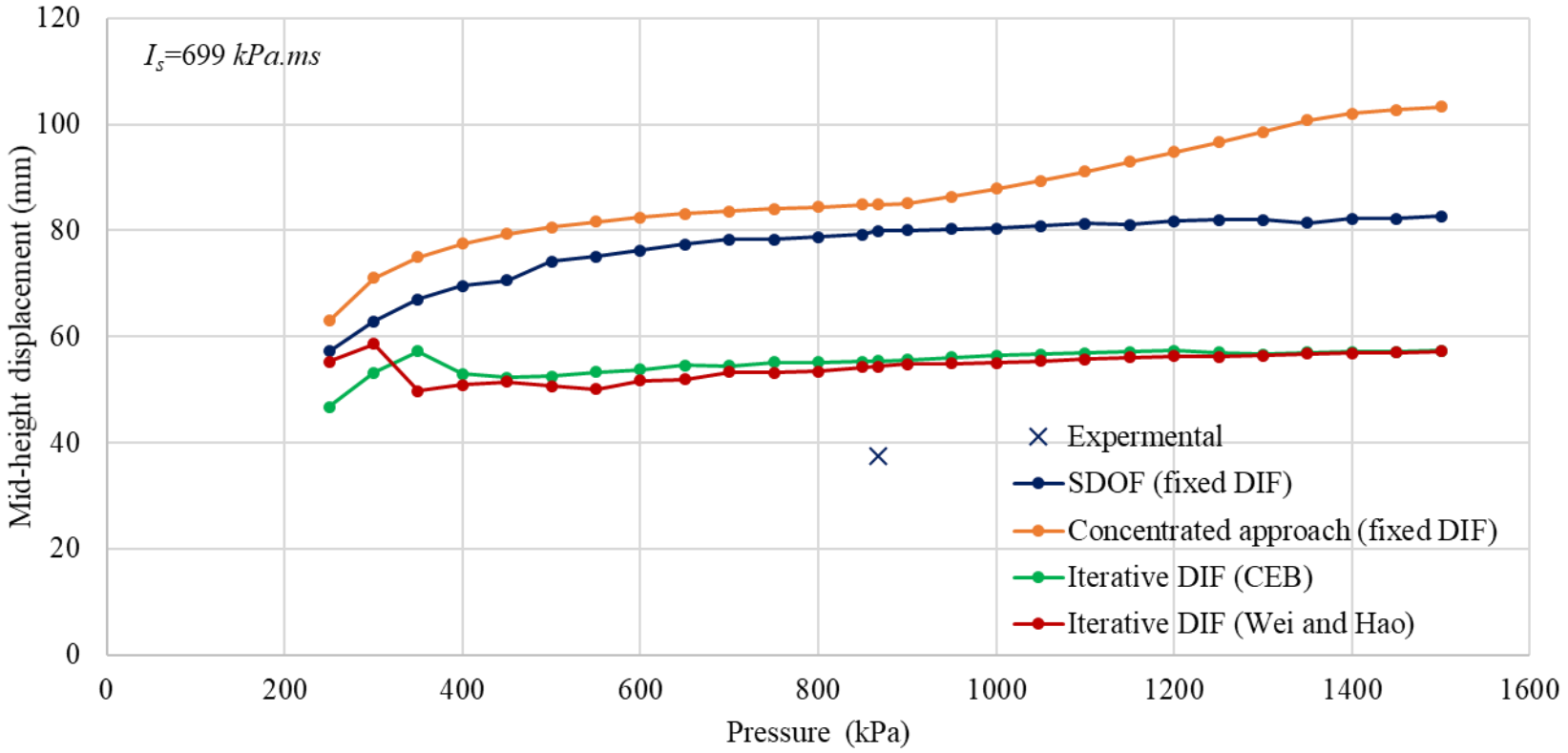

Figure 3.7: Influence of DIF on the blast response of wall L12

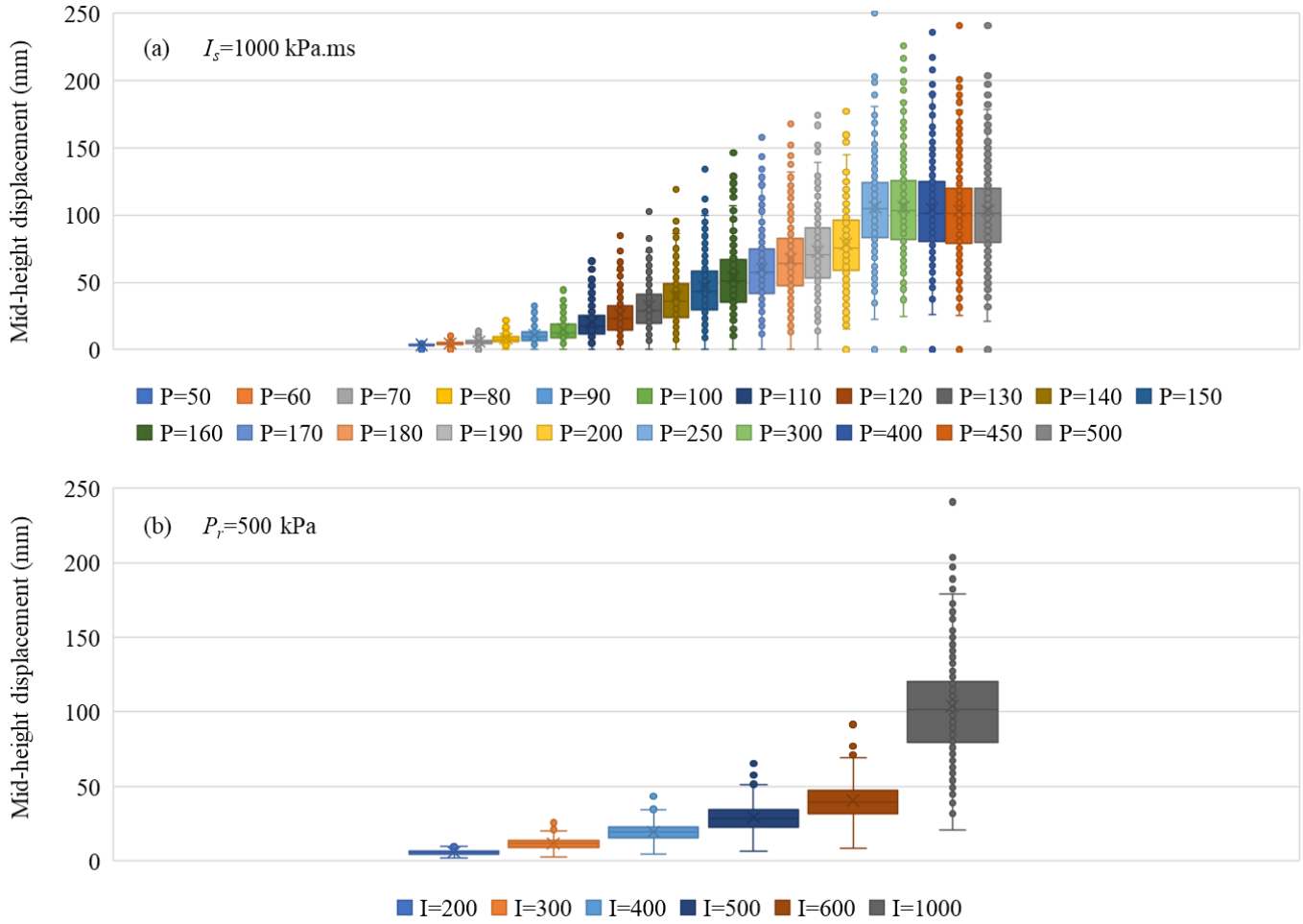

Figure 3.8: Effect of wavefront parameters uncertainty/variability on wall L12 performance: (a) constant I_s; (b) constant P_r

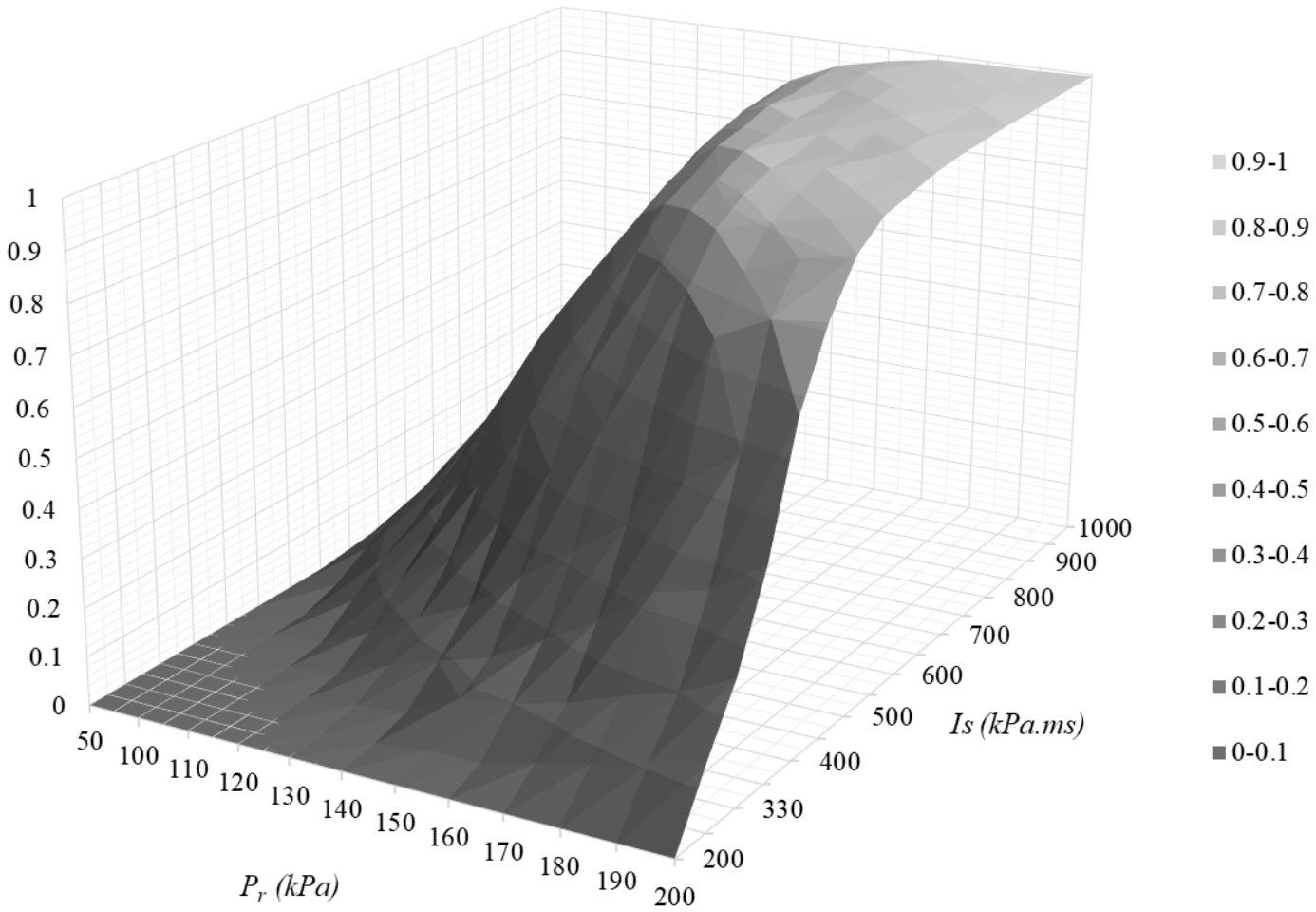
1
0.9
0.8
0.7
0.6
0.5
0.4
0.3
0.2
0.1
0
50
100
110
120
130
140
150
160
170
180
190
200
P_r (kPa)
200
330
400
500
600
700
800
900
1000
Is (kPa.ms)
0.9-1
0.8-0.9
0.7-0.8
0.6-0.7
0.5-0.6
0.4-0.5
0.3-0.4
0.2-0.3
0.1-0.2
0-0.1

(a)

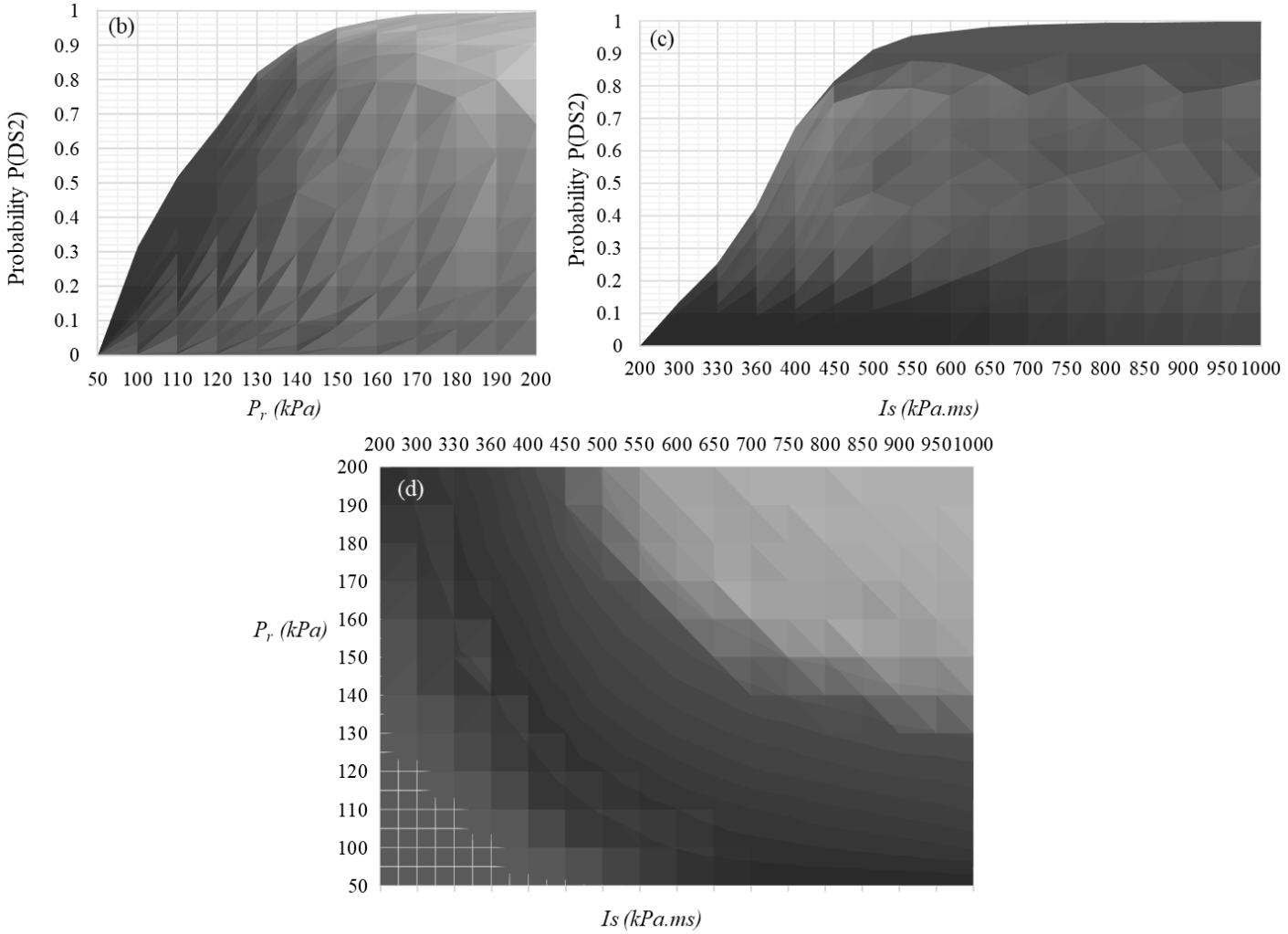

Figure 3.9: Blast fragility surface for wall L12 (θ=2°): (a) 3D view; (b) elevation (c) side view; (d) plan

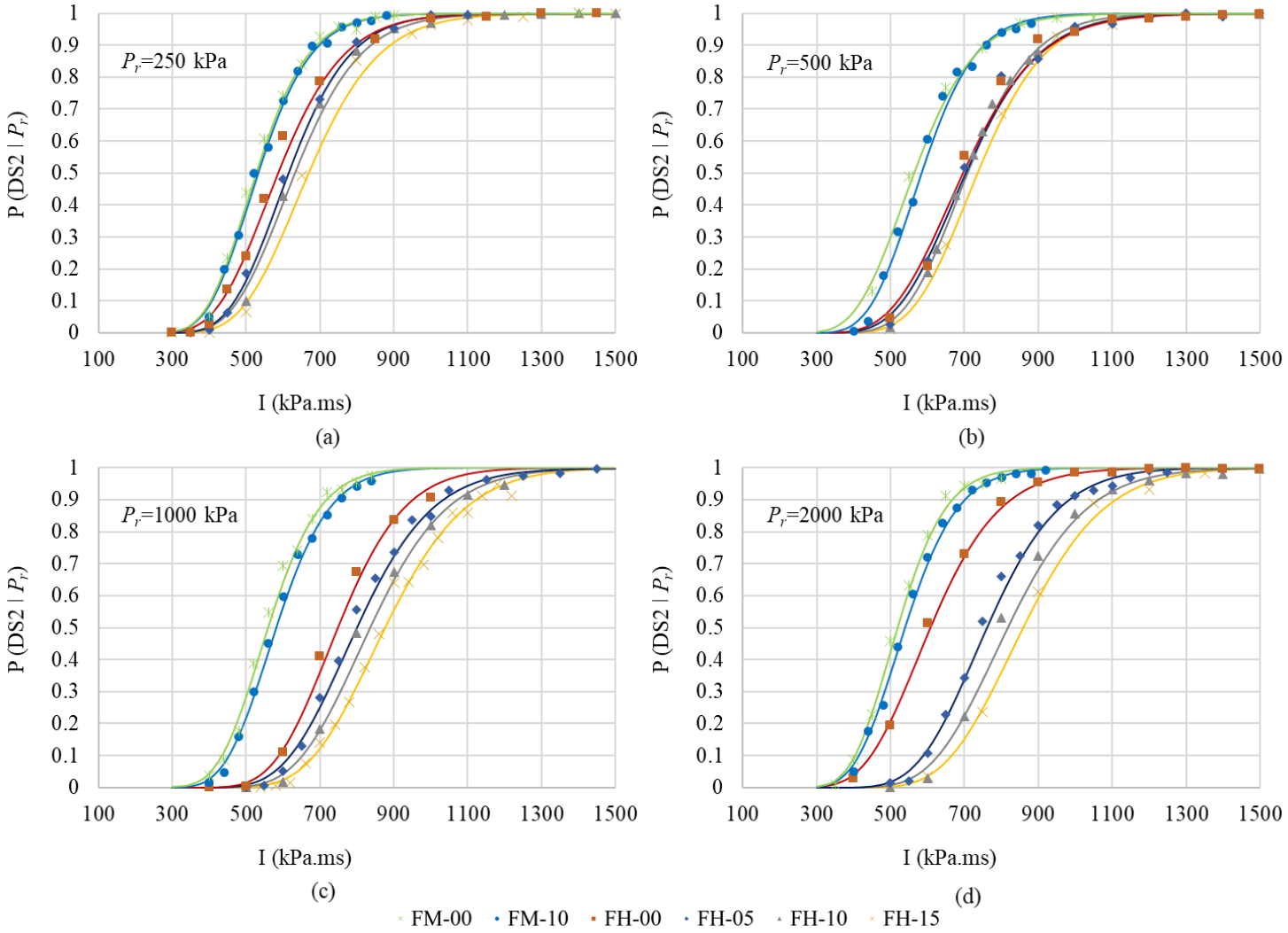

Figure 3.10: Conditional fragility curves for different RMSWs at Pr (kPa)= (a) 250; (b) 500; (c) 1000; (d) 2000

Chapter 4

RESILIENCE-BASED DESIGN OF URBAN CENTRES: APPLICATION TO BLAST RISK ASSESSMENT

4.1 ABSTRACT:

The design provisions of current standards for the blast protection of buildings are primarily focused to the response of single components and do not provide adequate tools to quantify the overall performance of complex structural systems, not to mention an array thereof. Methodologies that can translate probable structural damage into information actionable by policymakers are greatly needed to support the risk mitigation decision process. The best efforts produced to date towards a comprehensive analysis of the built environment under blast threats can be classified under the umbrella of probabilistic risk assessment, which can provide the public with projected casualties and economic loss associated with different blast threat levels. However, additional metrics are needed in order to capture the post-blast operational functionality and loss of productivity, which are directly linked to the resilience of the target facilities. The current study is focused on integrating elements of risk assessment and resilient thinking within a unified framework, wherein new design criteria—the functionality loss index and the resilience indicator—are proposed as instrumental to the assessment of a building's post-blast functionality and resilience in an integrated fashion. The results from a hypothetical blast scenario are used to demonstrate the utility of resilience-based design, an approach that can support executive decisions by providing more meaningful information than what is currently available by standard practices and thus be greatly beneficial for the selection of the most cost-effective measures of blast risk mitigation.

4.2 INTRODUCTION

A cursory analysis of the casualties and economic losses caused by natural and anthropogenic disasters reveals an alarming trend instigated by classical risk mitigation strategies, which historically led to a risk upsurge when the opposite was in fact the desired objective. The 1997 flood in the Red River Valley (Manitoba, Canada), the 2005 Hurricane Katrina (Louisiana, US), and the post 9/11 expenditures in airport security by the US Department of Homeland Security (DHS) are three case studies that exemplify this phenomenon, whereby policies of land development, urban planning, subsidized insurance and terrorism mitigation measures lead to a significant risk increase by moving entire communities in harm's way. In the Red River Valley, initiatives undertaken to curb the risk of flooding included a C$ 63.2 million "floodway project" and disaster funding assistance, the latter provided by the local (municipal), regional (provincial), and federal governments (Emdad Haque, 2000). With these policies enacted, the Red River Valley has suffered from several disasters, the most severe of which occurred in 1997, when the "flood of a century" covered 1,836 km^2 of land with water and caused damages in excess of C$ 500 million (Robert, Forget, & Rousselle, 2003). Yet, paradoxically, property values in flood-prone areas have grown at a rate equivalent to, if not greater than, that reported for safer areas. This seemingly reckless trend in urban development has been attributed to the false sense of security spawned by the floodway (Robert et al., 2003).

In Louisiana, the "Hurricane Protection Project" was implemented to protect the Mississippi watershed and the areas surrounding Lake Pontchartrain from storm surges—by means of control structures such as floodwalls and levees. The US Federal Government covered 72% of the cost and subsidized a system of flood insurance (USACE 2005). As a result, in 2005 Hurricane Katrina caused more than 1,500 fatalities and destroyed over 283,000 homes in Louisiana alone, while direct economic losses and insured losses tallied in the amounts of US$ 125 billion and US$

40.6 billion overall, respectively (FEMA 2006). Burby (2006) ascribed these losses to the extraordinary urban development prompted by the allure of the enhanced levee system. In his analysis, Burby (2006) identified the "safe development paradox", which explains why measures designed to mitigate risk led to its increase—via intensive development of a system of levees and floodwalls in highly vulnerable areas of Louisiana, as made apparent by the previous Hurricane Betsy, and policies of subsidized flood insurance—all of which conspired to greatly increase the population density in flood-prone areas, inflate a false sense of security in the residents, and discourage property owners from taking common sense actions to improve the buildings' safety. Investments in airport security by DHS include the installation of x-ray backscatter scanners for the screening of passengers. The risk countered by this technology is quantified as a yearly probability of one in 3.5 million of being involved in a terrorist plot, with death as a result (Mueller & Stewart, 2011). On the other hand, the risk of cancer mortality attributed to the scanners is 10-7 per exposure (Brenner, 2011). Assuming an average of one billion scans per year in the US alone, and given its current total US population of 321.4 million, that is equivalent to each person in the US being exposed to an average of 3.1 scans/year, resulting in a probability of death of one in 3.2 million. Therefore, although the foregoing data are somewhat uncertain, measures designed to counter the terrorist threat in the context of airport security would seem to produce a 9% increase in yearly cancer-related mortality rates.

4.3 RESILIENCE TO NATURAL HAZARDS

To shed some light on the disastrous interactions between the built and natural environments and overcome the pitfalls of land use planning recapped thus far, it may be useful to view the paradox discussed by Burby (2006) through the lens of resilience—a concept used across several disciplines to explain the behaviour of complex systems under shock. In broad terms, resilience has been defined by Martin-Breen & Anderies (2011) as the continued ability of a system, organization,

community, or individual to adapt in the face of acute crises and chronic stresses. In engineering, the National Infrastructure Advisory Council (NIAC) defines infrastructure resilience as "[enhancing] the ability of critical infrastructure systems, networks, and functions to withstand and rapidly recover from damage and disruption and adapt to changing conditions" (NIAC 2010). Intrinsic to these definitions are the notions of system functionality and its recovery over time, which may help resolve Burby's paradox by widening the scope of the analysis: Not only the new levees in Louisiana need be assessed against the expected design wind speed, but the *entire city network* need be revaluated under the assumption of a potential failure of the protective infrastructure, in order to gauge the immediate loss of functionality—in terms of essential services, utilities, etc.—and the time required to restore the network to pre-disaster conditions. In essence, from a resilience standpoint, the safety of a land use plan need be revaluated by broadening the investigation to a greater number of variables, whose complex interdependent relationships will determine the functionality of the new built infrastructure; the analysis need also be protracted in time, to estimate the capacity to recover from disaster while accounting for variable hazard exposure (e.g. caused by variability in population density) as well as other time-dependent properties of the system. Based on the NIAC definition and with the benefit of hindsight, it is apparent that the practices of land development criticized by Burby (2006) and Robert et al. (2003) had ultimately led to the opposite effect if significantly affecting the community resilience.

4.4 RESILIENCE TO ANTHROPOGENIC HAZARDS

When the attention is shifted to anthropogenic (man-made/induced) disasters and, more specifically, to civil structure and infrastructure exposed to the hazard of blast overpressure—generated by high explosives, propellants, flammable vapour clouds, bursting pressure vessels, and the likes—the need for risk-based design and resilient thinking is also apparent. In such a context, special attention has been garnered by terrorism, which is considered one of the least predictable

anthropogenic hazards because of the intelligent and adaptive nature of the attacker (Ezell, Bennett, von Winterfeldt, Sokolowski, & Collins, 2010). Terrorist attacks are often characterized by exceptionally high social/emotional impact, which may result in a community response that fits the definition of "black swan" (Mueller & Stewart, 2016). Historically, the losses caused by terrorist attacks, for which the general public has demonstrated exceptionally high aversion (Stewart, Ellingwood, & Mueller, 2011), have been brought at the forefront of security concerns in recent decades, especially after the Oklahoma City bombing, the 9/11 attacks on the World Trade Center and the subsequent anthrax attacks (Bier, Nagaraj, & Abhichandani, 2005; Morrill, Malvar, Crawford, & Ferritto, 2004). The insured costs of the 9/11 attacks were estimated to be approximately US$ 40 billion, which amounts to twice the insured losses claimed for the largest natural catastrophe reported at the time in the USA (Fitzpatrick, 2005). Worldwide, terrorism accounts for 15% of the aggregate casualties from all man-made disasters reported in 2015 (Swiss Re Ltd., 2016), which has focused the public attention on the severity of such a hazard and its limited coverage by insurance policies. The lack of adequate insurance for terrorist acts is generally attributed to the complexity of the ensuing cascading effects and their potential for besetting the global economy. Domino/cascading effects on the economy are typically hard to track for an evaluation by actuaries, which explains the growing tendency to resort to reinsurance as a way to deal with black swan events, like 9/11, that have the potential for causing disproportionately large losses. However, although reinsurance is an effective tool for spreading the financial risk, it may also contribute to feedback loops that would ultimately yield a greater risk: Similarly to the effect of land development initiatives, which resulted in the unintended rise in hazard exposure by moving entire communities in harm's way, risk transfer has been identified by Journeay et al. (2015) as one of the mechanisms by which a false sense of security arises and promotes risky behaviour—a phenomenon usually referred to as moral hazard. Given these past failures, the only viable

alternative to a complete denial of insurance coverage for rare events—a de facto victory for terrorism (Schaad, 2002)—lies in resilience–based insurance policies (MMC & CFIRE 2015) grounded in a new generation of risk assessment tools—able to track the evolution of risk in time, account for feedback loops instigated by anthropogenic activities, and integrate elements of resilient thinking at a the level of the city and community networks.

4.5 RESEARCH OBJECTIVE AND SCOPE: RESILIENCE TO BLAST HAZARDS

Historically, the threat of terrorism in North America has led to the development of design guidelines and technologies for the reduction of damage caused by explosive devices, which represent the weapon of choice in approximately 60% of all attacks led by terrorist organizations worldwide (Institute for Economics and Peace, 2015). Within the purview of blast protection of civilian buildings, the problem of effective risk mitigation is addressed by codes and design practices that are still anchored to deterministic notions of threat and hazard, as exemplified by the concept of design basis threat (DBT) found in Canadian (CSA, 2012) and American (ASCE 2011) standards. In this respect, it should be acknowledged at the outset that CSA (2012) does recommend a risk assessment methodology for the determination of the applicable DBT—based on the concepts of threat, vulnerability, and consequences; however, no guidelines are provided as to the specifics of such a methodology, which is left to the best judgment of the designer. A further limitation of both North American standards is represented by the specified performance criteria, which are focused on the deformation of *single* structural components. The narrow scope of the underlying design philosophy finds its analogue in construction practices of infrastructure against natural disasters, wherein the continued functionality/resilience of an entire city may be overlooked in favour of more easily quantifiable design targets (e.g. height of the floodwalls): On the one hand, the overall structural performance under blast loading in not addressed at the system–level via an integrated analysis; on the other, the performance metrics provided by the standards—namely, the

ductility ratio and support rotation—are useful only to structural engineers tasked with gauging the incurred damage in a local sense and from the sole standpoint of structural safety rather than infrastructure resilience. No metrics are offered to evaluate the loss of functionality and time of recovery of the impacted assets, which are key information for a comprehensive estimate of direct, indirect, and insured economic losses, and thus the overall system/network resilience.

To plot a course forward and address the limitations outlined thus far in current standards, a shift in the direction of risk and resilience-based thinking is currently being pursued, in an effort to account for the high degree of uncertainty associated with blast loading—including epistemic uncertainty (parameter and model error) and aleatory uncertainty (inherent variability), as pointed out by Stewart et al. (2006). A comprehensive framework aimed at the probabilistic risk assessment (PRA) of blast-induced damage was introduced by Grant & Stewart (2015; 2012), wherein the blast risk is quantified in terms of expected casualties and loss of property value per building per year. To mitigate these losses, a cost-benefit methodology was also made available in support of rational decision making, in order to select cost-effective protective strategies, e.g. structural strengthening and enhanced perimeter protection (Stewart, 2010). The body of literature on risk analysis is based on the well–established definition of risk given in Eq. (1), which requires the determination of hazard probability, asset vulnerability, and consequences of a successful attack:

$$Risk = Hazard \times Vulnerability \times Consequences \tag{1}$$

However, in the past, valuable consequence evaluation schemes, when adopted in the service of blast protection, have failed to integrate key elements of post-disaster building performance into a global index. In this respect, the recovery time is a prime example of an often-neglected factor of crucial importance to decision makers. To correct for these deficiencies, elements of resilience need be incorporated within the existing PRA methodology, as it is currently practice for the purpose of

blast-resistant design. The concept of resilience has permeated a diverse group disciplines, including physics, ecology, economics, sociology, anthropology, and engineering. A total of 46 definitions have been classified in the work of Rose & Krausmann (2013) and Plodinec (2009), and their analyses show core attributes shared across all fields of inquiry. A common thread found in engineering and, more specifically, in the field of structural design, is the assessment of post-disaster recovery—for instance, recovery after a major earthquake (Almufti & Willford, 2013)—which explains the current progress towards resilience–based design. The latter methodology is based on the assessment of a system performance under a specified hazard and is carried out by processing the hazard effects on the structural performance (system fragility) and subsequent functionality losses, in accordance with sensible performance criteria; and by selecting, whenever appropriate, protective measures for enhancing system resilience by recourse to estimates, i.e. post-event predictions, and evaluations—driven by post-event observations, decision support tools, and technology developed to promote preparedness and aid recovery (Bruneau et al., 2003).

The application of resilience within the context of blast protection holds significant promise; hence, in this paper a first attempt is made at broadening the methodology known as blast resistant design, so as to promote a global approach to the problem of safeguarding the resilience of complex systems—such as buildings, infrastructure, and cities—and outgrow narrow definitions of blast risk and failure that may promote unsafe behaviour, in analogy with the experience accumulated on natural disasters and land development. The focus of the following sections is the evaluation of the post-blast functionality and resilience of an isolated building subjected to a blast scenario, i.e. the unconfined airblast detonation of a charge of high explosive. At the local level, the incurred damage is evaluated by calculating the deformation of single structural members under blast overpressure, and by comparing it with known thresholds of structural performance (response limits) provided by the applicable design standards (ASCE, 2011; CSA, 2012). Afterwards, a

simplified framework is proposed, wherein the building's post-blast functionality and resilience are quantified at the system–level—by introducing two new metrics, namely, the *functionality loss index* and the *resilience indicator*. The building's downtime is also estimated, on the basis of FEMA P-58 (FEMA, 2012c) recommendations for computing the downtime following a seismic event. The example of an eleven–storey administrative building is provided to illustrate the proposed methodology, in which the computation of all resilience metrics is carried out in a deterministic fashion. Future work will investigate the functionality of the same system—as well as more complex ones, up to the city-level—as a stochastic phenomenon, in order to perform a PRA of the applicable resilience metrics and achieve a unified framework—founded on both risk and resilience principles.

4.6 EXISTING METHODOLOGIES FOR RESILIENCE QUANTIFICATION

The attributes of resilience shared across disciplines stem from the similarities in behaviour of the different social units, including individuals, communities, organizations, nations, etc. Generally, the behaviour of a system under shock shows a temporary drop in performance and a subsequent recovery to pre-shock, pre-disaster levels, as exemplified in Figure 4.1 by the so–called "resilience triangle" (Ayyub, 2015) adapted from Salem et al. (2016), which is supported by a number of case studies of post-disaster recovery patterns reported by Brown et al. (2010) and Reed et al. (2009). Figure 4.1 shows alternate recovery paths/functions, each mapping the variation in functionality resulting from the degree of preparedness of the social units experiencing a given hazard. The functionality curves *a*, *b*, and *c* in Figure 4.1 represent, respectively, an exponential recovery path driven by initial inflow of resources decreasing over time; a linear recovery path, typically assumed when no information about preparedness is available; and a trigonometric path driven by lack of resources (Gian Paolo Cimellaro, Reinhorn, & Bruneau, 2010). Curve *d* represents a stepped recovery path instead, associated with incremental repair steps as well as a defined sequence of

target performance levels (Burton, Deierlein, Lallemant, & Lin, 2016; G. P. Cimellaro, Tinebra, Renschler, & Fragiadakis, 2016).

Within the scope of building systems, Almufti & Willford (2013) proposed three recovery states as the sensible targets of resilience-based design, namely, re-occupancy, pre-disaster functionality, and full recovery. Re-occupancy is the state in which users are allowed to reoccupy a non–life-threatening facility where utilities are not available; functional recovery implies the regaining of all primary functions, e.g. electrical power, water supply, and HVAC systems; and full recovery requires complete restoration of pre-disaster aesthetic conditions. Significant effort has been made to provide a rigorous, quantitative definition of resilience that can summarize the entire recovery history with a single parameter. Among the most influential works, Bruneau et al. (2003) defined the loss of resilience as the loss of functionality integrated over the time of recovery; however, a more direct definition has been provided in Attoh-Okine et al. (2009), wherein the *resilience index* (I_r) is broadly designated as the mean functionality over the time of recovery, in accordance with Eq. (2):

$$I_r = \frac{\int_{t_0}^{t_f} Q(t)\,dt}{100\left(t_f - t_0\right)} \tag{2}$$

where Q denotes the functionality of the system—its performance level, its functional history from the time of first damage to the time of complete recovery—as measured by any meaningful metric; t_0 is the time at which first damage occurs, as a result of the incurred hazard; and t_f is time when the post–hazard target performance is achieved—typically, full recovery to pre-disaster functionality, as illustrated in Figure 4.1. A number of problem-specific definitions of the resilience index exist,

yet none can comprehensively replace the wealth of information provided by the full functional history.

The pioneering framework on seismic resilience by Bruneau et al. (2003) identified four dimensions of community resilience—technical, economic, social and organizational—as well as four properties (or pillars)—robustness, rapidity, redundancy, and resourcefulness—and it is often referred to as the 4R methodology. Within this framework, robustness is defined as the ability of a system to withstand a given level of shock with minimal or no functional loss—as measured immediately after the hazard via applicable performance metrics, while rapidity accounts for the time of recovery to pre-shock performance levels. To evaluate a system's rapidity, it is useful to recall the distinction between repair time and downtime. As defined by Almufti & Willford (2013), repair time is the time required to repair or replace all damaged components to restore a building to a specific state; downtime, in addition to repair and replacement, also includes the time associated with impeding factors—i.e. the delay between hazard occurrence and the initiation of repairs, as necessity dictates, in order to conduct inspections, mobilize engineering services, etc.—and utility disruption—i.e. the time required for the recovery of backup systems, refuelling of generators, refilling of water tanks, etc. Redundancy is what keeps a system functional after the loss of part of its elements, whose role is undertaken by, and shared amongst, the undamaged elements. And finally, resourcefulness is the capacity to identify and mobilize the resources required to recover from a disruption. These definitions denote robustness and rapidity as the goals of resilient design, while redundancy and resourcefulness are the means to achieve them (Rose & Krausmann, 2013). Figure 4.2 illustrates the interrelationships among the four pillars of resilience: Redundancy affects both robustness and rapidity, because redundant elements can compensate for the loss of damaged ones, thus increasing robustness, and operational redundancy can lead to shorter downtime while regaining full functionality, thereby increasing rapidity; resourcefulness, on the other hand, affects

only the system rapidity as it is an idle property during normal operations—prior to hazard occurrence; a partial dependency of rapidity on robustness is also noted, as exemplified by the causal chain initiated by after–shock losses (perfectly correlated with robustness) followed by the selection of an appropriate repair technique, which in turn determines, to a significant degree, the system downtime.

A cursory analysis of the resilience triangle reveals the main factors affecting the resilience index introduced in Eq. (2). With reference to Figure 4.3, three different post-disaster recovery paths are considered, named *a*, *b*, and *c*; for the sake of simplicity, linear recovery is assumed in all cases. Path *a* describes the response of the control system (baseline case)—a highly robust system incurring low initial loss (λ) and short recovery time (t). Path *b* is characterized by the same level of robustness ($1\text{-}\lambda$) as path *a* but with slower recovery ($2t$). Path *c* shows high initial loss (2λ) and fast recovery (t). When the integrated functionality losses (cumulative losses) are compared, cases *b* and *c* produce the same result ($\lambda \cdot t$), which is twice the cumulative losses incurred by the control system ($0.5\lambda \cdot t$). However, when the resilience indices are compared, both recovery paths *a* and *b* give $I_r = 1 - 0.5\lambda$, while the value from path *c* is $I_r = 1 - \lambda$. This trivial example demonstrates that, in case of linear recovery, the downtime strongly affects the cumulative functionality loss but has no effect on the resilience index, which is congruent with the relationship proposed by Quiel et al. (2016):

$$\text{Resilience} \propto f(\text{hazard, robustness}) \tag{3}$$

Equation (3) implies that resilience is proportional to the combined output of hazard level and system robustness, while the time of recovery may or may not be significant in the determination of the constant of proportionality. For instance, in the case of hospitals, Bruneau & Reinhorn (2007) have argued that robustness and rapidity may be strongly correlated, in which case rapidity would

become a redundant, idle variable. A similar argument may be formulated for the case of blast-induced damage: Given its localized nature, the initial loss is expected to be more easily quantifiable and linked to the expected recovery time, hence resilience could be based solely on the initial loss of performance, as proposed by Quiel et al. (2016). Although there is merit to the latter approach, the framework presented in this study is based on the assumption that robustness and rapidity can be independent variables, in order to provide decision-makers with a tool of broader applicability, albeit less problem–specific and accurate in its predictions; furthermore, resilience is estimated in terms of quantities (indices) integrated over the time of recovery, in order to provide the stakeholders with an overall appraisal of post-disaster performance.

4.7 FUNCTIONALITY

System functionality refers to the capacity of a system to deliver the products or services it was designed to provide and it is usually monitored over the so–called "control time", e.g. the system life cycle (G. P. Cimellaro et al., 2016). Of interest to the current discussion is the evaluation of the change in functionality in the aftermath of a disaster. The metrics and indices selected to quantify functionality are problem–dependent and their definition may evolve over time. At the community level, resiliency metrics typically target the availability of housing and infrastructure as well as social, economic, institutional, and environmental capitals (Cutter, Ash, & Emrich, 2014). Within the field of highway bridges, Mackie & Stojadinović (2006) proposed the traffic loading capacity, lane closures, allowed axle load, and speed limit as apt functionality indices. Normalized gas flow rate and total length of a gas distribution elements have been proposed as functionality indices of gas distribution networks (G. P. Cimellaro, Villa, & Bruneau, 2015). With regard to building infrastructure, its performance has been described by Grussing et al. (2009) as the synthesis of its physical condition and functional state, which may or may not be coupled. In the specific case of hospitals, Cimellaro et al. (2009) defined their functionality through qualitative and quantitative

indices as well as their combined effect: The qualitative functionality, or quality of service, was based on the patients' waiting time in the emergency room and the ambulance response time, while the quantitative indicator was proposed as the ratio of treated to total number of patients (G P Cimellaro et al., 2009). In the following sections, two functionality metrics of general applicability to the built environment are introduced, in order to aid the designer in the assessment of resilience to blast hazards and the broader consequences of infrastructure disruption on the community network.

4.8 POST-BLAST FUNCTIONALITY

When the blast protection of buildings and their post–blast serviceability levels are considered, it is noted that the scope of current design provisions is mostly limited to the localized response of individual structural components—as a way to assess the level of protection (LOP) of a facility. The pertinent Canadian standard CSA S850 (CSA, 2012) classifies the LOP of a structure into four categories, based on its post–blast damage, operational status and functionality as well as the anticipated repair cost, as summarized in Table 4.1. The four damage levels outlined in the standard—namely, superficial, moderate, heavy, and hazardous—are defined in terms of the so–called response limits, i.e. upper bounds of the ductility ratio and support rotation experienced by structural members and correlated with their post–blast serviceability, as shown in Table 4.2. As they are focused on the damage incurred by single elements, the current CSA provisions are not suitable to quantify the global functionality loss suffered by a building after a blast event; the LOP of a building is not sufficient to determine its post–blast operational capacity, unless overly conservative assumptions are made, e.g. basing the loss estimate solely on the most damaged structural member. To take a more sensible approach, a three-stage methodology is proposed, based on damage mapping, practical/rational correlation between structural damage and functionality

loss, and a coherent definition of functionality loss at the building system–level as a weighted aggregate of local damages.

Blast damage mapping has been adopted by a number of researchers to assess the blast risk of glass facades (Stewart, 2010; Stewart & Netherton, 2008) and the likelihood of progressive collapse following the destruction of columns at several locations in a building's topology (Gombeda, Naito, Quiel, & Fallon, 2016). In the current study, a similar procedure is followed to calculate the blast overpressure and ensuing damage at several locations across a building's façade facing an explosive charge. Relevant details about this calculation are discussed in a later section, where an illustrative example is provided. Given a sufficiently detailed representation of the structural damage, a plausible assumption is then made about the relationship between structural deterioration and accessibility: Each architectural unit (bay) is considered to be accessible and fully functional when all the components of its pertinent structure experience a damage that can be classified as superficial; conversely, a non–functional bay area is assumed whenever one or more of its structural members experience any damage level other than superficial, as shown in Figure 4.4. The latter assumption is based on the standards' definition of superficial damage, which may or may not be visible and it may require cosmetic repair, if any at all. Therefore, it is reasonable to assume a superficially damaged bay area as accessible and fully operational, with no significant loss of functionality. On the other hand, moderate and heavy damage states would entail significant repairs, thereby rendering the affected area temporarily inaccessible to regular occupants; hence the consequent loss, at the local level, would be 100% for the entire duration of the repairs. These considerations are codified in the following *loss indicator*, λ:

$$\lambda = \begin{cases} 0 & \text{Bay enclosed by components incurring superficial damage} \\ 1 & \text{Bay enclosed by components incurring moderate or heavy damage} \\ \text{N/A} & \text{Bay enclosed by components incurring hazardous damage or blowout} \end{cases} \tag{4}$$

Note that Eq. (4) explicitly indicates that the proposed approach is not applicable when one or more elements experience severe deformation; in such a case, the possibility of progressive collapse need be evaluated and immediate evacuation may be required. States that would require that these steps be taken include hazardous damage and blowout, the latter being below anti-terrorism standards (USACE, 2008b) and therefore outside the scope of any design guidelines.

To aggregate all local losses into a global descriptor, the *functionality loss index* (I_F) is introduced in Eq. (5), which represents the immediate post–blast functionality loss at the system–level and is complementary to the building robustness (loss and robustness add up to one):

$$I_F = \frac{\sum_{i=1}^{n} A_i I_i \lambda_i}{\sum_{i=1}^{n} A_i I_i} \tag{5}$$

where A_i is the area of the i-th bay, n is the total number of bays in the building, I_i is the importance factor ascribed to bay area A_i—which can be attributed based on criticalities in the chain of production, services, or communication—and λ_i is the loss indicator describing the damage experienced by the i-th bay, in accordance with Eq. (4). It should be noted that the functionality loss index is based on independent analysis of each component, considered in isolation from its surrounding structure and architecture; although there is merit to this simplification, given the typically localized nature of the blast-induced damage, future work should be directed at a more rigorous analysis encompassing the system interdependencies, by means of structural analysis,

fragment penetration analysis, etc. Although outside the scope of the current study, it is noted that when secondary and non–structural elements are also considered in the analysis, λ = 1 can be assumed in the cases of hazardous damage and blowout as well, given that these elements are not responsible for progressive collapse.

4.9 PROPOSED FRAMEWORK

The framework proposed in this section can be applied to the design of new structures as well as the assessment of existing ones when blast hazard is a concern. Its scope is limited to the evaluation of direct functionality losses, and related quantities, experienced within the confines of the affected facility as a result of physical damage. Indirect losses, including the societal consequences of terrorism, are beyond the scope of this investigation and are captured by the metrics adopted to quantify resilience. Furthermore, secondary effects on post-blast resourcefulness, e.g. delayed repair operations caused by a disruption of the transportation system, are not accounted for; to include such effects, a comprehensive analysis of the building's premises and its surrounding environment will be required in future developments.

To evaluate the building performance, in addition to the functionality loss index introduced earlier to assess the building robustness, a *resilience indicator* (I_R) is proposed in order to account for the cumulative functionality loss though time:

$$I_R = \frac{1}{2}(t_f - t_0)I_F \tag{6}$$

where the dependencies of I_R on immediate loss and downtime are made explicit. Figure 4.5 shows a graphical representation of the resilience indicator, defined in Eq. (6) as the area enclosed between the recovery function and the line Q = 100%. The recovery time (t_f - t_0), a key element in the blast resilience framework, is the number of labour hours or days needed to complete the repairs and it

is estimated as the baseline repair cost divided by the effective labour hourly rate provided in FEMA P-58 (FEMA, 2012a). For more accurate estimates, a more comprehensive approach should be adopted however, in which the downtime should be inclusive of the impeding factors and disruption of utilities, as pointed out in Almufti & Willford (2013).

A flowchart of the proposed framework is illustrated in Figure 4.6. First, acceptable resilient–based design/assessment criteria need be selected, including a design basis threat—in the form of a plausible blast scenario—and thresholds for the functionality index and resilience indicator, based on risk acceptance criteria agreed on by the stakeholders. In the following step, the elements at risk are identified, e.g. the components of a facility under threat, and importance factors (Ii) are attributed to them based on value tree analysis, which may account for environmental, social, and physical impacts (Apostolakis, 2008; Apostolakis & Lemon, 2005); in the current analysis, Ii = 1 is assumed for all i = 1,…,n. Hazard mapping follows, involving, for instance, the determination of overpressure distribution across the exposed façade. Based on the latter, the subsequent loop is dedicated to a component by component evaluation of the blast load and consequent damage state and functionality index. If no elements experience a level of damage classified beyond heavy, the functionality index is calculated via Eq. (5); otherwise, critical elements need be strengthened and the overall building need be revaluated. The global building performance is then evaluated by appraising the functionality index: If I_F is found to be greater than the acceptable design target, the overall building needs to be strengthened or retrofitted, otherwise the resilience indicator (I_R) is determined as well, in accordance with Eq. (6). If I_R falls within the acceptable range the process is concluded; otherwise, blast risk mitigation measures are necessary, either in the form of greater resources for a more expedient recovery or as interventions aimed at increasing robustness (e.g. via perimeter protection and structural strengthening).

4.10 CASE STUDY

The following example is presented to illustrate the process by which the functionality and resilience indices are calculated in the case of a multi-storey building and it should be regarded as a simple demonstration of the proposed framework to a single building façade. In order to avoid introducing numerous details that would distract from understanding the framework application, the computation of the building's functionality accounts only for the damage experienced by bays sharing one side with the façade directly facing the explosive charge. Phenomena such as the propagation of the blast waves through the building's premises and towards the building's core; wave diffraction over the building's envelope; interaction between structural and non–structural components and their incurred damage as a result of earth ejecta; and primary and secondary fragmentation are neglected. Future developments of the proposed methodology will account for all the foregoing effects and include an analysis of the building's premises, in order to detect possible interactions of the shock waves with nearby constructions, the ground, and the geometry of the building's envelope. Some simplifications are also made about the recovery path: Generally, the rate of recovery, and thus the shape of $Q(t)$ in Eq. (2), is dictated by the availability of resources and level of preparedness; in the absence of this information, a linear recovery is assumed.

Figure 4.7 shows the selected example, an 11–storey reinforced concrete block (masonry) building adapted from NEHRP (2010). The plan view in Figure 4.7(a) shows the primary load–bearing system: The area most affected by the blast wave is that behind the façade directly facing the explosive charge, that is the area enclosed between axes A and B; any effects beyond axis B are neglected in the current analysis. The elevation in Figure 4.7(b) reveals the façade components, two load–bearing reinforced masonry shear walls (RMSW) at every floor—the detailing of which is shown in Figure 4.7(c)—and one infill, unreinforced brick wall (UBW) sandwiched in between. Regarding the material properties, the average compressive strength of grouted masonry is 20 MPa

and its reinforcement is selected to bear low axial stresses—approximately 3% of the RMSW axial strength (NEHRP, 2010); UBWs feature a 50 MPa compressive strength and elastic-plastic behaviour (no arching effect is instigated). The three blast scenarios simulated herein are identified in Table 4.3 by charge mass and standoff distance—the minimum distance between the centre of the explosive charge and façade–A shown in Figure 4.7(a)—and involve the outdoor detonation of improvised explosive devices (IEDs) at the ground floor, on the left side of the building and in front of its center. Each IED detonation is modeled as a hemispherical surface burst of bare TNT at sea–level; the associated scaled distances Z, used to determine the blast overpressure, are also reported in Table 4.3. Hazard scenarios #1 and #2 feature small explosive charges (50 kg) located relatively close to the building, at R = 10 and 20 m, respectively, and can be characterized as person-borne IEDs; scenario #3 features a considerably larger charge—500 kg at a distance R = 40 m—which can be considered representative of a vehicle-borne IED subjected to the access restrictions produced by common measures of perimeter protection—including barriers, fences, controlled entry gates, etc. For each scenario, the slanted standoff distance, angle of incidence, and distance from the edges of the reflecting surface are calculated on a 64×64 grid across façade–A (see Figure 4.8) and used to determine four key wavefront parameters—namely, the reflected peak pressure, specific impulse, duration, and decay coefficient of the positive pressure phase (Campidelli, Tait, El-Dakhakhni, & Mekky, 2015; DoD, 2014); clearing effects on the specific impulse generated nearby the edges of façade–A are also considered. The results of the analysis are summarized in Table 4.3, where the LOP, functionality index, downtime, and resilience indicator are reported for all three scenarios, while the following discussion is a detailed presentation of the steps followed in the simulation of scenario #1.

The results, in terms of reflected peak pressure and specific impulse contours, are presented in Figure 4.9. From the figure, it can be noticed that the peak pressure ranges from a minimum of

50 kPa at the 8th floor and above, to a maximum of 400 kPa at the ground floor, at the region of the façade closest to the charge; similarly, the specific impulse ranges from a minimum of 150 kPa.ms at the last floor, farthest from the explosive, to a maximum of 900 kPa.ms at the ground floor. When this information is coupled with the spatial distribution of the other two wavefront parameters (duration and decay coefficient), a pressure history can be calculated for every point on the grid and a blast hazard map can be drawn; subsequently, the integration of such pressure over the surface area of every single wall on the façade can be used to map the damage—that is the wall response––by means of single degree of freedom models, finite element analysis, or design charts. For the sake of simplicity, in the current analysis the wall response, quantified by either the maximum ductility ratio (μ) or support rotation (θ) as per ASCE (2011) and CSA (2012), is determined on the basis of pressure–impulse diagrams generated by the SBEDS software (USACE, 2008a); the latter has been implemented to predict the response of structures subjected to unconfined airblast detonations, hence it is applicable in the present case study. The results are shown in Figures 4.10(a and b) for the reinforced and unreinforced walls, respectively, based on the average peak pressure and impulse exerted on their surface. To identify the damaged elements, each wall is tagged using its pertinent floor number and typology. For instance, 5RMSW refers to a reinforced wall at the fifth floor, while 11UBW refers to an unreinforced wall at the eleventh floor; note that given the symmetry of the blast scenario, there is no need for further distinction between RMSWs. Based on Figure 4.10(a), it can be concluded that any RMSWs between floors 1 and 5 are expected to exhibit moderate damage, whereas RMSWs between the 6th and the 11th floors would experience only superficial damage, if any. As for the brick masonry, Figure 4.10(b) indicates that elements 1UBW and 11UBW are expected to exhibit greater than hazardous (blowout) and moderate damage, respectively; other walls in between would likely experience either heavy or hazardous damage, depending on their distance from the explosive. The damage to the entire façade is mapped in Figure

4.11, where the information from the pressure–impulse diagrams is translated into functionality indicators, as per Eq. (4): The bays supported by RMSWs at floor 6 through 11 are expected to be functional after the blast ($f = 0$), whereas the remaining bays, associated with walls 1RMSW through 5RMSW and 1UBM through 11UBM, are expected to be in need of extensive repairs and therefore inaccessible ($f = 1$). Given that the only elements expected to suffer hazardous or greater damage do not carry axial load, progressive collapse analysis is deemed unnecessary and $f = 1$ is assumed for the associated bay areas.

The overall reduction in functionality is estimated via the functionality loss index from Eq. (5), under the assumption of importance factors all equal to unity ($I_i = 1.0$):

$$I_F = \frac{\sum_{i=1}^{n} A_i I_i \lambda_i}{\sum_{i=1}^{n} A_i I_i} = \frac{2\times 8\times 11\times 5\times 1 + 7\times 11\times 11\times 1}{23\times 77\times 11} = 8.9\%$$

Under the simplified assumptions stated earlier, the explosion would result in 8.9% functionality loss, which, in the case of identical importance factors, would translate into an equal loss of products and services provided by the facility. Should this impairment be deem unacceptable by the stakeholders ($I_F > I_{F,\text{acc}}$), measures of blast risk mitigation would be considered by weighing their costs and benefits. To complete the assessment, the resilience indicator from Eq. (6) is calculated on the basis of the 90$^{\text{th}}$ percentile of the repair cost provided in FEMA P-58 (FEMA, 2012b), as reported in Table 4.4. The RMSW repair cost is assumed to be that of a flexure dominated, special reinforced masonry walls with fully grouted cells (thickness = 8”–12” and height ≤ 12’); the UBM repair price is taken as the cost of masonry parapets, which includes demolition and construction anew. Based on Figure 4.10(a) and FEMA’s definitions, the failed RMSWs (floors 1 to 5) fall under the second damage state category (DS2), whose price is reported in Table 4.4 as US$ 487.93 /m^2.

On the other hand, UBWs are forecasted to exhibit different damage states, as shown in Figure 4.10(b); however, FEMA (2012b) does not provide sufficient information regarding the associated repair costs, thus the cost of brick elements classified as "repairable" is simply assumed, i.e. US$ 240.39 /m^2. Therefore, given the total surface area of the damaged RMSWs as 256 m^2 (8×3.2×2×5), the associated repair cost is US$ 487.93×256 = 124,910; in the case of unreinforced walls, their surface area measures 246.4 m^2 (7×3.2×11), which leads to a repair cost of US$ 240.39×246.4 = 59,232. The incidence of labour on the total cost—termed by FEMA (2012b) as the labor production commencement time—is 69% and 60% for reinforced and unreinforced masonry, respectively, as recalled in Table 4.4. Therefore, the total labour cost can be estimated as US$ 124,910×0.69 + 59,232×0.60 = 121,727 and, given a crew rate of US$ 255 /hr, the expected repair time can be calculated as 121,727/255 = 477 hr or ~60 days, assuming 8 working hours per day. Finally, the resilience indicator from Eq. (6) can be calculated as $I_R = 0.5(t_f - t_0)I_F = 0.5\times60\times0.089 = 2.67$ days. Its interpretation is as follows: Given the 60 day estimate to full recovery, 2.67 days will be lost in terms of unrealized products and services, giving an average normalized loss $I_R/(t_f - t_0) = 2.67/60 = 4.45\%$, which is also the resilience index in Eq. (2), barring the 100 factor.

The benefits of the proposed framework are apparent when the results of all blast scenarios are compared in Table 4.3. In terms of LOP—determined from the response of the most severely damaged walls—all three scenarios yield the same outcome, i.e. very low protection, thereby making them undistinguishable from the viewpoint of the building owner. Yet, the resilience metrics support a very different conclusion: Compared to scenario #1, scenario #2 entails significantly lower instantaneous losses (4.3%), downtime (17 days), and cumulated losses (0.37 days), while the opposite is true for scenario #3, for which I_F = 14.3%, downtime = 110 days, and I_R = 7.89 days. Based on these numbers, it would be rational for all stakeholders to give precedence to mitigating the blast risk associated with the last scenario, as all resilience metrics forecast greater

potential losses. Furthermore, when compared to the scaled distance, Z, all resilience metrics return a different ranking of the blast scenarios: Based on Z, increasing physical damage is expected for scenarios #2, #3, and #1, whereas increasing functional losses, i.e. poorer resilience metrics, are predicted for scenarios #2, #1, and #3.

4.11 CONCLUSIONS

Moral hazard arguably represents the greatest pitfall of risk assessment methodologies and building codes based on exceedingly narrow objectives. Past experiences of land development in floodplains, both in Canada and the US, have demonstrated that urban planning should be based on a comprehensive assessment of city network vulnerabilities in the event of a natural disaster. Similarly, current standards for the blast protection of buildings are found to be greatly limited in scope—mostly confined to the response of single components; their performance criteria should be broadened to encompass notions of resilience in complex systems and outgrow narrow definitions of failure that may unduly lower the threshold of risk acceptance. The proposed framework for blast resilience sets new design targets, namely, the functionality loss index and resilience indicator, which can prove instrumental to the assessment of a building's post-blast functionality and resilience in an integrated fashion. The results from an example scenario demonstrate the utility of resilience-based design: Based on current standard practice, the 11–storey administrative building examined in this study is expected to provide low level of protection under the DBT selected for scenario #1—50 kg of TNT detonated at 10 m from the building side façade—corresponding to moderate damage to the most affected load-bearing element. On the other hand, resilience analysis predicts a decline in functionality immediately after the explosion of 8.9%, which corresponds to a robustness of 91.1%; a downtime of ~60 days; 2.67 days of lost production during the 60–day recovery—corresponding to 267 units of lost product given a steady state production rate of 100 units/day; and a total repair cost of US$ 124,910+59,232 = 184,142. In addition, the proposed

framework succeeds where a classical analysis fails, namely, in differentiating between the three blast scenarios considered: While all three are found to generate the same damage classification—in accordance to current standards—the resilience metrics reveal significantly different levels of global losses, which would suggest an allocation of resources that would prioritize scenario #3 over the others, because greater losses are forecasted for scenario #3 at the global level. It is therefore apparent that a resilience-based approach can provide stakeholders with a wealth of information unparalleled by current practices and be greatly beneficial to the selection of the most cost-effective measures of blast risk mitigation and the assessment of cascading effects on the city and community networks.

Limitations to the application presented to illustrate the proposed methodology include the type of scenario, i.e. an external unconfined explosion, a deterministic computation of all resilience metrics, and a range of simplifying assumptions concerning the building's response and its interaction with the shock waves. Future work will investigate the functionality of the same building as a stochastic phenomenon, in order to perform a PRA of the applicable resilience metrics under a unified framework—founded on both risk assessment and resilience evaluation principles and able to incorporate the high degree of uncertainty inherent to blast hazards. The propagation of the blast waves towards the building's core, secondary fragment penetration, interaction between load–bearing and non–structural members will be accounted for in future refinements of the proposed framework, as well as possible interactions of the shock waves with nearby structures, the ground, and the geometry of the building's envelope. A more extensive investigation on the economics of blast reliance is also desirable, with particular attention to a detailed breakdown of the costs and benefits entailed by strategies of risk reduction—including perimeter protection, structural strengthening, enhanced security, and others.

4.12 ACKNOWLEDGMENTS

Financial support has been provided through a Collaborative Research and Development Grant funded by the Natural Sciences and Engineering Research Council (NSERC) of Canada. Industrial support has been provided through the Canadian Concrete Masonry Producers Association and the Canada Masonry Design Centre. Additional support has been provided through the McMaster Institute for Multi-Hazard Systemic Risk Studies.

4.13 NOTATION

A	=	Area of a single bay
A_t	=	Total building area (sum of all bay areas)
I_A	=	Importance factor associated with bay area A
I_F	=	Functionality index
I_R	=	Resilience index
Q	=	System functionality
R	=	Standoff distance, measured from charge center building's facade
r	=	Resilience indicator
t_0	=	Time of hazard occurrence
t_f	=	Time of full recovery to pre-disaster functionality
W	=	TNT–equivalent mass of the explosive
Z	=	Scaled distance
θ	=	Maximum support rotation
λ	=	Loss indicator
μ	=	Maximum ductility ratio

4.14 REFERENCES

Almufti, I., & Willford, M. (2013). *REDiTM Rating System: Resilience-based Earthquake Design Initiative for the Next Generation of Buildings*. Arup Co.

Apostolakis, G. E. (2008). Probabilistic Risk Assessment (PRA). In *Wiley Handbook of Science and Technology for Homeland Security*. Hoboken, NJ, USA: John Wiley & Sons, Inc. http://doi.org/10.1002/9780470087923.hhs017

Apostolakis, G. E., & Lemon, D. M. (2005). A Screening Methodology for the Identification and Ranking of Infrastructure Vulnerabilities Due to Terrorism. *Risk Analysis*, *25*(2), 361–376. http://doi.org/10.1111/j.1539-6924.2005.00595.x

ASCE. (2011). *Blast Protection of Buildings*. (American Society of Civil Engineers, Ed.) *Blast Protection of Buildings*. Reston, VA, VA: American Society of Civil Engineers. http://doi.org/10.1061/9780784411889

Attoh-Okine, N. O., Cooper, A. T., & Mensah, S. A. (2009). Formulation of Resilience Index of Urban Infrastructure Using Belief Functions. *IEEE Systems Journal*, *3*(2), 147–153. http://doi.org/10.1109/JSYST.2009.2019148

Ayyub, B. M. (2015). Practical Resilience Metrics for Planning, Design, and Decision Making. *ASCE-ASME Journal of Risk and Uncertainty in Engineering Systems*, *1*(3), 1–11. http://doi.org/10.1061/AJRUA6.0000826

Bier, V. M., Nagaraj, A., & Abhichandani, V. (2005). Protection of simple series and parallel systems with components of different values. *Reliability Engineering & System Safety*, *87*(3), 315–323. http://doi.org/10.1016/j.ress.2004.06.003

Brenner, D. J. (2011). Are X-Ray Backscatter Scanners Safe for Airport Passenger Screening?

For Most Individuals, Probably Yes, but a Billion Scans per Year Raises Long-Term Public Health Concerns. *Radiology*, *259*(1), 6–10. http://doi.org/10.1148/radiol.11102347

Brown, D., Platt, S., Bevington, J., Saito, K., Adams, B., Chenvidyakarn, T., … Spence, R. (2015). Monitoring and Evaluating Post-Disaster Recovery Using High-Resolution Satellite Imagery–Towards Standardised Indicators for Post-Disaster Recovery, (March). Retrieved from http://www.carltd.com/sites/carwebsite/files/CAR Brown Monitoring recovery standardised indicators.pdf

Bruneau, M., Chang, S. E., Eguchi, R. T., Lee, G. C., O'Rourke, T. D., Reinhorn, A. M., … von Winterfeldt, D. (2003). A Framework to Quantitatively Assess and Enhance the Seismic Resilience of Communities. *Earthquake Spectra*, *19*(4), 733–752. http://doi.org/10.1193/1.1623497

Bruneau, M., & Reinhorn, A. (2007). Exploring the Concept of Seismic Resilience for Acute Care Facilities. *Earthquake Spectra*, *23*(1), 41–62. http://doi.org/10.1193/1.2431396

Burby, R. J. (2006). Hurricane Katrina and the Paradoxes of Government Disaster Policy: Bringing About Wise Governmental Decisions for Hazardous Areas. *The ANNALS of the American Academy of Political and Social Science*, *604*(1), 171–191. http://doi.org/10.1177/0002716205284676

Burton, H. V., Deierlein, G., Lallemant, D., & Lin, T. (2016). Framework for Incorporating Probabilistic Building Performance in the Assessment of Community Seismic Resilience. *Journal of Structural Engineering*, *142*(8), C4015007. http://doi.org/10.1061/(ASCE)ST.1943-541X.0001321

Campidelli, M., Tait, M. J., El-Dakhakhni, W. W., & Mekky, W. (2015). Inference of Blast

Wavefront Parameter Uncertainty for Probabilistic Risk Assessment. *Journal of Structural Engineering*, *141*(12), 4015062. http://doi.org/10.1061/(ASCE)ST.1943-541X.0001299

Cimellaro, G. P., Fumo, C., Reinhorn, A. M., & Bruneau, M. (2009). *Quantification of Disaster Resilience of Health Care Facilities*. (Multidisciplinary Center for Earthquake Engineering Research, Ed.). University at Buffalo, The State University of New York, Buffalo, NY, USA. Retrieved from: https://mceer.buffalo.edu/pdf/report/09-0009.pdf

Cimellaro, G. P., Reinhorn, A. M., & Bruneau, M. (2010). Framework for analytical quantification of disaster resilience. *Engineering Structures*, *32*(11), 3639–3649. http://doi.org/10.1016/j.engstruct.2010.08.008

Cimellaro, G. P., Tinebra, A., Renschler, C., & Fragiadakis, M. (2016). New Resilience Index for Urban Water Distribution Networks. *Journal of Structural Engineering*, *142*(8), C4015014. http://doi.org/10.1061/(ASCE)ST.1943-541X.0001433

Cimellaro, G. P., Villa, O., & Bruneau, M. (2015). Resilience-Based Design of Natural Gas Distribution Networks. *Journal of Infrastructure Systems*, *21*(1), 5014005. http://doi.org/10.1061/(ASCE)IS.1943-555X.0000204

CSA. (2012). *Design and assessment of buildings subjected to blast loads. CSA standard S850-12*. (Canadian Standards Association, Ed.). Mississauga, ON, Canada, ON, Canada: (CSA), Canadian Standards Association.

Cutter, S. L., Ash, K. D., & Emrich, C. T. (2014). The geographies of community disaster resilience. *Global Environmental Change*, *29*, 65–77. http://doi.org/10.1016/j.gloenvcha.2014.08.005

DoD, (Department of Defense). (2014). Structures to Resist the Effects of Accidental Explosions.

Unified Facilities Criteria 4-340-02.

Emdad Haque, C. (2000). Risk Assessment, Emergency Preparedness and Response to Hazards: The Case of the 1997 Red River Valley Flood, Canada. *Natural Hazards*, *21*(2/3), 225–245. http://doi.org/10.1023/A:1008108208545

Ezell, B. C., Bennett, S. P., von Winterfeldt, D., Sokolowski, J., & Collins, A. J. (2010). Probabilistic Risk Analysis and Terrorism Risk. *Risk Analysis*, *30*(4), 575–589. http://doi.org/10.1111/j.1539-6924.2010.01401.x

FEMA. (2012a). *Seismic Performance Assessment of Buildings. Volume 2 – Implementation Guide* (Vol. 2). Redwood City, California: Federal Emergency Management Agency.

FEMA. (2012b). Seismic Performance Assessment of Buildings. Volume 3 - Performance Assessment Calculation Tool (PACT) Version. Redwood City, California: Federal Emergency Management Agency.

FEMA. (2012c). *Seismic Performance Assessment of Buildings. Volume 1 - Methodology* (Vol. 1). Redwood City, California: Federal Emergency Management Agency.

FEMA (Federal Emergency Management Agency). (2006). *FEMA 549, Hurricane Katrina in the Gulf Coast: Mitigation Assessment Team Report, Building Performance Observations, Recommendations, and Technical Guidance*. Washington, DC: Federal Emergency Management Agency (FEMA).

Fitzpatrick, J. H. (2005). The Impact of a new large-scale Terrorism Attack on Insurance, Reinsurance and the Economy. *Workshop Session at the World Economic Forum in Davos*, 2001–2003.

Gombeda, M. J., Naito, C. J., Quiel, S. E., & Fallon, C. T. (2016). Blast-Induced Damage

Mapping Framework for Use in Threat-Dependent Progressive Collapse Assessment of Building Frames. *Journal of Performance of Constructed Facilities*, 4016089. http://doi.org/10.1061/(ASCE)CF.1943-5509.0000949

Grant, M., & Stewart, M. G. (2012). A systems model for probabilistic risk assessment of improvised explosive device attacks. *International Journal of Intelligent Defence Support Systems*, *5*(1), 75. http://doi.org/10.1504/IJIDSS.2012.053664

Grant, M., & Stewart, M. G. (2015). Probabilistic Risk Assessment for Improvised Explosive Device Attacks That Cause Significant Building Damage. *Journal of Performance of Constructed Facilities*, *29*(5), B4014009. http://doi.org/10.1061/(ASCE)CF.1943-5509.0000694

Grussing, M. N., Uzarski, D. R., & Marrano, L. R. (2009). Building Infrastructure Functional Capacity Measurement Framework. *Journal of Infrastructure Systems*, *15*(4), 371–377. http://doi.org/10.1061/(ASCE)1076-0342(2009)15:4(371)

Institute for Economics and Peace. (2015). *Global Terrorism Index 2015: Measuring and Understanding the Impact of Terrorism*.

Journeay, J. M., Talwar, S., Brodaric, B., & Hastings, N. L. (2015). *Disaster resilience by design: a framework for integrated assessment and risk-based planning in Canada*. Ottawa, ON.

Mackie, K. R., & Stojadinović, B. (2006). Post-earthquake functionality of highway overpass bridges. *Earthquake Engineering & Structural Dynamics*, *35*(1), 77–93. http://doi.org/10.1002/eqe.534

Martin-Breen, P., & Anderies, J. M. (2011). *Resilience: A Literature Review* (The Bellagio Initiative).

MMC (Multihazard Mitigation Council), & CFIRE (Council on Finance Insurance and Real Estate). (2015). *Developing Pre-Disaster Resilience Based on Public and Private Incentivization*. Washington, DC: National Institute of Building Sciences (NIBS).

Morrill, K. B., Malvar, L. J., Crawford, J. E., & Ferritto, J. M. (2004). Blast Resistant Design and Retrofit of Reinforced Concrete Columns and Walls. In *Structures 2004* (pp. 1–8). Reston, VA: American Society of Civil Engineers. http://doi.org/10.1061/40700(2004)154

Mueller, J., & Stewart, M. G. (2011). Witches, Communists, and Terrorists Evaluating the Risks and Tallying the Costs. *Human Rights*, *38*(1).

Mueller, J., & Stewart, M. G. (2016). The curse of the Black Swan. *Journal of Risk Research*, *19*(10), 1319–1330. http://doi.org/10.1080/13669877.2016.1216007

NEHRP, C. J. V. (2010). *Evaluation of the FEMA P-695 Methodology for Quantification of Building Seismic Performance Factors*. Gaithersburg, MD.

NIAC (National Infrastructure Advisory Council). (2010). *A Framework for Establishing Critical Infrastructure Resilience Goals*. Washington, D.C.: Department of Homeland Security.

Plodinec, M. J. (2009). *Definitions of Resilience: An Analysis. Community and Regional Resilience Initiative*. Oak Ridge, TN, USA. Retrieved from http://www.resilientus.org/library/

Quiel, S. E., Marjanishvili, S. M., & Katz, B. P. (2016). Performance-Based Framework for Quantifying Structural Resilience to Blast-Induced Damage. *Journal of Structural Engineering*, *142*(8), C4015004. http://doi.org/10.1061/(ASCE)ST.1943-541X.0001310

Reed, D. A., Kapur, K. C., & Christie, R. D. (2009). Methodology for Assessing the Resilience of Networked Infrastructure. *IEEE Systems Journal*, *3*(2), 174–180.

http://doi.org/10.1109/JSYST.2009.2017396

Robert, B., Forget, S., & Rousselle, J. (2003). The Effectiveness of Flood Damage Reduction Measures in the Montreal Region. *Natural Hazards*, *28*(2/3), 367–385. http://doi.org/10.1023/A:1022982108593

Rose, A., & Krausmann, E. (2013). An economic framework for the development of a resilience index for business recovery. *International Journal of Disaster Risk Reduction*, *5*, 73–83. http://doi.org/10.1016/j.ijdrr.2013.08.003

Salem, S., El-Dakhakhni, W., & Tait, M. (2016). Resilience-based design of reinforced masonry wall buildings under blast loading. In *Brick and Block Masonry* (pp. 1007–1014). CRC Press. http://doi.org/10.1201/b21889-137

Schaad, W. (2002). *Terrorism: Dealing with the New Spectre*. Zurich. Retrieved from https://scholar.google.ca/scholar?q=Terrorism-dealing+with+the+new+spctre&hl=en&as_sdt=0,5#1

Stewart, M. G. (2010). Risk-informed decision support for assessing the costs and benefits of counter-terrorism protective measures for infrastructure. *International Journal of Critical Infrastructure Protection*, *3*(1), 29–40. http://doi.org/10.1016/j.ijcip.2009.09.001

Stewart, M. G., Ellingwood, B. R., & Mueller, J. (2011). Homeland security: a case study in risk aversion for public decision-making. *International Journal of Risk Assessment and Management*, *15*(5/6), 367. http://doi.org/10.1504/IJRAM.2011.043690

Stewart, M. G., & Netherton, M. D. (2008). Security risks and probabilistic risk assessment of glazing subject to explosive blast loading. *Reliability Engineering & System Safety*, *93*(4), 627–638. http://doi.org/10.1016/j.ress.2007.03.007

Stewart, M. G., Netherton, M. D., & Rosowsky, D. V. (2006). Terrorism Risks and Blast Damage to Built Infrastructure. *Natural Hazards Review*, *7*(3), 114–122. http://doi.org/10.1061/(ASCE)1527-6988(2006)7:3(114)

Swiss Re Ltd. (2016). *Natural catastrophes and man-made disasters in 2015 : Asia suffers substantial losses*. Zurich, Switzerland: Swiss Re Ltd.

USACE. (2008a). *Methodology Manual for the Single-Degree-of- Freedom Blast Effects Design Spreadsheets. Report No. PDC TR-06-01 Rev 1*. Omaha, NE: US Army Corps of Engineers (USACE), Protective Design Center (PDC).

USACE. (2008b). *Single Degree of Freedom Structural Response Limits for Antiterrorism Design. Rep. No. PDC–TR 06–08, Rev. 1*. Omaha, NE: US Army Corps of Engineers (USACE), Protective Design Center (PDC).

USACE (US Army Corps of Engineers). (2005). *Lake Pontchartrain and Vicinity Hurricane Protection Project*. Washington, D.C.

Table 4.1: Definition of buildings' level of protection, adapted from CSA S850–Cl. 4.4.2 (CSA, 2012)

Buildings' LOP	Physical description
Very Low	Safe re-entry is unlikely and building contents may be damaged
Low	Evacuation and temporary reoccupation are likely; building contents are undamaged but non–functional; repair may be costly
Medium	Temporary evacuation may be necessary; reoccupation is possible after clean–up and repairs; building contents are expected to be partially functional; repair costs are worthwhile
High	Operations and occupancy are mostly unaffected; building contents are expected to be fully functional

Table 4.2: LOP description for building components, adapted from CSA S850 (CSA, 2012)

LOP	Building performance	Building component damage levels			
		Primary structural	**Secondary structural & non–structural**	**Glazing**	**Doors**
Very low	Collapse prevention	Heavy	Hazardous	Low hazard rating	Failure
Low	Life safety	Moderate	Heavy	Very low hazard rating	Category IV
Medium	Immediate occupancy	Superficial	Moderate	Minimal hazard rating	Category III
High	Operational	Superficial	Superficial	No break	Category I or II

Table 4.3: Different blast scenarios, the accompanied LOP and proposed indices

Scenario #	Charge weight (kg TNT) (W)	Standoff distance (m) (R)	Scaled distance (m/kg$^{1/3}$) (Z)	LOP	Functionality index (I_F)	Downtime (days)	Resilience indicator (I_R)(days)
1	50	10	2.71	very low	8.9%	60	2.67
2	50	20	5.42	very low	4.3%	17	0.37
3	500	40	5.04	very low	14.3%	110	7.89

Table 4.4: Repair cost in US$/m^2, adapted from FEMA (2012b) —DS = damage state

Element	Repair cost (US$, 90th percentile)			Labor production commencement time
	DS1	DS2	DS3	
RMSW	100.43	487.93	906.00	69%
UBW	240.39			60%

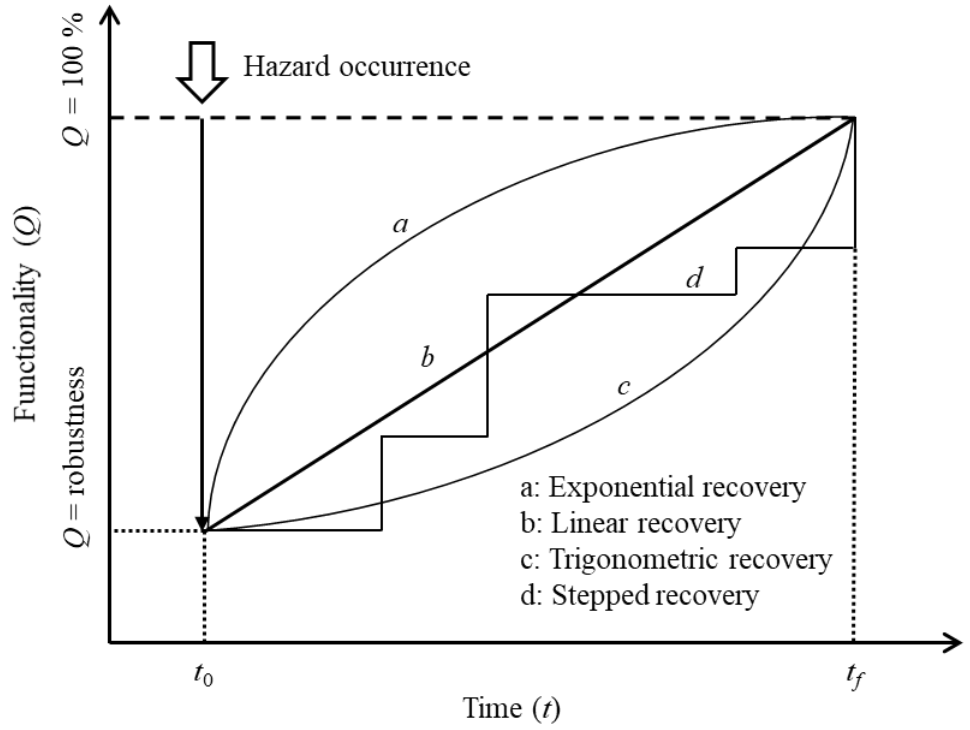

Figure 4.1: Resilience triangle representing the post-disaster recovery of different social units (Salem et al. 2016)

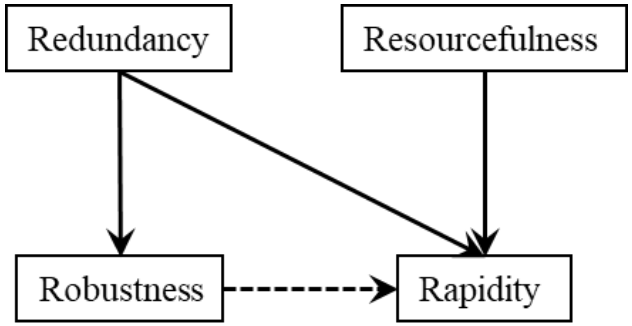

Figure 4.2: Interrelationships among the four pillars of resilience

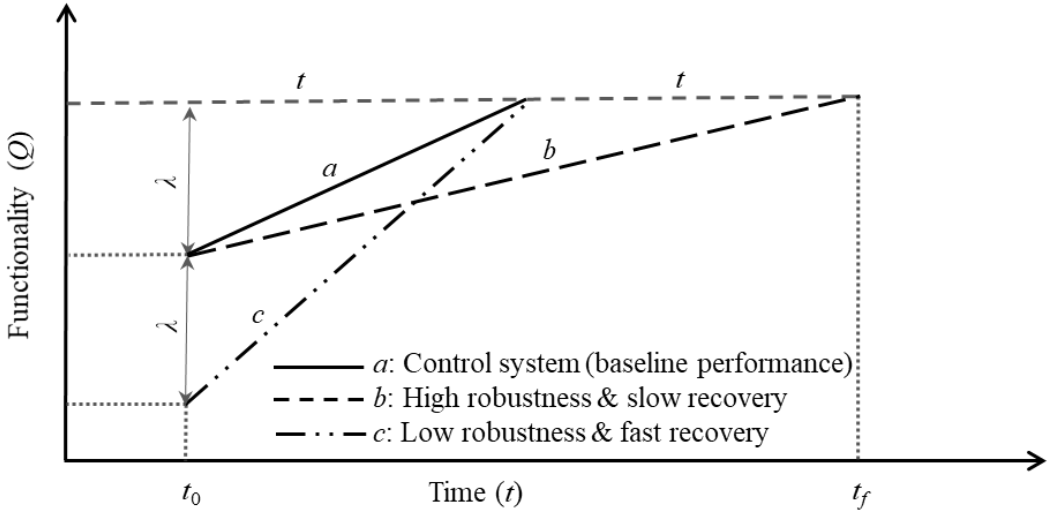

Figure 4.3: Post-disaster recovery paths

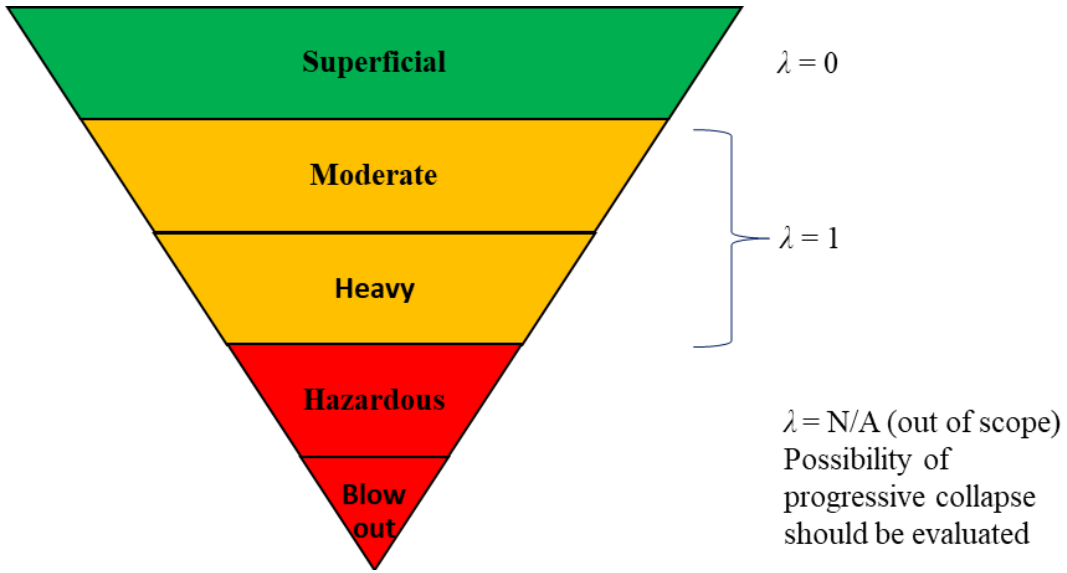

Figure 4.4: Proposed functionality indicator (λ) scheme for primary elements

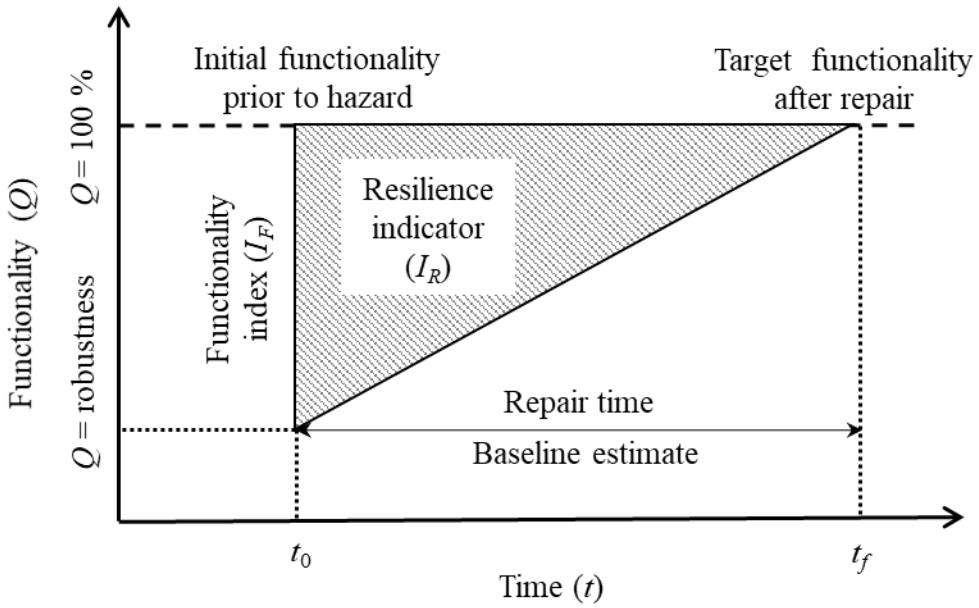

Figure 4.5: Geometrical interpretation of the resilience indicator (I_R)

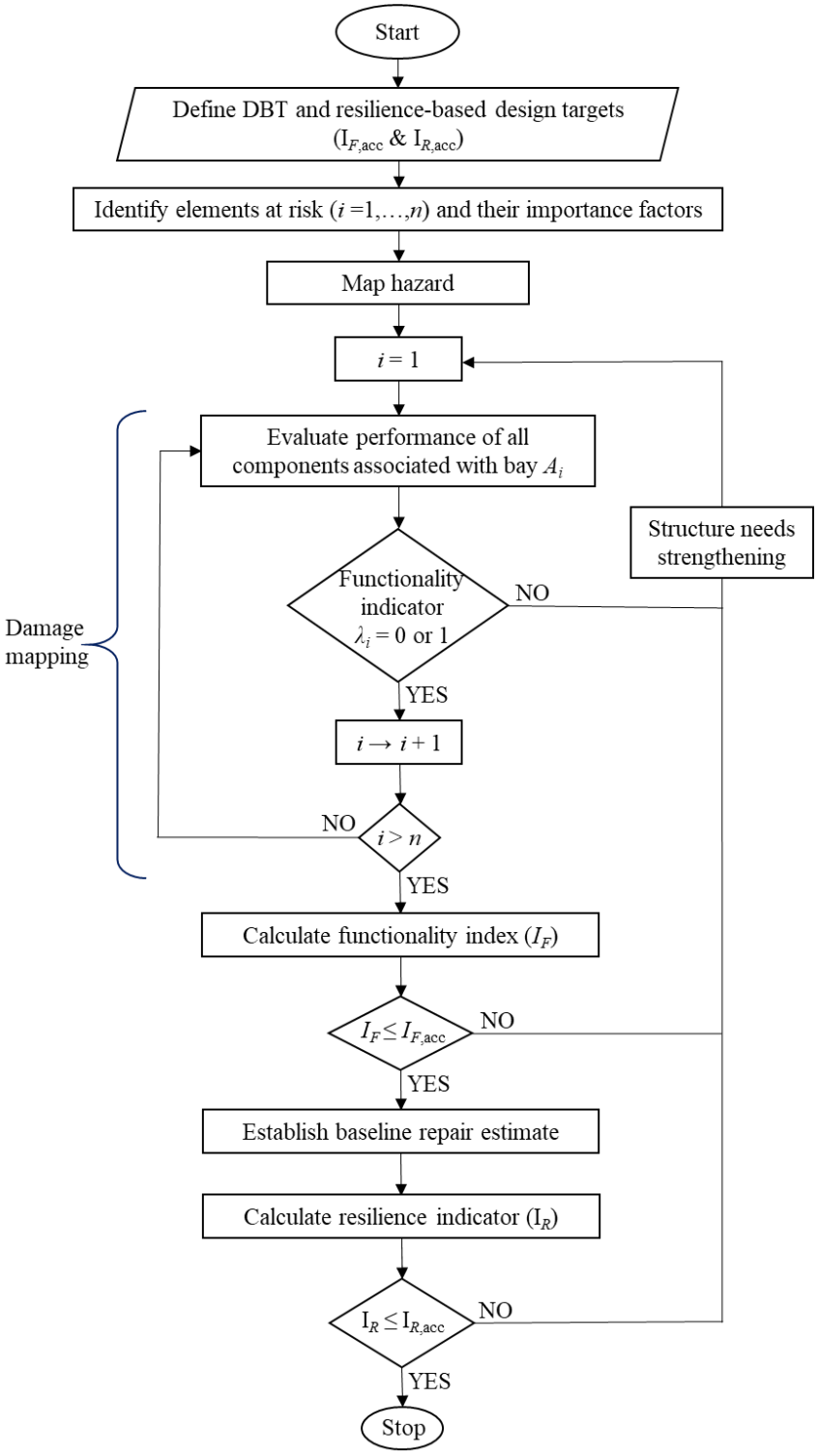

Figure 4.6: Proposed blast resilience framework

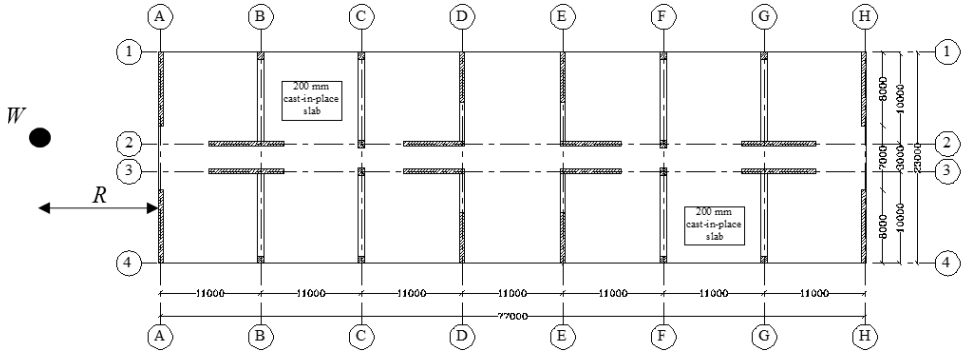

(a)

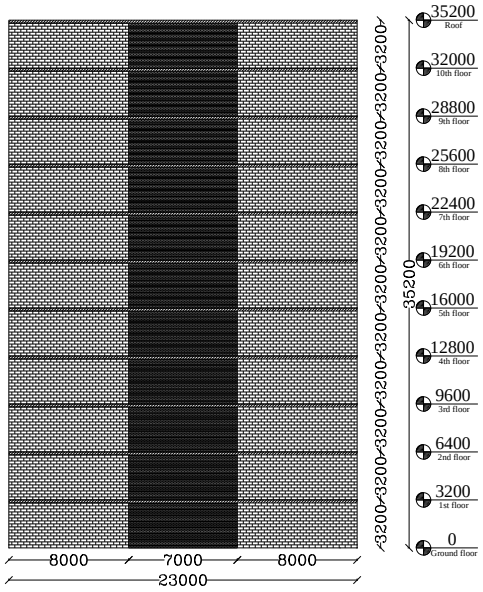

(b)

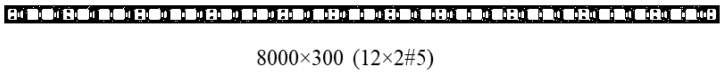

(c)

Figure 4.7: Reinforced masonry building prototype, adapted from NEHRP (2010), units in mm: (a)Plan view showing the DBT (charge weight "*W* " *and standoff distance "R"*); (b) Elevation; (c) Reinforced masonry wall detailing

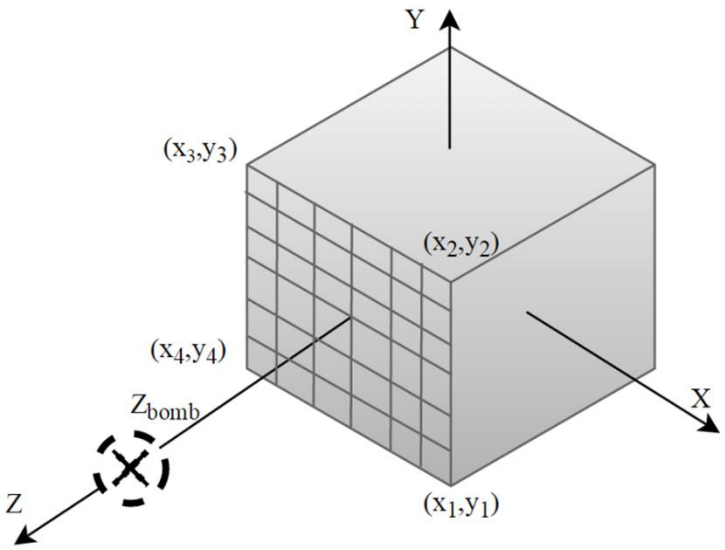

Figure 4.8: Geometrical grid adopted for the determination of blast wavefront parameters on the building's façade directly exposed to the explosive charge

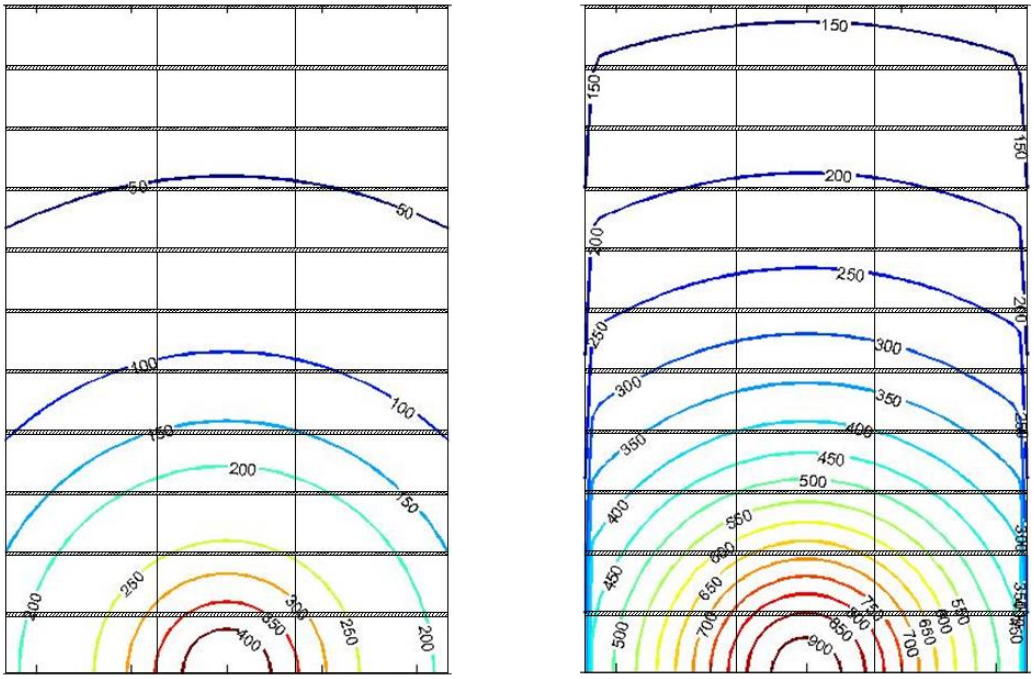

Figure 4.9: Reflected blast wavefront parameters on the exposed façade due to scenario 1:

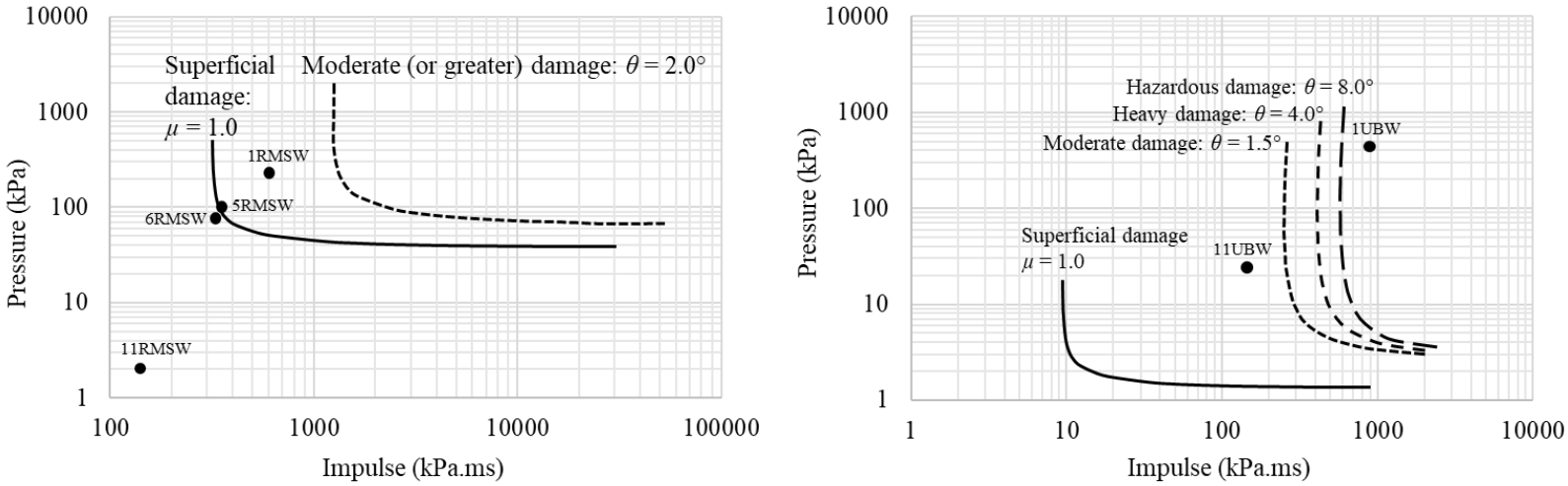

(a) (b)

Figure 4.10: Pressure-impulse diagrams of the exposed façade generated by the software SBEDS (USACE 2008):

(a) RMSW; (b) UBW

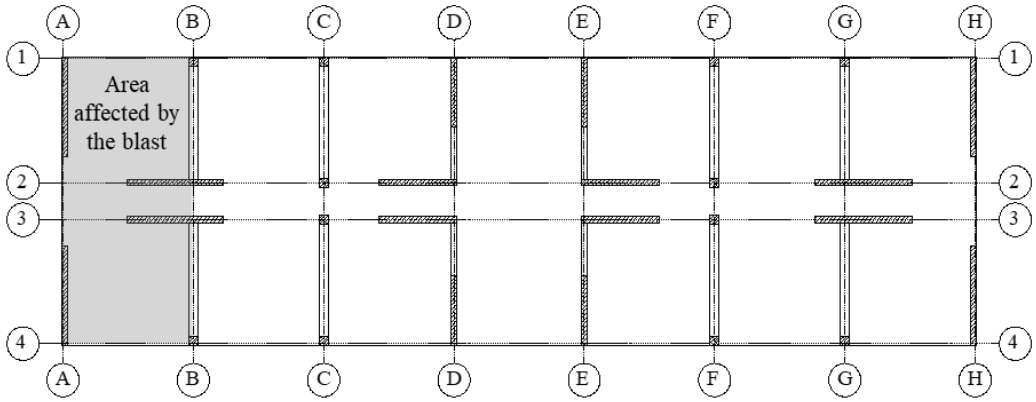

(a)

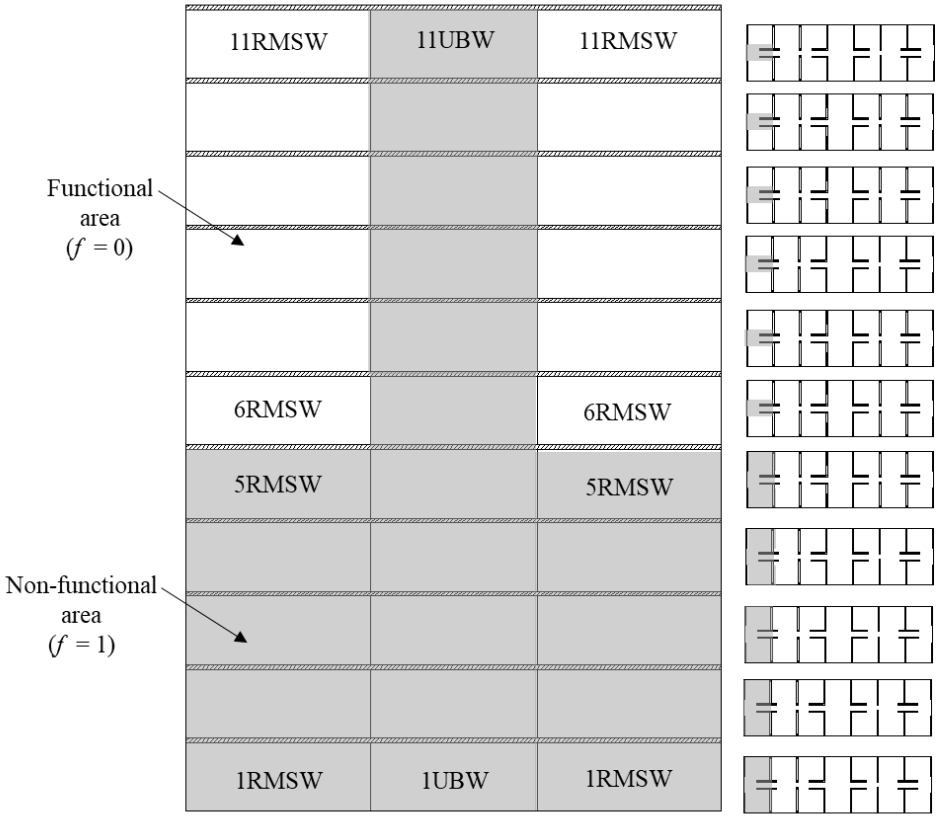

(b)

Figure 4.11: Building damage map (shaded areas are damaged): (a) Plan view, showing the bay areas affected by the blast hazard; (b) Elevation, showing the damage distribution over the exposed façade

Chapter 5

PROBABILISTIC RESILIENCE-BASED BLAST DESIGN FRAMEWORK

5.1 ABSTRACT:

Within the last decade, the cascading impact of different natural and anthropogenic hazard events has created a need to adopt resilience-based thinking within risk mitigation planning. Furthermore, deliberate explosion events—considered as low-probability high-consequence events—have increased over the past two decades. This in turn has resulted in the development of multiple blast design standards and highlighted the importance of relevant consideration in urban centers resilience planning. Several attempts aimed at producing comprehensive frameworks for the built environment against terrorist attacks; however, most of which falls under the umbrella of probabilistic risk assessments. In such approaches, the *instantaneous* projected direct and indirect losses are considered (causalities and economic) without the consideration of the *subsequent* loss evolution. In this respect, a novel resilience-based framework for the built environment resilience planning under blast events is introduced in this paper. The framework is based on the probabilistic assessment of general system functionality, recovery time and resilience indicators using deductive analysis techniques. The applicability of the proposed framework is demonstrated through a case study representing a mid-rise building subjected to different blast threat scenarios. The proposed probabilistic resilience framework lays the foundation for further work dealing with other forms of natural and/or anthropogenic hazard events in urban centers.

5.2 INTRODUCTION

One of the main objectives in natural and anthropogenic hazard risk predictions and mitigations is to support the rationality of the decision makers regarding pre- and post-disaster preparedness and planning. However, several disasters have been escalated due to the miscommunication of risk between the analysts and the decision makers, such as the 2017 Hurricane Maria, the 2017 Kabul terrorist attacks, and the 1995 Oklahoma City bombing. Risk communication is achieved through translating the outcomes of a hazard event into quantifiable metrics representing different risk aspects (economic, social, political, environmental, etc.) (Ayyub 2014). For example, the German Embassy, as well as multiple nearby embassies, in Afghanistan were heavily damaged after the 2017 Kabul attacks although an imminent terrorist threat that was expected six days before the attacks prior to the attack (Deutsche Welle Network 2017). To overcome this miscommunication problem, numerous frameworks have been proposed to assess the expected consequences into common metrics. The proposed frameworks were based on the well-established general definition of risk, given in Eq. (1), entailing the determination of hazard, assessing the vulnerability, and estimating the consequences.

$$Risk = Hazard \times Vulnerability \times Consequences \quad (1)$$

Some of these frameworks attempted to integrate the uncertainties associated with different hazards through the instantaneous direct and indirect losses resulting in developing probabilistic risk assessment (PRA) frameworks (Grant and Stewart 2015; Hickman 1983; Parry 1996). The advancements in the PRA have facilitated its application within the context of terrorism risk due to the latter's high inherent uncertainty (Grant and Stewart 2012). More specifically, PRA has been recommended by the current North American blast standards for the analysis of improvised

explosive devices (IEDs) attacks (ASCE 2011; CSA 2012), which constitutes about 60% of the terrorist attacks during the past 15 years (Institute for Economics and Peace 2015).

However, available blast-related PRA frameworks focus on estimating the overall damage (presented in the form of *level of protection*) based on the critical performance of some individual components only. In addition, these frameworks focus on the instantaneous post-event losses without considering the subsequent loss histories that continue to evolve until the targeted asset reaches an acceptable performance comparable to (or better than) that of the pre-event. These drawbacks highlight the deficiency of current frameworks in terms of integrating the instantaneous and subsequent losses into a unified framework metrics. As such, a comprehensive framework is required to assess the system post-event dysfunctionality history. This requirement coincides with the policy directive from the President of the United States (Presidential Policy Directive 2013) which emphasizes accounting for the resilience targets (instantaneous and subsequent losses).

Resilience-based design frameworks have been successfully applied to deal with so called black swan events within multiple disciplines, typically defined as the unpredictable events having catastrophic effects (Rose and Krausmann 2013). As such, its application within the context of blast design is promising, since resilience-based design adopts a holistic approach to evaluate system functionality and its subsequent downtime. The resilience concept has been applied within the context of a few blast-related risk; however, these applications were typically preliminary and require more development. Specifically, the available resilience-based blast design frameworks either neglect the subsequent losses or the probabilistic nature of the blast hazard. In this respect, this paper aims to develop a probabilistic resilience-based blast design framework that can be applied to different infrastructure elements to overcome the drawbacks of previous attempts. The framework objective is to probabilistically integrate the building system loss and its subsequent

downtime into unified resilience indicators, to provide decision-makers with a comprehensive risk perspective. Finally, to demonstrate the applicability of the proposed framework, an illustrative example of a typical mid-rise building under different blast threats is presented later in this paper.

5.3 RESILIENCE QUANTIFICATION

The concept of resilience has emerged from ecology in the 60's and subsequently introduced to different fields such as anthropology, and environmental psychology, where the concept has evolved from the single steady state domain to multiple equilibrium targets (Folke 2006). The multiple equilibrium concept conforms with engineering problems of multi-attribute optimization (Folke 2006). For instance, in earthquake engineering, a paradigm shift is being developed—moving from performance to resilience-based design—in order to account for the post-disaster functionality loss with its multiple-attributes (Almufti and Willford 2013). Bruneau et al. (2003) proposed a resilience framework, mainly for pre/post-earthquake evaluation, where resilience is quantified by four indicators (4R): robustness, rapidity, redundancy, and resourcefulness. Robustness is the system's ability to operate under a given level of shock measured as the immediate system performance after the hazard occurrence. Rapidity is the system's recovery time — downtime — measured from the immediate post-hazard state to the predefined acceptable post-hazard state, which may or may not be similar to the pre-hazard state. A distinct difference between the downtime and repair time has been illustrated by Almufti and Willford (Almufti and Willford 2013, 2014). The repair time is the time required to repair, or replace the elements affected by the hazard, while downtime is total time required to reach the targeted post-hazard performance state. The downtime includes the repair time as well as other impeding factors — the delays between the hazards and beginning of repair to conduct inspection, mobilizing services, etc. — and utility disruption — time required for the initiation of the backup systems, refueling generators, etc. Redundancy —the third resilience property in the 4R methodology — is the ability of the system

to sustain its functionality requirements through a secondary/backup system after losing/damaging some of the system's elements. And finally, resourcefulness is the system's capacity to mobilize the resources required for recovery. These four indicators of system resilience are sub-grouped into "robustness and rapidity" and "redundancy and resourcefulness". The first sub-group "robustness and rapidity" is the system's resilience quantifiable targets, namely, "resilience goals", while the second sub-group "redundancy and resourcefulness" is the resilience means (Rose and Krausmann 2013).

The system resilience goals, visually presented in Figure 5.1, are the functionality time history illustration and typically known as "resilience triangle" (Ayyub 2015). The first goal "robustness" is based on the assessment of the system functionality, where system functionality is the quantified system capacity to deliver a service or product within a design period "control time" representing the system qualitative or quantitative performance (Cimellaro et al. 2009, 2016). From the robustness definition, functionality is considered a system-dependent parameter that changes from one system to another and may evolve over time (Salem et al. 2018). At the community scale, ISO 37120 (ISO 2014) proposed comprehensive indicators covering multiple community vital functions such as the economy, education, energy, environment, finance, emergency response, governance, health, recreation, safety, shelter, solid waste management, telecommunication, transportation, urban planning, water and waste water management. All the indicators are presented in the form of a ratio of the delivered function after the hazard occurrence to the initial delivered function for a control number of population. Within specific infrastructure elements, the functionality is dependent on the system outcome; for example, the normalized gas flow rate and the total gas length were proposed for the resilience quantification of gas distribution network (Cimellaro et al. 2015). The traffic loading capacity, lane closures, allowed axle load, and speed limit were the representing quantitative and qualitative resilience indices used for highway bridges

(Mackie and Stojadinović 2006). For resilience assessment of hospitals, the patients' waiting time in the emergency room and the ambulance response time were presented as the qualitative functionality, while the ratio of treated to total number of patients was proposed as the quantitative index (Cimellaro et al. 2009).

Rapidity, is the resilience's second goal is influenced by the recovery path, which is the functionality rate of change influenced by the system preparedness. For example, an exponential recovery path can occur if the initial inflow of resources decreases over time, whereas a trigonometric path is expected when there is lack of resources, and a linear recovery path can develop when there is no solid information about the post-disaster preparedness (Cimellaro et al. 2010). In addition to the aforementioned recovery paths, the stepped recovery path can be associated with a realistic repair schedule to meet multiple performances also known as the sequence of target performance levels (Burton et al. 2016; Cimellaro et al. 2016). Ouyang et al. (2012) accounted for the damage propagation time through quantifying the time to reach the maximum damage state.

Mathematically, the resilience can be quantified through one of the earliest urban infrastructure-relevant resilience definitions using the "resilience index" (I_r). I_r is the ratio of the functionality loss to the expected function delivered within a predefined control time (Attoh-Okine et al. 2009) as shown in Eq. (2):

$$I_r = \frac{\int_{t_0}^{t_f} Q(t)\,dt}{100(t_c - t_0)} \tag{2}$$

where Q(t) represents the system functionality with respect to time (t); t_0 is the first damage time that occurs due to the considered hazard; t_f is the time required to reach the targeted post-hazard performance; t_c is the control time used to evaluate the functionality loss, which is usually used as

t_f; however, this transforms the I_r to function loss averaging over the downtime — known as resilience linearity. The resilience linearity feature would overlook the effect of the recovery time on the resilience index (Bruneau and Reinhorn 2007; Salem et al. 2018); which may influence the rationality of the decision makers.

5.4 AVAILABLE BLAST RESILIENCE EVALUATION FRAMEWORKS

According to the published literature, two resilience-based have been applied within the context of blast design, however, these frameworks have various limitation that will be discussed in this section. The first framework, proposed by Quiel et al. (2016) and Marjanishvili (2017), focuses on the probabilistic prediction of a given system robustness subjected to a blast threat, but does not consider the resilience's second goal "rapidity". While, the second framework was proposed by Salem et al. (2017a and 2018) as a deterministic quantification procedure for the reserved system functionality in generic terms with an approximate estimation for the system post-blast downtime. A linear recovery path was assumed due to the approximation in the rapidity estimation. As such two indices have been proposed to overcome the resilience linearity problem; namely the functionality loss index (I_F), and the resilience indicator (I_R). Where I_F is the ratio of the residual post-blast immediate functionality to the system normal state functionality, while I_R is the integrated functionality loss over the downtime period. The functionality was derived using the functionality loss indicator (λ), a binary indicator, representing the accessibility of each area of the building after the hazard. The functionality loss indicator (λ) is based on the expected performance of the façade components, affected by the blast wave, surrounding the building area under investigation "architectural unit (bay)". The bay is considered functioning (i.e. λ=0) if all its surrounding components experienced superficial damage. Whereby definition, superficial damage may or may not be visible and it may require cosmetic repair, if any at all, which allows the functionality of its pertinent bay. Conversely, the bay is considered not functioning (i.e. λ=1) whenever one or more

of its surrounding façade components experience any damage rather than superficial. The framework did not consider the initiation of progressive collapse by not including the hazardous and the blow out states for the structural components. However, this framework would remain valid even if the non-structural components experience hazardous or blowout states as it would not affect the structural integrity of the investigated system. The λ for structural components and I_F can be formulated as shown in Eq. (3 and 4) (Salem et al. 2018).

$$\lambda = \begin{cases} 0 & \text{Bay enclosed by components incurring superficial damage} \\ 1 & \text{Bay enclosed by components incurring moderate or heavy damage} \\ \text{N/A} & \text{Bay enclosed by components incurring hazardous damage or blowout} \end{cases} \tag{3}$$

$$I_F = \frac{\sum_{i=1}^{n} A_i I_i \lambda_i}{\sum_{i=1}^{n} A_i I_i} \tag{4}$$

where A_i is the functioning area of the i-th bay, n is the total number of bays in the building, I_i is the importance factor ascribed to bay area A_i, and λ_i is the loss indicator describing the damage experienced by the i-th bay, in accordance with Eq. (3). On the other hand, the resilience's second goal "downtime" is presumed as the repair time estimated using the baseline estimate approach recommended by the FEMA P-58 (FEMA 2012a) to calculate the labor hours of repair (averaging the estimated overall labor repair cost with respect to the crew hourly rate) as shown in Eq. (5).

$$Baseline\ estimate(hr) = \frac{Repair\ cost\ (\$) \times LPCT\ (\%)}{Effective\ hourly\ rate(\$ / hr)} \tag{5}$$

LPCT (labor production commencement time) is the ratio of labor cost to repair a certain component to its total cost. Finally, the I_R can be calculated using Eq. (6) (Salem et al. 2018).

$$I_R = \frac{1}{2}(t_f - t_0)I_F \quad (6)$$

The framework proposed by Salem et al. (2017a and 2018) was mainly addressing the current blast standards (ASCE 2011; CSA 2012) to apply the resilience concept. As such, a deterministic approach was applied to facilitate a seamless design concept shift. However, the ignored probabilistic nature of the blast hazard/risk remains key for a comprehensive assessment (Campidelli et al. 2016a; Grant and Stewart 2015). Consequently, numerous studies accounted for various sources of blast uncertainty via PRA. Even more, it worth mentioning that the Canadian blast standards design has recommended the inclusion of the blast uncertainty, however, no clear guidelines are proposed (CSA 2012). Subsequently, the following sections discuss the available PRA blast-related frameworks and its adoption within the simplified resilience-based blast design proposed by Salem et al. (2018).

5.5 PROBABILISTIC BLAST RISK ASSESSMENT

Blast threat is characterized by high epistemic and aleatory uncertainties even under a given design basis threat (Stewart 2008; Stewart et al. 2006). The blast epistemic uncertainties include parameter uncertainty (detonation charge, stand-off distance, etc.) and model uncertainty (accuracy of predictive models), while aleatory uncertainties includes the inherent variability (weather, blast environment, etc.) (Stewart et al. 2006). The uncertainty of the blast wavefront parameters or the response of elements subjected to blast loading have been extensively studied to assess the response of structural/non-structural elements, for reliability analysis, or to highlight the high impact of the blast uncertainties on the components performance (Borenstein and Benaroya 2009; Campidelli et al. 2015a; Kelliher and Sutton-Swaby 2012; Low and Hao 2002; Stewart et al. 2006; Stewart and Netherton 2008). The blast reliability analysis has been integrated with PRA for different structural/non-structural elements as an optimization tool for the blast mitigation measurements

through finding the probability of failures and integrating the failure consequences. Stewart (2008) used the direct cost for the façade glazing optimization, Grant and Stewart (2015) and Stewart (2010) used the direct cost as well as the cost of the expected fatalities (using the value of single live in monetary units) derived from historical data of previous terrorist events. Campidelli et al. (2015a), and ElSayed et al. (2015) implemented the PRA for assessing reinforced masonry walls (RMWs) and estimating their repair costs.

The available blast-related PRA frameworks either adopts the conditional or the unconditional approaches to account for different sources of uncertainty associated with blast loading (Olmati et al. 2016). The unconditional approach integrates all the sources of uncertainty, load, component performance and capacity, into one model using Monte Carlo simulation. Subsequently, the unconditional approach would require a large computational advancements (Olmati et al. 2016). Conversely, the conditional approach decouples the uncertainty associated with the load, component performance, and capacity, requiring less computational advancements than the unconditional approach. As such, most of the available PRA frameworks use the conditional approach to account for the uncertainty associated with blast loading (Low and Hao 2001, 2002, Olmati et al. 2014, 2016; Stewart et al. 2006; Yu et al. 2018). The complexity of the conditional approach depends on the data availability and the number of considered parameters; as such, optimum parameter selection is a vital aspect of the application within the blast context design.

Within the blast context, multiple parameters may influence the blast response of different structural/non-structural components such as: charge weight and location, energetic equivalency, ambient pressure, and temperature, etc.. (Campidelli et al. 2015b; Netherton and Stewart 2010). However, Olmati et al. claimed that the charge weight (W) and the scaled distance (Z) are two main parameters affecting the blast load intensity (Olmati et al. 2016). Where the Z is one of the most

universally used blast scaling laws, known as "Hopkinson-Cranz law" (Baker et al. 1991), and can be calculated through Eq. (7).

$$Z = \frac{R}{\sqrt[3]{W}} \tag{7}$$

where R is the standoff distance measured from the center of the explosive charge to the investigated point; while W is the explosive TNT equivalent weight. Furthermore, according to the Unified Facilities Criteria (UFC) the Z and W are the only parameters required to estimate the idealized, induced and reflected, blast wavefront parameters as shown in Figure 5.2 (USDOD 2014). Where P_0 (in MPa) is the atmospheric ambient pressure; P_s^+ (in MPa) is the maximum reflected pressure; t_a (in seconds, m.s) is the arrival time; t_d (in m.s) is the blast duration; while the integration of the positive phase pressure through the blast duration is known as the positive phase specific impulse "I" (MPa.ms).

Typically, both the P_s^+ and I are the well-known blast parameters controlling the component performance (Olmati et al. 2016); even more, the P_s^+ and I are used for the generation of the iso-response curve for elements subjected to blast loading; namely P-I diagrams. The typical blast P-I diagram represented in Figure 5.3 divides the component response into three regions; impulsive region where the impulse is the dominating factor on the component response (most of the blast-resistant structural elements); dynamic region where the structural performance is controlled by both pressure and impulse; and finally, the quasi-static region where the peak pressure is the governing factor for the response of the components (governing for very stiff components) (Hayman 2014). Consequently, many researchers solely account for I, dominating for most cases, as the influential blast parameter within the conditional probabilistic assessments (Campidelli et al. 2017; Olmati et al. 2016; Stewart et al. 2006; Stewart and Netherton 2008). As such, the conditional

probabilistic blast assessment is formulated as shown in Eq. (8) and known as "fragility curve" (Olmati et al. 2016).

$$P_f = \int_0^{\infty} \mathrm{P}_r\left[G(X) < LS \mid I\right] \mathrm{P}_r\left[I\right] dI \tag{8}$$

where P_f is the probability of exceeding a specific limit state (LS); $P_r[G(X)<LS/I]$ is the probability of exceeding a specific limit state at a given specific impulse; $P_r[I]$ is the probability density function of the specific impulse. It should be noted that although both P_s^+ and I are the dominant parameters for the structural performance, depicted through the P-I diagrams, the approximation of using a 2D fragility curve instead of using a 3D fragility surface still represents a reasonable assumption for the impulsive region components (Olmati et al. 2016).

5.6 PROBABILISTIC RESILIENCE ASSESSMENT FRAMEWORK

This section encompasses comprehensive details about the application of uncertainty within the deterministic resilience-based blast design proposed by Salem et al. (2017a and 2018). The framework aims to calculate both the system's expected functionality loss and repair time and their standard deviations after blast hazard through the application of the conditional probabilistic approach as illustrated in Figure 5.4. It is worth noting that an earlier attempt for the application of blast uncertainty within the aforementioned framework was made by Salem et al. (2017b); however, within the earlier attempt, the unconditional approach was adopted. Although the framework proposed by Salem et al. (2017b) highlighted the importance of integrating the probabilistic nature of blast loading into the systems resilience assessment, it can be classified as a conceptual framework that cannot be applied to multiple systems due to the lack of information and the significant computational challenges.

As such, the conditional probability approach is proposed for the current framework to probabilistically assess the resilience goals (functionality loss and downtime). The assessment presented in the proposed framework is based on the decision-makers perception for the functionality loss caused by blast hazard through assessing probabilistically the functionality indicator (λ) and the repair cost controlling the downtime as illustrated next.

5.6.1 Functionality Loss

The proposed functionality loss index I_F (Salem et al. 2017a, 2018), illustrated in Eq. (4), can be presented as shown in Eq. (9). It can be seen that λ is the only variable influencing I_F, as C_i is a constant given by Eq. (10).

$$I_F = \sum_{i=1}^{n} C_i \lambda_i \tag{9}$$

$$C_i = \frac{A_i I_i}{\sum_{i=1}^{n} A_i I_i} \tag{10}$$

Due to the assumption of the individual components localized response used in the current blast standards and the proposed blast resilience frameworks (ASCE 2011; CSA 2012; Salem et al. 2017a, 2018); the probabilistic I_F ,for a given scenario, can be derived directly from λ due to the probabilistic linearity (Ang and Tang 2007). In other words, the determination of the expected value and the standard deviation of I_f depends on the probability of the binary function λ of each bay. Where P(λ)=1 is the probability of experiencing all the surrounding components of an area a no/superficial damage; while P(λ)=0 is the complimentary as expected damage state does not matter from the functionality perspective (the subsequent area will be closed for repairs). The P(λ=1) can be determined through the conditional probability approach as shown in Eq. (11); where LS_1 is the first damage state.

$$P(\lambda = 1) = \int_0^{\infty} \mathrm{P}_r\left[G(X) < LS_1 \mid I\right] \mathrm{P}_r\left[I\right]\, dI \tag{11}$$

5.6.2 Downtime Estimation

As per the deterministic framework proposed by (Salem et al. (2017a and 2018), the downtime is assumed as the repair time. The deterministic downtime can be calculated using Eq. (5) as previously mentioned, however, this linear equation solely depends on the repair cost as a unique variable. Subsequently, the expected value of the probabilistic downtime can be interpreted as the weighted average of the repair cost, as seen in Equation 12, divided by the effective labor hourly rate and can be calculated using Eq. (12); while the repair time standard deviation can be derived using the method of moments (MoM) with respect to the standard deviation of the repair cost.

$$\textit{Repair cost}\left(\$\right) = \sum_{s=1}^{nf} \sum_{k=1}^{q} \mathrm{P}_{rs}\left[LS_k \mid I < G(X) < LS_{k+1} \mid I\right].\mathrm{P}_{rs}\left[I\right].Q_{ks} \tag{12}$$

$$\textit{Repair time}\left(hr\right) = \frac{\sum_{s=1}^{nf} \sum_{k=1}^{q} \mathrm{P}_{rs}\left[LS_k \mid I < G(X) < LS_{k+1} \mid I\right].\mathrm{P}_{rs}\left[I\right].Q_{ks} \times LPCT_i \ \left(\%\right)}{\textit{Effective hourly rate}\left(\$ \diagup hr\right)}$$

(13)

where LS_k is the performance at limit state function "k" ranging from 1 to q depending on the element under investigation (the most severe damage state expected for the s), Q_{ki} is the expected repair cost for element "s" at the k-th damage state, nf is the total number of elements in the façade subjected to blast loading.

Although Eq. (11 and 13) probabilistically assess the post-blast functionality loss and the downtime (through conditional approach); both equations still based a deterministic load parameter (I). The application of a deterministic I ignores the input parameters uncertainty, which may propagate into a large variation within the structural response (Campidelli et al. 2015a). On the

other side, numerous researchers investigated the uncertainty associated with I through proposing coefficient of variation (c.o.v) for recorded blast scenarios ranging from 0.1 to 0.3 (Campidelli et al. 2015b; Lofton and Meyers 2001; Twisdale et al. 1994). Consequently; introducing the parameter uncertainty within the I_F and I_R alter their estimated values. Accordingly, a development for the proposed conditional probabilistic approach is required to account for the input parameters uncertainty. Subsequently, a Monte Carlo simulation can be adopted through randomly changing the input parameter based on the investigated blast scenario, using the MoM.

5.6.3 Framework Structure

Figure 5.5 illustrates a flowchart for the proposed framework in order to probabilistically assess an existing building or to optimize through different blast mitigation measurements. First, the design basis threat (DBT) (blast scenario) should be identified, the acceptable functionality index and resilience indicator ($I_{F,acc}$, $I_{R,acc}$) are determined as the acceptance thresholds based on the decision-makers loss acceptance. Also, the importance factors (I_i) should be assigned to building areas based on the value tree analysis performed by the decision makers to assign importance factors for the building different areas by weighting their economic, social, physical, and environmental aspects (Apostolakis 2008; Apostolakis and Lemon 2005). Furthermore, based on the DBT, the elements at risk (n) (façade elements facing the DBT) should be determined and the Monte Carlo sample size (N) should be defined. Subsequently, the Monte Carlo simulation starts, using the MoM, through mapping the hazard on the façade while checking the susceptibility to progressive collapse. The progressive collapse assessment is achieved through a deterministic valuation for the primary structural components to ensure that none of them would experience a hazardous or a blowout state to ensure the integrity of the structure after the blast occurrence. Consequently, the façade components are assessed for each damage state using the conditional approach through applying the mapped hazard. As such, the expected functionality loss and the downtime for the

building can be calculated using Eq. 11 and 13 respectively. Finally, the iterative Monte Carlo simulation continues till reaching the target sample size (N), which would allow the computation of the descriptive measures for the I_F and I_R (mean and standard deviation), while considering the input parameter uncertainty. The framework is ultimately applied within the iterative design context through comparing the probabilistic I_F and I_R with the previously defined thresholds ($I_{F,acc}$, $I_{R,acc}$). Where strengthening for the façade components can be applied if any of the primary elements experienced a hazardous or blow out through the deterministic analysis or any of the I_F and I_R did not meet the $I_{F,acc}$, $I_{R,acc}$. As a graphical representation of the results, the expected functionality loss and the downtime can be plotted assuming a linear recovery path to generate the resilience triangle, moreover, their confidence interval can be plotted to illustrate the uncertainty in both resilience aspects to illustrate the uncertain recovery rate band as shown in Figure 5.4. Furthermore, the 2D resilience triangle, with the confidence intervals, can be interpolated into a 3D resilience surface integrating all the calculated uncertainties into a comprehensive post-blast functionality time-history as illustrated later in the following demonstrative example.

5.7 DEMONSTRATION APPLICATION OF THE PROPOSED FRAMEWORK

This section presents an illustrative example for the proposed probabilistic blast resilience framework to demonstrate its applicability to real buildings. The case considered applies the proposed framework on a mid-rise building with simple architectural details. In order to avoid distracting the reader with complex blast load numerical calculations, the blast wave reflections through the building's premises and its propagation towards the building core; interaction between different building components; primary and secondary fragmentation effects are neglected. However, these neglected factors can be considered and implemented within the proposed framework. As such, the assumed affected area with the blast scenario is limited to the façade area facing the DBT. Also, the linear recovery path used in the resilience quantification implicitly

assumes a constant resource supply rate; which may not be the case, and a real repair scenario with respect to the expected damage should be included.

A mid-rise, four-story, reinforced concrete block masonry building is adapted from NEHRP (NEHRP 2010) is selected an illustrative example to typify a governmental administrative building as shown in Figure 5.6. Where Figure 5.6(a) shows the plan of the primary load bearing system; while Figure 5.6(b) illustrates the building's elevation revealing its components; 3 m panels non-load bearing RMWs and 2 m x 2 m simply supported toughened glass (6 mm) on all its four sides to form the designed architectural module. Figure 5.6(c) depicts the details of the details of the non-load bearing RMWs used as a typical panel in the building's façade constructed with 400 x 190 x 190 mm concrete blocks, 20 MPa average compressive strength, and 0.53% vertical reinforcement ratio (15 #5 (200 mm^2)). The façade components details are selected to facilitate the application of previously developed fragility curves into the current case study, as the investigation of the components blast performance is out of the study's scope. Three different scenarios adapted from Salem et al. (2018) are illustrated in this case study to present the applicability of the proposed framework. The three scenarios, shown in Table 5.1, are sorted in an ascending order according to the DBT scaled distance calculated using Eq. (7). Scenarios #1 and #2 presents a small charge weight (50 kg) with relatively small standoff distances (10 and 20 m respectively) representing a person-borne threat. On the other hand, scenario #3 resembles a vehicle-borne IED threat with 500 kg charge weight and 40 m standoff distance. According to the current blast standards (ASCE 2011; CSA 2012), the three selected scenarios yield to a very low level of protection (LOP) due to the low performance of the non-structural components. As such, the assumed scenarios would highlight the significance of the proposed framework to physically quantify the post-blast functionality.

The proposed framework is applied through a developed probabilistic infrastructure resilience assessment toolbox (PIRAT); a subroutine developed using MATLAB (The MathWorks

2014) to facilitate the assessment for the three scenarios. The PIRAT facilitates the iterative blast simulation considering the input parameter uncertainty through considering the uncertainty associated with *I* via the MoM. In the given example, the *I* is generated using the proposed normal distribution fitted by Campidelli et al. (mean value of 1.01 and c.o.v of 0.19) (Campidelli et al. 2015b). The PIRAT starts with calculating the wavefront parameters, specifically the positive phase specific impulse, across the façade facing the blast through an imaginary grid —100x100 in this case study — considering the clearing effect (Campidelli et al. 2015b; USDOD 2014). Figure 5.7 depicts the *I* contour on the façade subjected to scenario #1 DBT which ranges from 111 kPa.ms at the top corners of the façade to 929 kPa.ms at the center of the façade (shortest standoff distance). Subsequently, the susceptibility to progressive collapse is checked then the conditional probabilities of the facade components for the different applicable damage states (DS) are determined. The determined conditional probabilities are based on a previously developed fragility curves for similar components and shown in Figure 5.8 (Campidelli et al. 2016b; Stewart and Netherton 2008). Where Campidelli et al. (2016b) derived the fragility curves for a scaled RMWs (1/3 scale) similar to that used in the façade; as such, the fragility curves used in this example are scaled up following the Buckingham PI theorem (Baker et al. 1991). Moreover, Stewart and Netherton (2008) derived the fragility curves for the glazing used with the example proposed dimensions. The baseline estimate used to evaluate the repair time adopts the repair cost of the RMW from the FEMA P-58 based on the 90^{th} percentile cost associated with the repair of a special RMW flexural controlled of 200-300 mm (8-12'') thick wall with height not greater than 3.67 m (12') (FEMA 2012b). The repair cost for forth damage State (DS4) was assumed as DS3 as both would require wall replacement, while the average cost of a glass panel is assumed $820/ panel, which accounts for replacement cost of a similar unit (Salem et al. 2017a). The used RMWs and glazing LPCT is 69 and 30% respectively (Salem et al. 2017a); where all the repair costs are recalled in Table 5.2. For the sake of comparison,

a series repair scheme is assumed — repair activities are limited to one floor at a time —the number of repair workers has been fixed to eight workers (1 crew) based on FEMA P-58 (FEMA 2012a; b), which recommends assuming one worker for each 92m^2 (1000ft^2) with 255$/hr. Consequently, Equations 11 and 13 are applied to evaluate the functionality loss and its subsequent downtime for each iteration. Finally, the PIRAT probabilistically assess the descriptive measures for both the I_F and I_R (using Equations 4 and 6). The results of the three scenarios are summarized in Table 5.3 illustrating the expected value as well as the standard deviation of the I_F, the total repair cost, labor repair cost, repair time, and I_R.

The expected functionality loss for the three scenarios ranged from 39.4 to 43.2% with standard deviation ranges from 0.6 to 0.8%. These results can be interpreted as the as the instant loss of the products/service loss delivered by the building. The similar expected values and the small c.o.v. for the I_F of the three scenarios, 1.3-2.0%, is attributed to the vulnerability of the façade components to different damage states rather than the superficial state. In other words, the three considered scenarios will cause some damage to the façade rather than superficial. Figure 5.9 depicts the dysfunctionality (probability of exceeding DS1) mean distribution across the façade resulting from scenario #1. On the other side, the expected downtime and standard deviations for scenarios #1 and 2 are almost similar as seen in Table 5.3, expected value of 189 and 185 *hrs* with standard deviation of 7.3 and 10.6 *hrs* working hour respectively, which results into small c.o.v. (3.8 and 5.7%). These similar values, within scenarios #1 and 2, are attributed to the to the domination of the repair cost of the window glazing and its high probability (100%) of fracturing when subjected to the blast load and the relatively small masonry component affected by the blast considered under the DBT scenarios due to the small charge threat. Conversely, the expected repair time for scenario #3 is 347 *hrs* with a standard deviation of 83 *hrs*, resulting into 23.9% c.o.v. This high c.o.v. is backed to the large input parameter variability influencing the repair cost of the façade

RMSWs. Figure 5.10 depicts a 3D comprehensive surface for the building's functionality post-blast (scenario #1) time history at the 90th percentile confidence.

Although the three scenarios have a similar I_F, the expected I_R values for the three scenarios were not the case as illustrated in Table 5.3. Both scenarios # 1 and 2 have similar I_R (3799 and 3645 *hrs* respectively), due to the similar I_F and repair time as previously discussed; while scenario #3 has larger I_R (7495 *hrs*) due to its larger expected repair time.

Among the three different scenarios, the results of scenario #3 are comprehensively elaborated in the following section. For scenario #1, the expected total repair cost for the building (using Equation 11) is \$182,000 with a standard deviation of \$30,000 to reach the pre-blast performance; while the corresponding labor expected cost is \$88,500 with \$21,200 standard deviation. Figure 5.11 depicts the building, the façade, and the damaged façade component costs, where the estimated building total cost — \$8,500,000 — is derived from the average cost of office buildings under five stories \$1,300/m^2 (Altus Group Limited 2017), the façade cost estimate — \$340,000 — accounts for building/installation the façade components, and the details of the façade repair cost (\$95,000 for the glazing and \$87,000 for the RMWs). Figure 5.11 represents the ratio of the facade components repair cost ratio to the building cost, where the glazing repair cost is 1.1% (\$95,000) of the total building cost while the repair cost ratio of the RMWs is 1.0% (\$87,000) of the total cost. As such, the estimated damage of 2.1% of the total building cost due to Scenario #3 would cause the facility 7495 *hrs* of dysfunctionality which may be a proper communication form with the risk assessors than the current generic LOP proposed by the current blast standards. Figure 5.12 shows a graphical 2D representation to the probabilistic functionality loss and repair time required to reach the pre-hazard performance when subjected to Scenario #3.

The proposed probabilistic resilience framework clarified the vagueness of the current assessment criteria recommended by the North American blast standards (ASCE 2011; CSA 2012); since all the blast scenarios are classified the same LOP, as shown in Table 5.1, yet the proposed framework has demonstrated the difference of function loss between the blast scenarios through the I_F and I_R. Furthermore, the considered case study building with different DBT scenarios highlights the ambiguity of using Z as the only blast hazard severity indicator. This is demonstrated by observing that the Z value for Scenario #1 is greater than that in Scenario #3 while the expected losses under Scenario #3 is larger than that under Scenario #1. This is attributed to the combination of different performance of all the façade elements through the assessment. Finally, the proposed framework can be adapted to a reliable optimization tool for the blast mitigation through the effective placements of blast mitigation measurements to protect the areas responsible for the functionality loss or minimizing the losses.

5.8 CONCLUSIONS

A probabilistic resilience-based blast design framework is proposed to comprehensively assess the post-blast functionality history. The proposed framework is based on a conditional probability approach which facilitate repeatability of the assessment. The probabilistic resilience is quantified through two indices, namely, the functionality index and the resilience indicator. The functionality index describes the probable functional loss by integrating the expected local damage over the whole structure, while the resilience indicator is proposed as a measure of the expected cumulative loss dependent on the post-blast downtime. In this paper; the resilience metrics were linked to the functioning areas of the building, while the downtime is estimated using the baseline repair time provided in FEMA P-58. A case study of a mid-rise building subjected to a ground IED threat is included to illustrate the computation of the probabilistic functionality loss index and the resilience indicator, given the variation of the blast wavefront parameters across the exposed façade. The blast

uncertainties (epistemic and aleatory) have been integrated into the framework using the probabilistic infrastructure resilience assessment toolbox (PIRAT), which is based on the conditional probability approach that facilitates its application and repeatability. The probabilistic functionality and repair time, presented graphically, extend the 2D resilience triangle into a 3D resilience surface. The proposed methodology leads the way of introducing uncertainty in resilience–based infrastructure design tools under other forms of anthropogenic hazards.

5.9 ACKNOWLEDGMENT

Financial support has been provided through a Collaborative Research and Development Grant funded by the Natural Sciences and Engineering Research Council (NSERC) of Canada. Industrial support has been provided through the Canadian Concrete Masonry Producers Association and the Canada Masonry Design Centre. Additional support has been provided by the McMaster Institute for Multi-Hazard Systemic Risk Studies (INTERFACE).

5.10 NOTATION

A_i = Area of a single bay i

G = Component performance

I = Positive phase specific impulse

I_F = Functionality index

I_i = Importance factor associated with bay area i

I_r = Resilience index

I_R = Resilience indicator

LS = Limit state

P_0 = The atmospheric ambient pressure

P_s^+ = Blast maximum reflected pressure

Q = System functionality

R = Standoff distance, measured from charge center building's facade

t_0 = Time of hazard occurrence

t_a = Blast wave arrival time

t_d = Blast duration

t_f = Time of full recovery to pre–disaster functionality

W = TNT–equivalent mass of the explosive

Z = Scaled distance

λ = Loss indicator

5.11 ACRONYMS

PRA Probabilistic risk assessment;

IED Improvised explosive devices;

LPCT Labor production commencement time;

DBT Design basis threat;

RMWs Reinforced masonry walls;

LS Limit state;

PIRAT Probabilistic infrastructure resilience assessment toolbox;

DS Damage state.

5.12 REFERENCES

Almufti, I., and Willford, M. (2013). *REDiTM Rating System: Resilience-based Earthquake Design Initiative for the Next Generation of Buildings*. Arup Co.

Almufti, I., and Willford, M. (2014). "The REDi^{TM} rating system: A framework to implement resilience-based earthquake design for new buildings." *10th U.S. National Conference on Earthquake Engineering, Frontiers of Earthquake Engineering, July 21-25*.

Altus Group Limited. (2017). *Canadian cost guide*. Toronto, ON, Canada.

Ang, A., and Tang, W. (2007). *Probability Concepts in Engineering: Emphasis on Applications to Civil and Environmental Engineering*. John Wiley & Sons.

Apostolakis, G. E. (2008). "Probabilistic Risk Assessment (PRA)." *Wiley Handbook of Science and Technology for Homeland Security*, John Wiley & Sons, Inc., Hoboken, NJ, USA.

Apostolakis, G. E., and Lemon, D. M. (2005). "A Screening Methodology for the Identification and Ranking of Infrastructure Vulnerabilities Due to Terrorism." *Risk Analysis*, 25(2), 361–376.

ASCE. (2011). *Blast Protection of Buildings*. *ASCE 59-11*, (American Society of Civil Engineers, ed.), American Society of Civil Engineers, Reston, VA, VA.

Attoh-Okine, N. O., Cooper, A. T., and Mensah, S. A. (2009). "Formulation of Resilience Index of Urban Infrastructure Using Belief Functions." *IEEE Systems Journal*, 3(2), 147–153.

Ayyub, B. M. (2014). *Risk Analysis in Engineering and Economics*. *Risk Analysis in Engineering and Economics*, (Chapman and Hall/CRC, ed.).

Ayyub, B. M. (2015). "Practical Resilience Metrics for Planning, Design, and Decision Making."

ASCE-ASME Journal of Risk and Uncertainty in Engineering Systems, American Society of Civil Engineers, 1(3), 1–11.

Baker, W. E. (Wilfred E., Westine, P. S., and Dodge, F. T. (1991). *Similarity methods in engineering dynamics : theory and practice of scale modeling*. Elsevier.

Borenstein, E., and Benaroya, H. (2009). "Sensitivity analysis of blast loading parameters and their trends as uncertainty increases." *Journal of Sound and Vibration*, 321(3–5), 762–785.

Bruneau, M., Chang, S. E., Eguchi, R. T., Lee, G. C., O'Rourke, T. D., Reinhorn, A. M., Shinozuka, M., Tierney, K., Wallace, W. a., and von Winterfeldt, D. (2003). "A Framework to Quantitatively Assess and Enhance the Seismic Resilience of Communities." *Earthquake Spectra*, 19(4), 733–752.

Bruneau, M., and Reinhorn, A. (2007). "Exploring the Concept of Seismic Resilience for Acute Care Facilities." *Earthquake Spectra*, 23(1), 41–62.

Burton, H. V., Deierlein, G., Lallemant, D., and Lin, T. (2016). "Framework for Incorporating Probabilistic Building Performance in the Assessment of Community Seismic Resilience." *Journal of Structural Engineering*, American Society of Civil Engineers, 142(8), C4015007.

Campidelli, M., El-Dakhakhni, W., Tait, M., and Mekky, W. (2016a). "Probabilistic risk assessment of masonry buildings exposed to improvised explosive devices." *Brick and Block Masonry*, CRC Press, 959–966.

Campidelli, M., El-Dakhakhni, W., Tait, M., and Mekky, W. (2016b). "Risk– driven fragility evaluation of reinforced concrete block walls subjected to blast hazard." *Brick and Block Masonry*, CRC Press, 967–975.

Campidelli, M., El-Dakhakhni, W. W., Tait, M. J., and Mekky, W. (2015a). "Blast Design-Basis

Threat Uncertainty and Its Effects on Probabilistic Risk Assessment." *ASCE-ASME Journal of Risk and Uncertainty in Engineering Systems, Part A: Civil Engineering*, 1(4), 04015012.

Campidelli, M., El-Dakhakhni, W. W., Tait, M. J., and Mekky, W. (2017). "Resilience of Masonry Systems in Nuclear Power Plants Under Blast Risk." *Volume 4: Fluid-Structure Interaction*, ASME, Waikoloa, Hawaii, V004T04A020.

Campidelli, M., Tait, M. J., El-Dakhakhni, W. W., and Mekky, W. (2015b). "Inference of Blast Wavefront Parameter Uncertainty for Probabilistic Risk Assessment." *Journal of Structural Engineering*, 141(12), 04015062.

Cimellaro, G. P., Fumo, C., Reinhorn, A. M., and Bruneau, M. (2009). *Quantification of Disaster Resilience of Health Care Facilities*. (Multidisciplinary Center for Earthquake Engineering Research, ed.), University at Buffalo, The State University of New York, Buffalo, NY, USA.

Cimellaro, G. P., Reinhorn, A. M., and Bruneau, M. (2010). "Framework for analytical quantification of disaster resilience." *Engineering Structures*, 32(11), 3639–3649.

Cimellaro, G. P., Tinebra, A., Renschler, C., and Fragiadakis, M. (2016). "New Resilience Index for Urban Water Distribution Networks." *Journal of Structural Engineering*, American Society of Civil Engineers, 142(8), C4015014.

Cimellaro, G. P., Villa, O., and Bruneau, M. (2015). "Resilience-Based Design of Natural Gas Distribution Networks." *Journal of Infrastructure Systems*, 21(1), 05014005.

CSA. (2012). *CSA S850-12 Design and assessment of buildings subjected to blast loads*. Canadian Standards Association, Mississauga, ON, Canada.

Deutsche Welle Network. (2017). "Germany intelligence knew Kabul embassy truck bomb was

imminent."

ElSayed, M., Campidelli, M., El-Dakhakhni, W., and Tait, M. (2015). "Simplified Framework for Blast-Risk-Based Cost-Benefit Analysis for Reinforced Concrete-Block Buildings." *Journal of Performance of Constructed Facilities*, 04015077(13), 04015077.

FEMA. (2012a). *Seismic Performance Assessment of Buildings. Volume 2 – Implementation Guide*. Federal Emergency Management Agency, Redwood City, California.

FEMA. (2012b). "Seismic Performance Assessment of Buildings. Volume 3 - Performance Assessment Calculation Tool (PACT) Version." Federal Emergency Management Agency, Redwood City, California.

Folke, C. (2006). "Resilience: The emergence of a perspective for social–ecological systems analyses." *Global Environmental Change*, 16(3), 253–267.

Grant, M., and Stewart, M. G. (2012). "A systems model for probabilistic risk assessment of improvised explosive device attacks." *International Journal of Intelligent Defence Support Systems*, 5(1), 75.

Grant, M., and Stewart, M. G. (2015). "Probabilistic Risk Assessment for Improvised Explosive Device Attacks That Cause Significant Building Damage." *Journal of Performance of Constructed Facilities*, 29(5), B4014009.

Hayman, M. (2014). "Response of one-way reinforced masonry flexural walls under blast loading." McMaster University, Hamilton, ON, Canada.

Hickman, J. W. (1983). *PRA (Probablistic Risk Assessments) Procedures Guide: A Guide to the Performance of Probabilistic Risk Assessments for Nuclear Power Plants. Volume 2*. VA, USA.

Institute for Economics and Peace. (2015). *Global Terrorism Index 2015: Measuring and Understanding the Impact of Terrorism*.

ISO. (2014). "Sustainable development of communities: Indicators for city services and quality of life."

Kelliher, D., and Sutton-Swaby, K. (2012). "Stochastic representation of blast load damage in a reinforced concrete building." *Structural Safety*, 34(1), 407–417.

Lofton, S. C., and Meyers, G. E. (2001). "Preliminary Validation of Computer Programs for Prediction of Glazing Response to Explosive Airblast." *Structures 2001*, American Society of Civil Engineers, Reston, VA, 1–8.

Low, H. Y., and Hao, H. (2001). "Reliability analysis of reinforced concrete slabs under explosive loading." *Structural Safety*, 23(2), 157–178.

Low, H. Y., and Hao, H. (2002). "Reliability analysis of direct shear and flexural failure modes of RC slabs under explosive loading." *Engineering Structures*, Elsevier, 24(2), 189–198.

Mackie, K. R., and Stojadinović, B. (2006). "Post-earthquake functionality of highway overpass bridges." *Earthquake Engineering & Structural Dynamics*, 35(1), 77–93.

Marjanishvili, S. (2017). "Resilient Bridge Design to Extreme Events." *Engineering Mechanics Institute Conference*, Y. Bazilevs and J. S. Chen, eds., San Diego, California, USA.

NEHRP, C. J. V. (2010). *Evaluation of the FEMA P-695 Methodology for Quantification of Building Seismic Performance Factors*. Gaithersburg, MD.

Netherton, M. D., and Stewart, M. G. (2010). "Blast Load Variability and Accuracy of Blast Load Prediction Models." *International Journal of Protective Structures*, 1(4), 543–570.

Olmati, P., Petrini, F., and Gkoumas, K. (2014). "Fragility analysis for the Performance-Based Design of cladding wall panels subjected to blast load." *Engineering Structures*, 78, 112–120.

Olmati, P., Petrini, F., Vamvatsikos, D., and Gantes, C. (2016). "Simplified fragility-based risk analysis for impulse governed blast loading scenarios." *Engineering Structures*, 117, 457–469.

Ouyang, M., Dueñas-Osorio, L., and Min, X. (2012). "A three-stage resilience analysis framework for urban infrastructure systems." *Structural Safety*, 36–37, 23–31.

Parry, G. W. (1996). "The characterization of uncertainty in Probabilistic Risk Assessments of complex systems." *Reliability Engineering & System Safety*, 54(2–3), 119–126.

Presidential Policy Directive. (2013). "Critical Infrastructure Security and Resilience."

Quiel, S. E., Marjanishvili, S. M., and Katz, B. P. (2016). "Performance-Based Framework for Quantifying Structural Resilience to Blast-Induced Damage." *Journal of Structural Engineering*, 142(8), C4015004.

Rose, A., and Krausmann, E. (2013). "An economic framework for the development of a resilience index for business recovery." *International Journal of Disaster Risk Reduction*, 5, 73–83.

Salem, S., Campidelli, M., El-Dakhakhni, W., and Tait, M. (2017a). "Blast Resilient Design of Infrastructure Subjected to Ground Threats." *Volume 4: Fluid-Structure Interaction*, ASME, Hawaii, USA, V004T04A018.

Salem, S., Campidelli, M., El-Dakhakhni, W. W., and Tait, M. J. (2018). "Resilience-based design of urban centres: application to blast risk assessment." *Sustainable and Resilient*

Infrastructure, 3(2), 68–85.

Salem, S., Campidelli, M., Tait, M., and El-Dakhakhni, W. (2017b). "Probabilistic Resilience Framework for Blast Resistant Infrastructure." *Engineering Mechanics Institute Conference*, Y. Bazilevs and J. S. Chen, eds., San Diego, California, USA.

Stewart, M. G. (2008). "Cost Effectiveness of Risk Mitigation Strategies for Protection of Buildings against Terrorist Attack." *Journal of Performance of Constructed Facilities*, 22(April), 115–120.

Stewart, M. G. (2010). "Risk-informed decision support for assessing the costs and benefits of counter-terrorism protective measures for infrastructure." *International Journal of Critical Infrastructure Protection*, Elsevier B.V., 3(1), 29–40.

Stewart, M. G., and Netherton, M. D. (2008). "Security risks and probabilistic risk assessment of glazing subject to explosive blast loading." *Reliability Engineering & System Safety*, 93(4), 627–638.

Stewart, M. G., Netherton, M. D., and Rosowsky, D. V. (2006). "Terrorism Risks and Blast Damage to Built Infrastructure." *Natural Hazards Review*, American Society of Civil Engineers, 7(3), 114–122.

The MathWorks, I. (2014). "The MathWorks 2014. MATLAB—Statistics Toolbox User's Guide."

Twisdale, L. A., Sues, R. H., and Lavelle, F. M. (1994). "Reliability-based design methods for protective structures." *Structural Safety*, Elsevier, 15(1–2), 17–33.

Unified Facilities Criteria (UFC). (2008). *Structures to resist the effects of accidental explosions*.

USDOD, (U.S. Department of Defense). (2014). *Structures to resist the effects of accidental explosions. Unified Facilities Criteria 4-340-02*, Washington D.C., USA.

Yu, R., Chen, L., Fang, Q., and Huan, Y. (2018). "An improved nonlinear analytical approach to generate fragility curves of reinforced concrete columns subjected to blast loads." *Advances in Structural Engineering*, SAGE PublicationsSage UK: London, England, 21(3), 396–414.

Table 5.1: Different blast scenarios blast hazard parameters

Scenario #	Charge weight (kg TNT)	Standoff distance (m)	Scaled distance ($m/kg^{1/3}$)	LOP
1	50	10	2.71	very low
2	50	20	5.42	very low
3	500	40	5.04	very low

Table 5.2: Repair cost in $\$/m^2$, adapted from FEMA (2017a) and Salem at al. (2017b)

Element	Repair cost (in US$, 90th percentile)				Labor production commencement time (LPCT)
	DS1	DS2	DS3	DS4	
RMW*	100.4	487.9	906.0	906.0	69%
Glazing**	820.0				30%

* for 1 m x 1 m RMW panel

** per 2 m x 2 m toughened glazing panel (6mm thickness)

Table 5.3: Different blast scenarios resilience indicators

Scenario #	I_F* (%)	Repair cost* (US$ x10^4)	Labor repair cost* (US$ x10^3)	Repair time* (hr)	I_R (hr)
1	40.2, 0.8	12.4, 0.4	48.2, 1.8	189, 7.3	3799
2	39.4, 0.7	12.2, 0.6	47.2, 2.7	185, 10.6	3645
3	43.2, 0.6	18.2, 3.0	88.5, 21.2	347, 83	7495

* represented in the form of (E, σ)

E is the expected value; while σ is the standard deviation

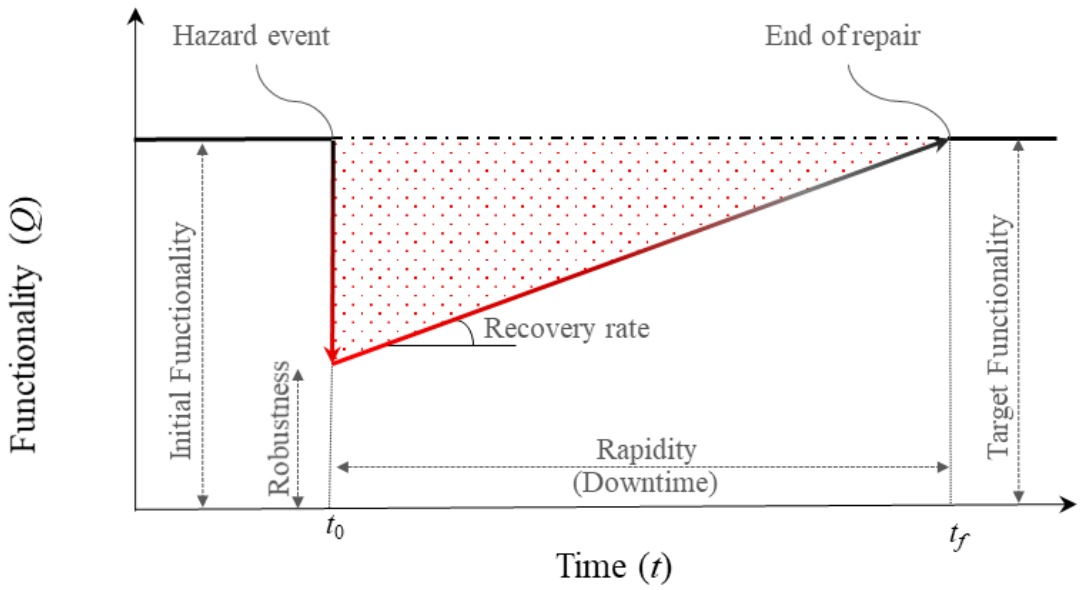

Figure 5.1: Idealized resilience triangle using linear recovery path

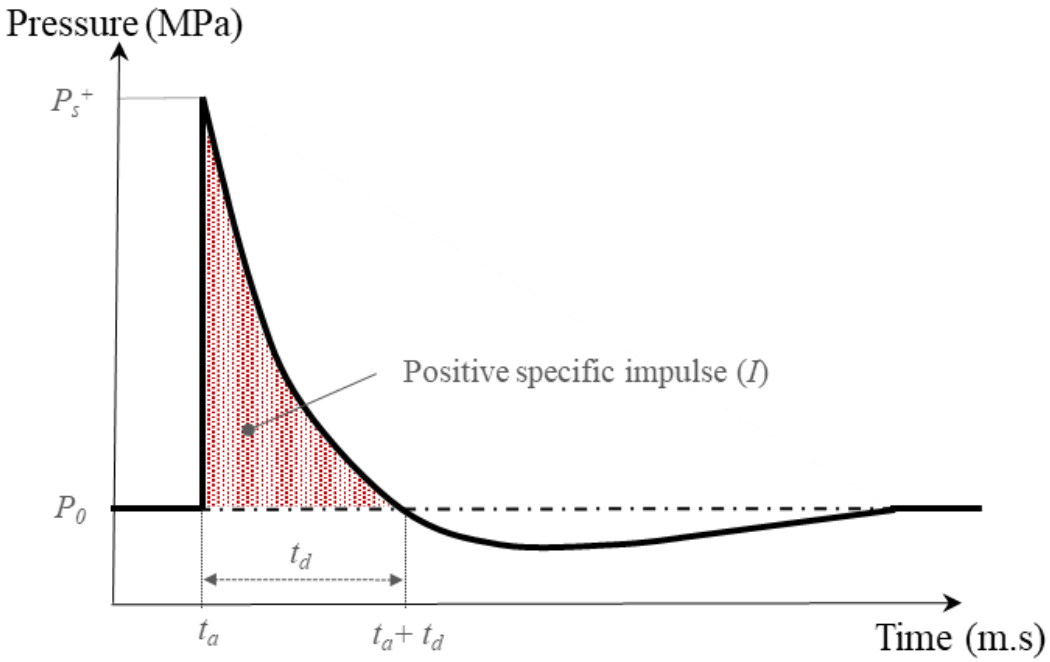

Figure 5.2: Typical blast wave profile

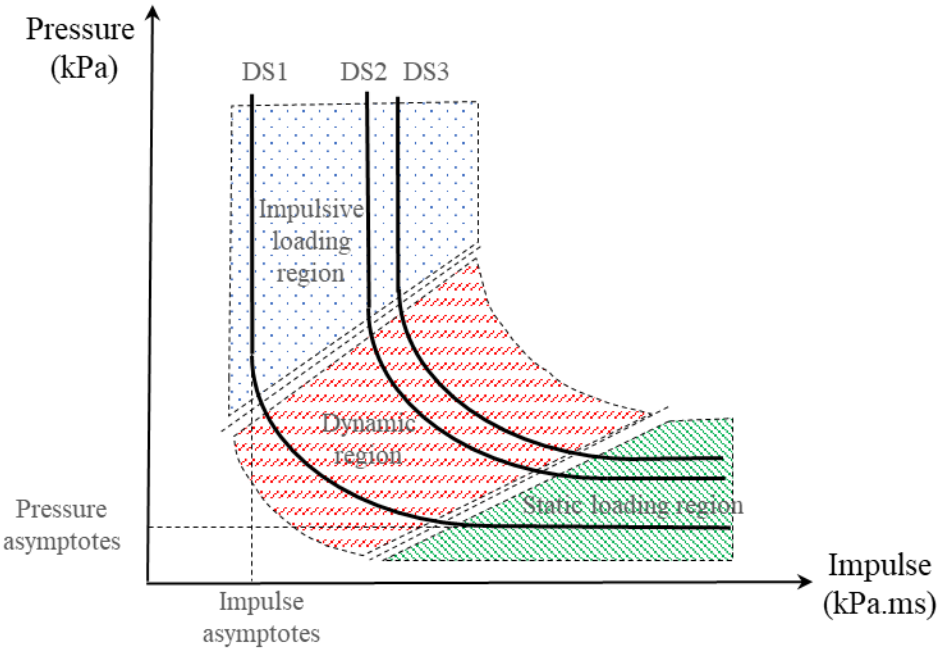

Figure 5.3: Typical P-I diagram (adapted from Hayman (2014))

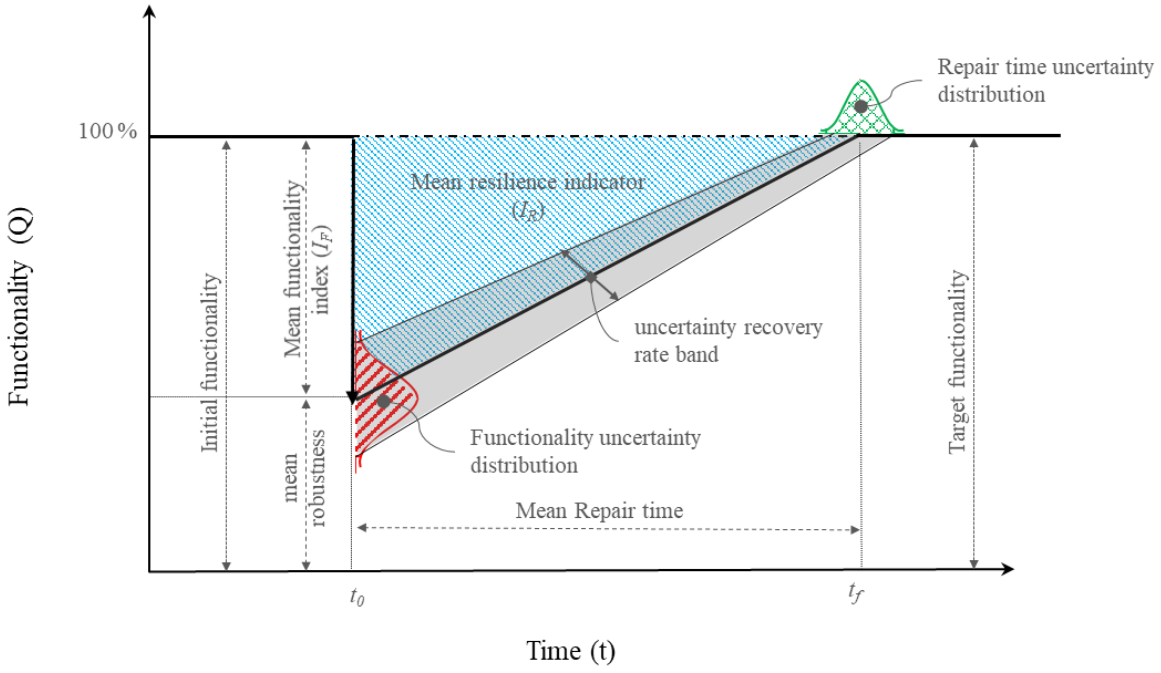

Figure 5.4: Typical probabilistic resilience triangle

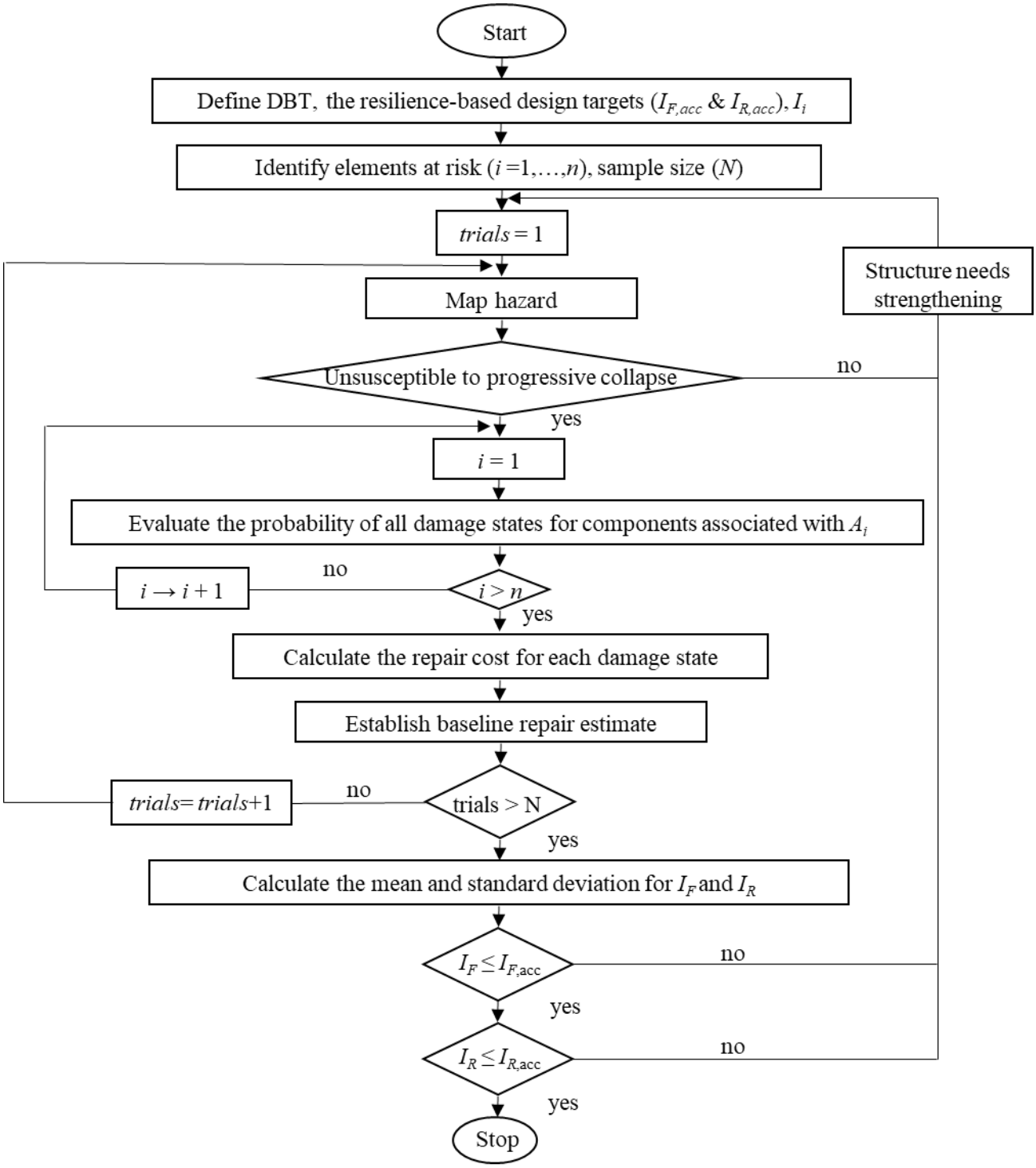

Figure 5.5: Proposed probabilistic blast resilience framework

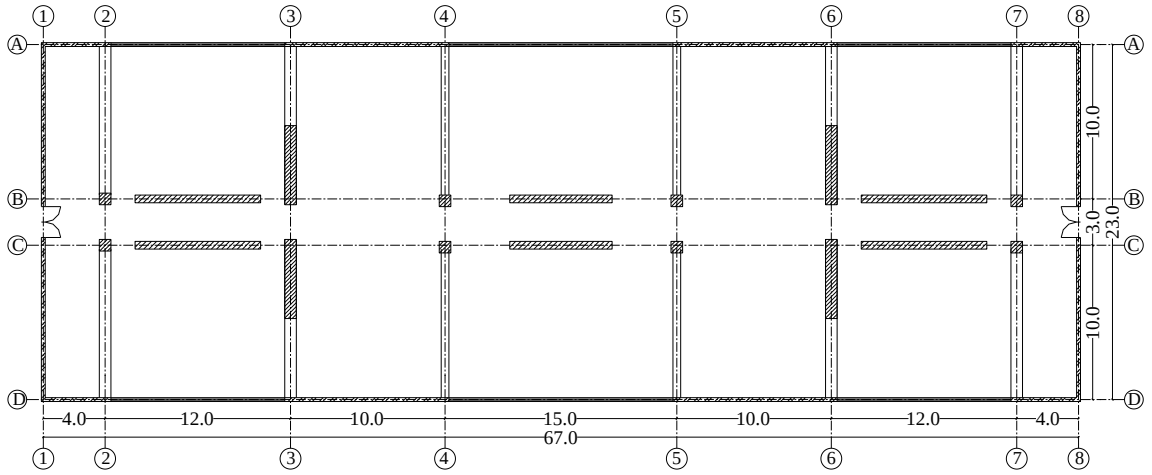

(a)

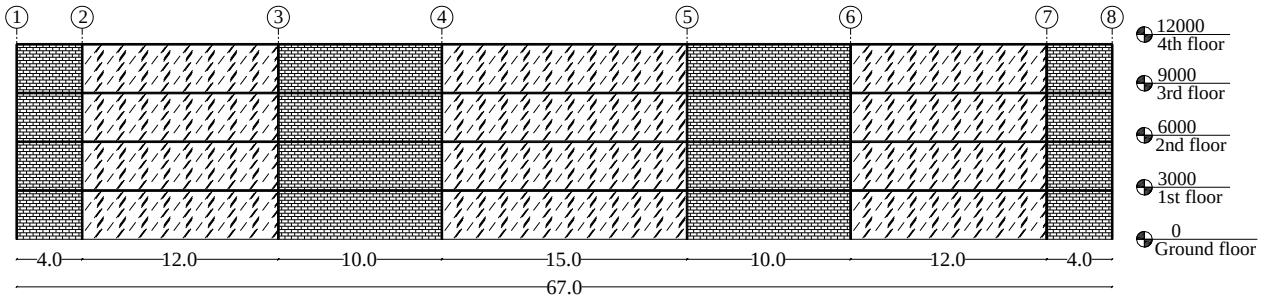

(b)

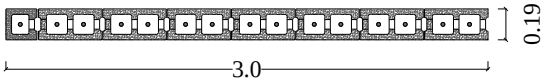

(c)

Figure 5.6: Reinforced masonry building prototype, adapted from NEHRP (2010), units in mm; (a) Building plan view; (b) Elevation view at axis "A and D"; (c) Reinforced masonry shear wall cross-section

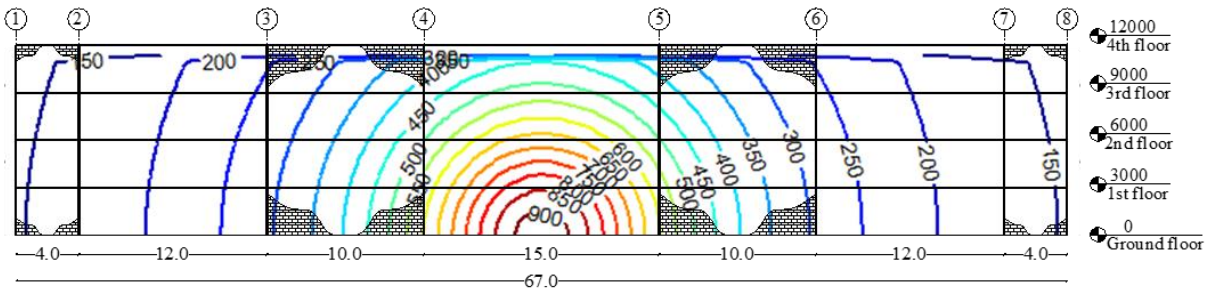

Figure 5.7: Reflected Specific impulse on the exposed façade due to scenario 1 (kPa.ms)

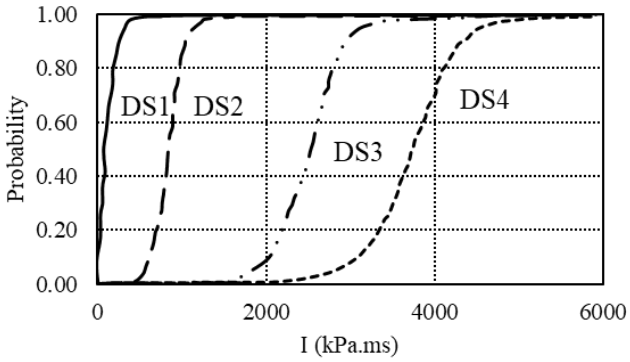

(a)

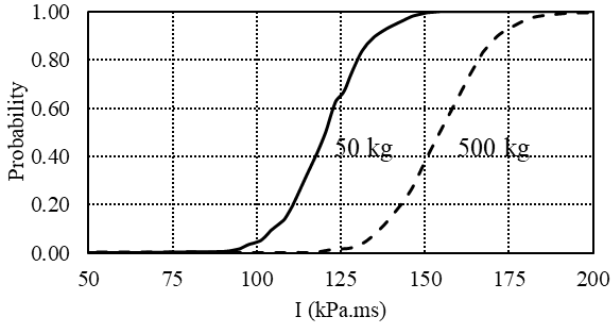

(b)

Figure 5.8: Fragility curves for the façade components: (a) RMSW; (b) 6mm toughened glass (adapted from Campidelli et al. (2016); Stewart and Netherton (2008))

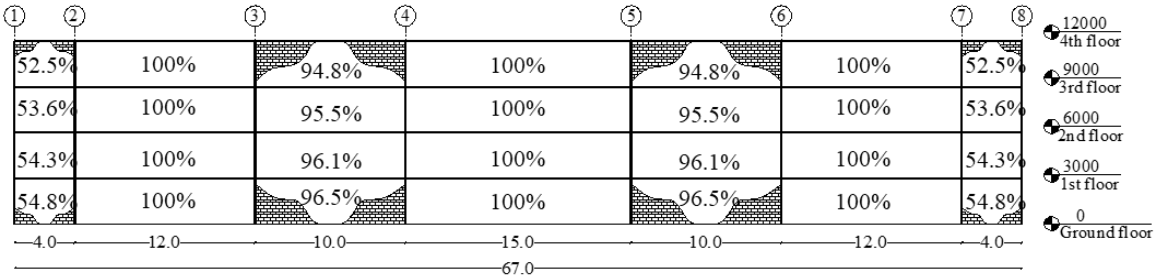

Figure 5.9: Dysfunctional probabilities across the façade due to scenario #1

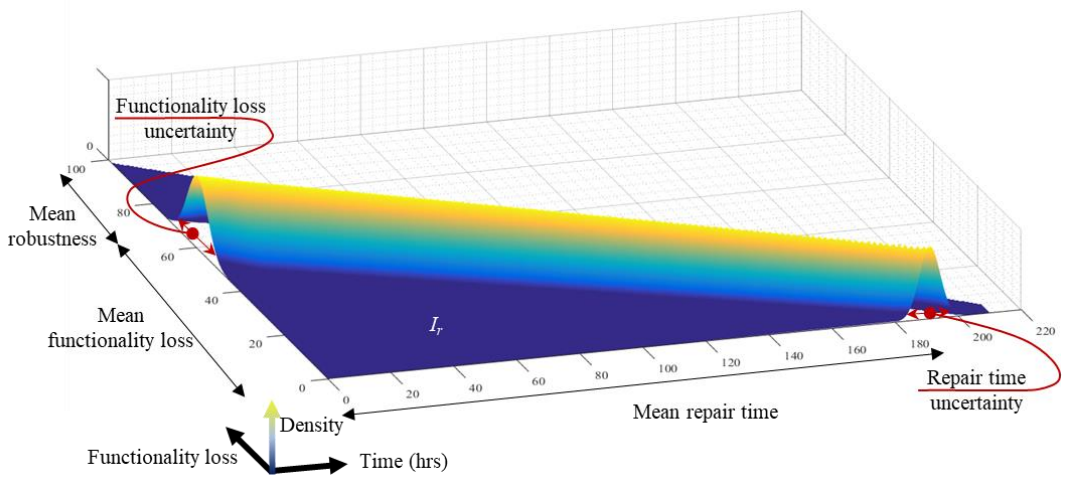

Figure 5.10: Resilience surface for scenario #1

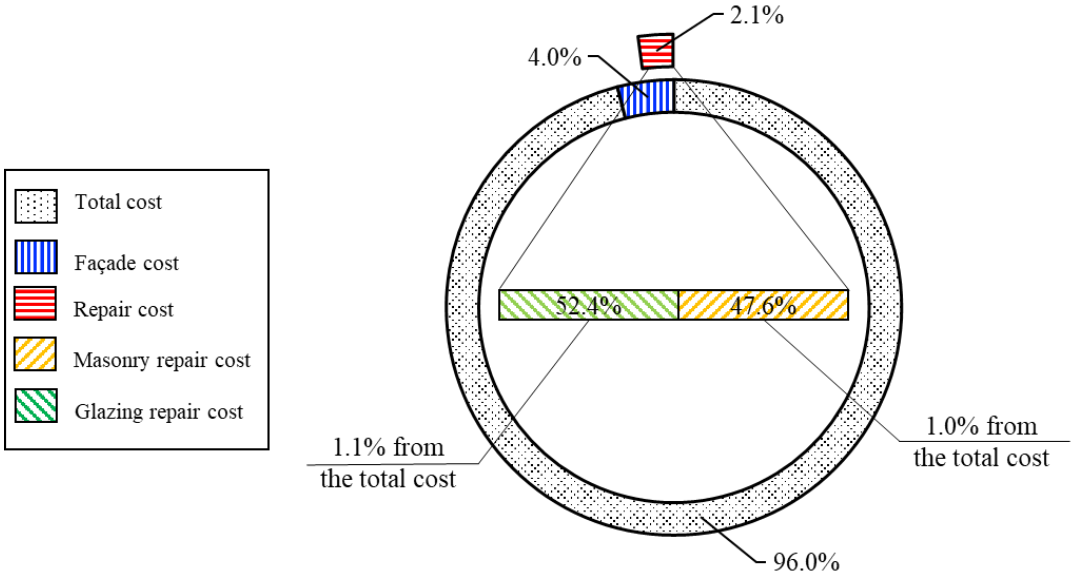

Figure 5.11: Breakdown percentages of contracting (both structural and non-structural elements) and repair costs (due to scenario #3) to the total building cost

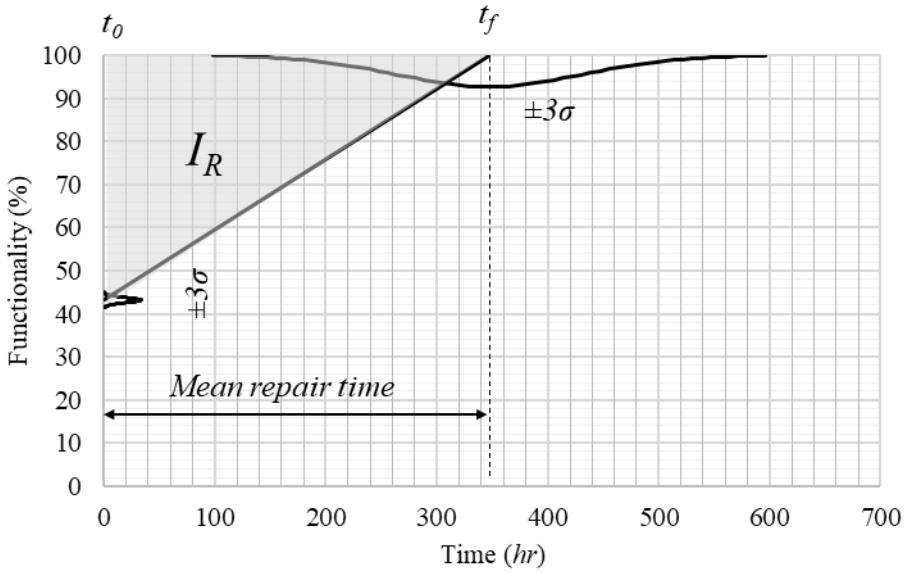

Figure 5.12: Probabilistic resilience triangle for scenario #3 at the 90th percentile confidence

Chapter 6

SUMMARY, CONCLUSIONS, AND RECOMMENDATIONS

6.1 SUMMARY

The research presented in this dissertation included experimental results of seven scaled RMSW, with different in-plane ductility seismic classifications and axial stress levels, subjected to out-of-plane loading. The influence of the test parameters, axial load, and vertical reinforcement ratio, were presented and discussed through examination of the wall damage sequence, load-displacement hysteretic response, stiffness degradation, and energy dissipation behaviour. Subsequently, the experimental results were used to assess the robustness of the resistance function proposed by the *Unified Facilities Criteria 3-340*. Moreover, a comprehensive analytical resistance function was proposed, considering both the post-peak behaviour and second-order effects of the RMSWs. Furthermore, the DIF was introduced to the numerical model during the simulation of the blast response of RMSWs, which was validated against free-field explosion results. In addition, an iterative framework, namely Blast OpenSees Simulation framework (BOSS), was proposed to assess the variability/uncertainty associated with the blast wavefront parameters on the response of RMSWs. The probabilistic results of the RMSWs blast response were presented through a 3D fragility surface, which is considered the second generation of the deterministic performance assessment charts (P-I diagram). The BOSS was also applied to probabilistically investigate the influence of the axial load at different vertical reinforcement ratios on the response of RMSWs. Furthermore, a deterministic resilience-based blast design framework was introduced to overcome the conservative estimation of the structure's level of protection (LoP) based on the lowest performance of its components of the current blast standards. The proposed resilience framework was based on quantifying the post-blast resilience aspects, functionality and repair time, through two introduced new metrics, namely the functionality loss index, and the resilience indicator.

Finally, a probabilistic resilience-based blast design framework was proposed and utilized through a developed toolbox, namely probabilistic infrastructure resilience assessment toolbox (PIRAT). The probabilistic resilience aspects were quantified and presented in graphical form via 3D resilience surface.

6.2 CONCLUSIONS

The experimental, analytical and numerical work reported in this dissertation has widened the knowledge of the blast response predictions of RMSWs. The presented work addressed the out-of-plane response of load-bearing RMSWs statically (i.e. through the resistance function) and dynamically (i.e. considering the response to blast loads). Furthermore, a deterministic- and probabilistic resilience-based blast design frameworks, were developed to cover the current blast standard limitations. Within this context, several conclusions can be drawn for the component-level RMSW out-of-plane response or the overall system-level response.

In terms of the component-level (i.e. individual RMSW) out-of-plane response:

- Load-bearing and non-load-bearing RMSWs exhibits similar out-of-plane displacement profile and cracking pattern regardless of their design parameters. As expected, the increases in the wall vertical reinforcement ratio and axial load reduced significantly the out-of-plane displacement ductility. Moreover, the vertical reinforcement ratio was found to be directly proportional to the energy dissipated and the normalized secant stiffness. Finally, the axial load increased the wall energy dissipation but reduced its corresponding normalized secant stiffness.
- The resistance function formulation given by the *Unified Facilities Criteria 3-340* showed inadequate values when compared to experimental results, especially at the post-peak stage.

In contrast, the analytical resistance function developed within the current study accounted for the moment redistribution, curvature concentrations, and the second order effects.

- The application of the concentrated plasticity approach within the context of blast response prediction has been validated for both the static resistance function and the dynamic response under blast load.
- The predictions of the RMSWs blast response sensitivity to the DIFs was demonstrated. The fixed DIFs values recommended by the *Unified Facilities Criteria 3-340* (USDOD 2014) showed a trend of overestimation with a large deviation (114% deviation) compared to the blast response results of RMSWs. However, both the DIF recommended by the CEB-FIP Model Code 1990 (Béton 1990) and the homogenized DIF accounting for the orthotropic behavior in the masonry walls (Wei and Hao 2009) showed approximately similar results with better predictions. Where the homogenized DIF (Wei and Hao 2009) resulted in 39% average deviation for the tested database.
- The influence of the blast waveform has also been addressed, where the numerical model has been validated against the experimental database using the idealized exponential Friedlander wave and a linear wave path. The exponential waveform provided better predictions with an average deviation of 29% compared to 39% average deviation using the linear wave path.
- The axial load, ranging from 0-15%, was found to be inversely proportional to the blast performance of the RMSWs. This is attributed to the enhanced section capacity due to the axial confinement.

In terms of the system-level (i.e. full building) overall response:

- The post-blast functionality and resilience were quantified at the system–level by introducing two new metrics, namely, the *functionality loss index* and the *resilience indicator*. The application of the resilience concept within the blast design context has provided more meaningful information for the post-disaster functionality and its corresponding downtime.
- The proposed resilience metrics allowed a comprehensive assessment for the global post-blast functionality which may not be depicted by the level of protections (LOPs) recommended by the current blast standards (ASCE 2011; CSA 2012). Moreover, the proposed resilience metrics account for the variation of wavefront parameters and the vulnerability of the building different components, which may lead to different judgments based solely on the scaled distance.
- The proposed probabilistic resilience-based blast design framework provides an enhancement for the current probabilistic risk assessment to account for the probabilistic post-blast functionality and its subsequent recovery time. The proposed framework is considered a proper communication form for the risk assessors as it addresses the probabilistic meaningful resilience aspects.

6.3 RECOMMENDATIONS FOR FUTURE RESEARCH

In light of the research findings reported in this dissertation; this section presents possible research extensions to expand the blast-resilience knowledge for RMSW buildings.

- The current study presented an experimental investigation of different seismically-detailed RMSWs, however, additional experimental tests are still required to develop the reliable judgment on the test parameters. These additional tests should cover other horizontal reinforcement details, boundary conditions, and axial load levels.
- Although the reported experimental work in this dissertation was mainly focused on the flexural assessment of RMSWs, an extensive investigation of the shear behavior of RMSWs is still required. The additional investigation is to create a comprehensive failure envelop for RMSWs subjected to out-of-plane loading.
- Additional investigations for a wider spectrum of axial load levels are still required to assess their influence on the out-of-plane response of RMSWs. Moreover, field/arena blast tests for loadbearing RMSWs are also required to reliably validate the proposed numerical blast model.
- Some limitations of the presented resilience-based blast design methodology, which hinders its comprehensive application, should be addressed. These limitations include different blast scenarios (i.e. an external unconfined explosion, and internal explosions), the range of explosions (i.e. far-field, and near-field explosions), and the simplified assumptions of the building response and its interaction with the shock waves. Moreover, the propagation of the blast waves towards the building's core, secondary fragment penetration. Whereas the interaction between load–bearing and non–structural members should also be considered. Furthermore, the interactions of the shock waves with nearby structures, the ground, and the geometry of the building's envelope should be deliberated.

- Although the proposed probabilistic resilience-based blast design accounts for the structural blast response uncertainty, other sources of uncertainty should be adapted. More specifically, uncertainties associated with the loading, response, and the consequences may aggregate into larger variations for the resilience parameters, and thus the decision-making process.

6.4 REFERENCES

ASCE. (2011). *Blast Protection of Buildings*. *ASCE 59-11*, (American Society of Civil Engineers, ed.), American Society of Civil Engineers, Reston, VA, VA.

Béton, C. E.-I. du. (1990). "CEB-FIP model code 1990.pdf."

CSA. (2012). *CSA S850-12 Design and assessment of buildings subjected to blast loads*. Canadian Standards Association, Mississauga, ON, Canada.

USDOD, (U.S. Department of Defense). (2014). *Structures to resist the effects of accidental explosions*. *Unified Facilities Criteria 4-340-02*, Washington D.C., USA.

Wei, X., and Hao, H. (2009). "Numerical derivation of homogenized dynamic masonry material properties with strain rate effects." *International Journal of Impact Engineering*, Pergamon, 36(3), 522–536.